

**UNIVERSITY OF GAZIANTEP
GRADUATE SCHOOL OF
NATURAL & APPLIED SCIENCES**

May, 2017

Ph.D. in Physics Engineering

DİLEK TOKTAMIŞ

**THE INVESTIGATION OF THE EFFECTS OF PRE-
IRRADIATION ANNEALING PROCEDURES ON
THERMOLUMINESCENCE DOSIMETRIC PROPERTIES OF
DIFFERENT NATURAL SAMPLES**

Ph.D. THESIS

IN

PHYSICS ENGINEERING

BY

DİLEK TOKTAMIŞ

MAY 2017

**The Investigation of the Effects of Pre-Irradiation Annealing Procedures on
Thermoluminescence Dosimetric Properties of Different Natural Minerals**

Ph.D. Thesis

in

Physics Engineering

University of Gaziantep

Supervisor

Prof. Dr. A. Necmeddin YAZICI

by

Dilek TOKTAMIŞ

May 2017



© 2017 [Dilek TOKTAMIŞ]


REPUBLIC OF TURKEY
UNIVERSITY OF GAZİANTEP
GRADUATE SCHOOL OF NATURAL & APPLIED SCIENCES
PHYSICS ENGINEERING DEPARTMENT

Name of the thesis: The Investigation of the Effects of Pre-Irradiation Annealing Procedures on Thermoluminescence Dosimetric Properties of Different Natural Minerals

Name of the student: Dilek TOKTAMIŞ


Exam date: 18.05.2017

Approval of the Graduate School of Natural and Applied Sciences


Prof. Dr. A. Necmeddin YAZICI

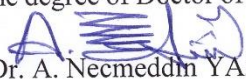
Director

I certify that this thesis satisfies all the requirements as a thesis for the degree of Doctor of Philosophy.


Prof. Dr. Ramazan KOÇ

Head of Department

This is to certify that we have read this thesis and that in our consensus opinion it is fully adequate, in scope and quality, as a thesis for the degree of Doctor of Philosophy.


Prof. Dr. A. Necmeddin YAZICI

Supervisor

Examining Committee Members:

Prof. Dr. Zihni ÖZTÜRK






Prof. Dr. Kasım KURT

Prof. Dr. Metin BEDİR

Prof. Dr. A. Necmeddin YAZICI

Doç. Dr. Cumhur CANBAZOĞLU

Signature


.....

.....

.....

.....

.....

I hereby declare that all information in this document has been obtained and presented in accordance with academic rules and ethical conduct. I also declare that, as required by these rules and conduct, I have fully cited and referenced all material and results that are not original to this work.

Dilek TOKTAMIŞ

ABSTRACT

THE INVESTIGATION OF THE EFFECTS OF PRE-IRRADIATION ANNEALING PROCEDURES ON THERMOLUMINESCENCE DOSIMETRIC PROPERTIES OF DIFFERENT NATURAL SAMPLES

TOKTAMIŞ, Dilek

Ph.D. in Physics Engineering

Supervisor: Prof. Dr. A Necmeddin YAZICI

May 2017

103 pages

Many thermoluminescence properties of dosimetric minerals may be affected by external effects and environmental condition. Annealing is one of the most known external effects and has different process. As a result of annealing process, the defect distribution of a specimen can be altered and thereby its sensitivity changes. In spite of fact that standard annealing procedures exist for the dosimetric purposes of the synthetic materials, these can be different for natural minerals. As the thermoluminescence properties of different natural minerals are unequal, different thermoluminescence properties are observed for the same natural minerals collected in the different region of the world. Therefore, annealing may alter the thermoluminescence properties of each natural minerals, differently. This thesis reveals that how the thermoluminescence properties of different natural minerals are affected by different pre-irradiation annealing processes. The origins of natural minerals used in this thesis were different and obtained from the different regions of Turkey. The thermoluminescence properties of four different natural minerals which are calcite minerals in sand used in making roasted chickpea, fluorapatite minerals in tooth enamel, plagioclase minerals in basaltic rocks and biogenic minerals in seashell have been studied under different thermal treatments.

Key Words: Thermoluminescence, Annealing, Natural Minerals, Dosimeter

ÖZET

FARKLI DOĞAL ÖRNEKLERİN TERMOLÜMINESANS DOZİMETRİK ÖZELLİKLERİ ÜZERİNDE IŞINLAMA ÖNCESİ TAVLAMA İŞLEMLERİ ETKİLERİNİN İNCELENMESİ

TOKTAMIŞ, Dilek

Doktora Tezi, Fizik Müh. Bölümü

Tez Yöneticisi: Prof. Dr. A. Necmeddin YAZICI

Mayıs 2017

103 sayfa

Dozimetrik minerallerin birçok özellikleri dış etkenlerden ve çevresel durumlardan etkilenebilir. Tavlama bilinen en önemli dış etkenlerden biri olup farklı işlemleri mevcuttur. Tavlamanın bir sonucuna göre numunenin kusur dağılımı değişir ve böylece duyarlılığında değişim gözlenir. Her ne kadar sentetik materyallerin dozimetrik amaçları için standart tavlama prosedürleri mevcut olsa da doğal minerallerde tavlama protokolleri farklılık gösterebilir. Farklı doğal minerallerin termolüminesans özellikleri farklı olduğu gibi, dünyanın farklı bölgelerinden toplanmış aynı doğal minerallerin termolüminesans özellikleride farklı olabilir. Böylece tavlama her bir doğal mineralin termolüminesans özelliğini farklı şekilde değiştirebilir. Bu tezde ışınlama öncesi, tavlama işlemlerinin doğal minerallerin termolüminesans özelliklerini nasıl etkilediği ortaya konmuştur. Bu çalışmada kullanılan doğal minerallerin orijinleri farklı olup, Türkiye'nin farklı bölgelerinden temin edilmiştir. Dört farklı doğal numune olan kalsit minerali; leblebi yapımında kullanılan kumdan, floropatit minerali; diş minesinden, plajiyoklaz minerali; bazaltik kayadan ve biyojenik minerali ise deniz kabuğundan elde edilerek farklı tavlama işlemleri altında termolüminesans özellikleri çalışılmıştır.

Anahtar Kelimeler: Termolüminesans, Tavlama, Doğal mineraller, Dozimetre



To me ...

ACKNOWLEDGEMENT

The scope of this thesis was conceived in my first year as a PhD student. Due to the results of my experiments, I'm excited to write my thesis. Thus, I thought it would be worth to write my results of TL experiment and research.

The first person that inspired me to take stock and summaries thermoluminescence research, I would like to thank to my supervisor Prof. Dr. Ahmet Necmeddin YAZICI, in the process of this study for interest and support makes me every time. He has been an inexhaustible source of new ideas and his luminescence research and his information sharing has led me.

The second person that has inspired me since the first years of my work, I am extremely grateful to Assoc. Prof. Dr. Hüseyin TOKTAMIŞ. I was lucky enough that he introduced me to the exciting and mysterious world of thermoluminescence phenomena and he makes me for guiding experiences. The high-quality work has strongly contributed to transferring of so many scientific ideas into experimental practice.

I would like to thank Prof. Dr. Metin BEDİR and Prof. Dr. Kasım KURT for constructive criticism, insightful comments on improving my qualifications.

I would like to express my particular gratitude to my mother Nesrin TUTCU and my father Ahmet Asım TUTCU for encouraging me.

Last but not least I want to thank my sons Birant and Bilgehan for her patience and warm support.

TABLE OF CONTENTS

CONTENTS	Page
TABLE OF CONTENTS	ix
LIST OF FIGURES	xii
LIST OF TABLES	xx
CHAPTER 1: INTRODUCTION	1
CHAPTER 2: LITERATURE SURVEY	5
2.1. Luminescence	5
2.2. Thermoluminescence	7
2.3. Defects and Color centers.....	9
2.4. Models in Thermoluminescence	11
2.4.1. Randall-Wilkins Model (First Order Kinetics).....	11
2.4.2. Garlick-Gibson Model (Second Order Kinetics)	16
2.4.3. May-Partridge Model (General Order Kinetics).....	17
2.4.4. Advanced Models	18
2.5. Cycle of Measurements (Reproducibility)	20
2.6. Annealing	20
2.7. Natural Minerals Used in Experiments	22
2.7.1. Calcite Extracted from Natural Sand Used in Making Roasted Chickpea (Leblebi).....	22
2.7.2. Fluorapatite Mineral ($\text{Ca}_5\text{F}(\text{PO}_4)_3$) In Tooth Enamel.....	23
2.7.3. Biogenic Minerals Present in the Seashells.....	25
2.7.4. Plagioclase Minerals in Basaltic Rocks.....	26
CHAPTER 3: EXPERIMENTAL EQUIPMENT AND PROCEDURES.....	31

3.1. Equipment in the Laboratory	31
3.1.1. Radiation Source and Irradiator	32
3.1.2. TL Reader and Peak Analyzer	33
3.1.3. Microprocessor Controlled Electrical Oven	35
3.1.4. Equipment Used Before Irradiation Process.....	36
3.2 Material and Preparation	36
3.2.1 Calcite Extracted from Natural Sand Used in Making Roasted Chickpea.....	36
3.2.2 Fluorapatite Mineral ($\text{Ca}_5\text{F}(\text{PO}_4)_3$) In Tooth Enamel.....	37
3.2.3 Biogenic Minerals Present In the Seashells.....	37
3.2.4 Plagioclase Minerals in Basaltic Rocks.....	38
3.3. XRD Analysis of the Samples	38
3.3.1 Calcite Extracted from Natural Sand Used in Making Roasted Chickpea.....	39
3.3.2 Fluorapatite Mineral ($\text{Ca}_5\text{F}(\text{PO}_4)_3$) In Tooth Enamel.....	40
3.3.3 Biogenic Minerals Present in the Seashells.....	41
3.3.4 Plagioclase Minerals in Basaltic Rocks.....	42
3.4. Procedure	44
CHAPTER 4: EXPERIMENTAL RESULTS	46
4.1. Grain Size Effect	46
4.1.1 Calcite Extracted from Natural Sand Used in Making Roasted Chickpea.....	46
4.1.2 Biogenic Minerals Present in the Seashells.....	48
4.1.3 Plagioclase Minerals in Basaltic Rocks.....	49
4.2. Annealing Effects at Different Annealing Temperatures	51

4.2.1 Calcite Extracted from Natural Sand Used in Making Roasted Chickpea.....	51
4.2.2 Fluorapatite Mineral ($\text{Ca}_5\text{F}(\text{PO}_4)_3$) In Tooth Enamel.....	54
4.2.3 Biogenic Minerals Present In the Seashells.....	57
4.2.4 Plagioclase Minerals in Basaltic Rocks.....	60
4.3. Annealing Effects at Different Annealing Times	62
4.3.1 Calcite Extracted from Natural Sand Used in Making Roasted Chickpea.....	62
4.3.2 Fluorapatite Mineral ($\text{Ca}_5\text{F}(\text{PO}_4)_3$) In Tooth Enamel.....	65
4.3.3 Biogenic Minerals Present in the Seashells.....	67
4.3.4 Plagioclase Minerals in Basaltic Rocks.....	70
4.4. Reproducibility at Different Annealing Temperatures.....	72
4.4.1 Calcite Extracted from Natural Sand Used in Making Roasted Chickpea.....	72
4.4.2 Fluorapatite Mineral ($\text{Ca}_5\text{F}(\text{PO}_4)_3$) In Tooth Enamel.....	74
4.4.3 Biogenic Minerals Present in the Seashells.....	78
4.4.4 Plagioclase Minerals in Basaltic Rocks.....	79
CHAPTER 5: DISCUSSION AND CONCLUSION.....	82
REFERENCES	94

LIST OF FIGURES

LIST OF FIGURES	Page
Figure 2.1 Basic concepts of irradiation, thermally and optically process between trap centers and recombination centers in a simple phenomenological band model. The transitions define whether a defect is a trap center T or a recombination center R . A recombination of an electron into a R center is assumed to be followed by photon emission [4].	6
Figure 2.2 Typical thermoluminescence glow curve from a sedimentary K-feldspar substance exposed by a beta dose (8 Gy) plus the natural dose (~200 Gy). The peak located 150°C peak in this figure has been created by the recent beta dose. The shaded part is the black body radiation [4].....	8
Figure 2.3 Energy levels in an insulator in equilibrium at absolute zero.....	10
Figure 2.4 Energy band model showing the electronic transitions in a thermoluminescence material according to a simple two-level model (a) generation of electrons and holes; (b) electron and hole trapping; (c) electron release due to thermal stimulation; (d) recombination. (●) shows electrons, (○) shows holes. Level T is an electron trap, level R is a recombination center, E_f is Fermi level [1].....	11

Figure 2.5	A bell-shaped glow curve as a result of Randall-Wilkins model.....	16
Figure 2.6	Comparison of first order ($b = 1$), second order ($b = 2$) and intermediate order ($b = 1.3$ and 6) thermoluminescence peaks, with $E = 1eV$, $s = 1 \times 10^{12} s^{-1}$, $n_0 = N = 1 m^{-3}$, and $\beta = 1 K/s$ [16].....	18
Figure 2.7	Advanced models describing the thermally stimulated release of trapped charged carriers including: (a) a shallow trap (ST), a deep electron trap (DET), and a active trap (AT); (b) two active traps and two recombination centers; (c) localized transitions; (d) defect interaction (trapping center interacts with another defect).....	19
Figure 2.8	Photomicrograph of the tested vesicular basalt showing a mixture of plagioclase, pyroxene and vesicles [61].....	27
Figure 2.9	The original basaltic rocks in the Karataş region of Gaziantep, Turkey.....	29
Figure 2.10	Geological map of Gaziantep city and near its vicinity (MTA 1994) [61].....	29
Figure 3.1	Thermoluminescence Laboratory.....	31
Figure 3.2	^{90}Sr - ^{90}Y β -source.....	32

Figure 3.3	Irradiator.....	33
Figure 3.4	Harshaw TLD System 3500 Manual TL Reader.....	34
Figure 3.5	Basic block diagram of TL reader.....	35
Figure 3.6	Microprocessor controlled Electrical Oven.....	35
Figure 3.7	Some of the used equipment; chemicals, sieves and digital balance.....	36
Figure 3.8	(a) Natural sand used in making roasted chickpea, (b) usage of sand sample during making roasted chickpea.....	37
Figure 3.9	The seashells which were collected from the shores of the Mediterranean (a) as bulk form (b) as powder form.....	38
Figure 3.10	The XRD measurement of sand used in making Ağın leblebi.....	39
Figure 3.11	X-ray diffraction (XRD) pattern of tooth enamel.....	40
Figure 3.12	The XRD measurement of un-annealed seashell as powder form.....	41
Figure 3.13	The XRD measurement of annealed seashell at 700 °C as powder form.....	42
Figure 3.14	The XRD measurement of powdered basaltic rock.....	43
Figure 4.1	Effect of different grain size of sand sample on the shape of TL glow curve.....	47

Figure 4.2	Effect of different grain size of sand sample on the area under the glow curve.....	47
Figure 4.3	The effect of different grain sizes of the seashell sample on glow curve shape.....	48
Figure 4.4	The effect of different grain sizes of the seashell sample on the area under the TL glow curve.....	49
Figure 4.5	Variation of TL glow curve at different grain sizes of basalt sample.....	50
Figure 4.6	Variation of area under the glow curve at different grain sizes of basalt sample.....	50
Figure 4.7	Variation of TL glow curve shape as a function of annealing temperature.....	52
Figure 4.8	Variation of area under the curve as a function of annealing temperature.....	52
Figure 4.9	Variation of TL peak intensities as a function of annealing temperature.....	53
Figure 4.10	Variation of peak temperatures as a function of annealing temperature.....	53
Figure 4.11	The variation of the shape of TL glow curve as a function of annealed temperatures at 500-800 °C and about 30 min....	54
Figure 4.12	The variation of TL glow curve as a function of annealed temperatures at 900-1100 °C about 30 min.....	55
Figure 4.13	The variation of area under the glow curve as a function of annealing temperatures at 500°C -1100°C about 30 minutes.	55

Figure 4.14	The variation of TL peak intensity as a function of annealing temperatures at 500°C -1100°C about 30 minutes.....	56
Figure 4.15	The variation of peak temperature as a function of annealing temperatures at 500°C -1100°C about 30 minutes.....	56
Figure 4.16	The effects of different annealing temperatures on TL glow curve (a) between 200 and 600 °C, (b) between 700 and 1100 °C.....	57
Figure 4.17	The effects of different annealing temperatures on the area under the glow curve.....	58
Figure 4.18	The effects of different annealing temperatures on the TL peak intensity.....	58
Figure 4.19	The effects of different annealing temperatures on the peak temperatures.....	59
Figure 4.20	Variation of TL glow curve as a function of annealing temperature.....	60
Figure 4.21	Variation of area under the curve as a function of annealing temperature.....	61
Figure 4.22	Variation of TL peak intensity as a function of annealing temperature.....	61
Figure 4.23	Variation of peak temperature as a function of annealing temperature.....	62
Figure 4.24	Variation of shape of TL glow curve as a function of annealing time at 900 °C.....	63

Figure 4.25	Variation of area under the glow curve as a function of annealing time at 900 °C.....	63
Figure 4.26	Variation of TL peak intensity as a function of annealing time at 900 °C.....	64
Figure 4.27	Variation of peak temperatures as a function of annealing time at 900 °C.....	64
Figure 4.28	Effects of different annealing times at fixed annealing temperature (1000 °C) on the glow curve.....	65
Figure 4.29	Effects of different annealing times at fixed annealing temperature (1000 °C) on the area under the curve.....	66
Figure 4.30	Effects of different annealing times at fixed annealing temperature (1000 °C) on the TL peak intensity.....	66
Figure 4.31	Effects of different annealing times at fixed annealing temperature (1000 °C) on the TL peak intensity.....	67
Figure 4.32	Effect of different annealing time on the TL glow curve for annealing time between (a) 30min-180min and (b) 240min-360min.....	68
Figure 4.33	Effect of different annealing time on the area under the curve.....	68
Figure 4.34	Effect of different annealing time on the TL peak intensity...	69
Figure 4.35	Effect of different annealing time on the peak temperature...	69

Figure 4.36	Variation of TL glow curve as a function of annealing time at 200 °C.....	70
Figure 4.37	Variation of area under the curve as a function of annealing time at 200 °C.....	71
Figure 4.38	Variation of TL peak intensity as a function of annealing time at 200 °C.....	71
Figure 4.39	Variation of peak temperature as a function of annealing time at 200 °C.....	72
Figure 4.40	Normalized area under the glow curve versus cycle of measurement for annealed samples between 200°C-400°C..	73
Figure 4.41	Normalized area under the glow curve versus cycle of measurement for annealed samples between 200°C-400°C..	73
Figure 4.42	Normalized area under the glow curve versus cycle of measurement for annealed samples between 800°C-1100°C.	74
Figure 4.43	Reproducibility of the un-annealed sample at fixed annealing time (30 min) and standard deviation.....	75
Figure 4.44	Reproducibility of the sample annealed at 600°C at fixed annealing time (30 min) and standard deviation.....	75
Figure 4.45	Reproducibility of the sample annealed at 700°C at fixed annealing time (30 min) and standard deviation.....	76
Figure 4.46	Reproducibility of the sample annealed at 800°C at fixed annealing time (30 min) and standard deviation.....	76

Figure 4.47	Reproducibility of the sample annealed at 900°C at fixed annealing time (30 min) and standard deviation.....	77
Figure 4.48	Reproducibility of the sample annealed at 1000°C at fixed annealing time (30 min) and standard deviation.....	77
Figure 4.49	Normalized area under the glow curve versus cycle of measurement for annealed samples between 500 °C and 700 °C.....	78
Figure 4.50	Normalized area under the glow curve versus cycle of measurement for annealed samples between 800 °C and 1100 °C.....	79
Figure 4.51	Normalized area under the glow curve versus cycle of measurement for annealed samples between 200°C-400°C.	80
Figure 4.52	Normalized area under the glow curve versus cycle of measurement for annealed samples between 500°C-700°C.	80
Figure 4.53	Normalized area under the glow curve versus cycle of measurement for annealed samples between 800°C-1100°C.	81
Figure 5.1	The glow curves of (a) unannealed and (b) annealed seashell samples at 700°C after irradiating 36Gy.	87

LIST OF TABLES

TABLES		Page
Table 2.1	List of the luminescence phenomena and the methods of excitation.....	7
Table 3.1	The analysis of XRD measurement of the sand sample.....	39
Table 3.2	The Peak ID Extended Report of tooth enamel.....	40
Table 3.3	The analysis of XRD measurement of the un-annealed seashell.....	41
Table 3.4	The analysis of XRD measurement of the annealed seashell at 700 °C.....	42
Table 3.5	The analysis of XRD measurement of the powdered basaltic rock.....	43
Table 4.1	Mean and standard deviation of normalized area under the curve for different annealing temperature.....	81
Table 5.1	Summary of grain size experiment for the natural minerals used in the thesis.....	85
Table 5.2	Summary of effects of annealing at different temperatures on TL properties of the four natural minerals.....	90

Table 5.3	Summary of effects of annealing at different times on TL properties of the four natural minerals.....	92
Table 5.4	Summary of effects of annealing at different temperatures on the cycle of measurement (reproducibility) of the four natural minerals.....	93



CHAPTER 1

INTRODUCTION

In recent years, thermoluminescence (TL) and associative methods have been most useful process in the studies of radiation dosimetry. Nowadays, many radiation applications such as the solid-state dosimetry and study of radiotherapy are based on luminescence detectors. Thermoluminescence has an obvious advantage with its ability to isolate signals that appear at different temperatures.

Thermoluminescence is a kind of luminescence differ from other types by stimulation method. To observe a thermoluminescence light, three conditions must be supplied. First condition is that thermoluminescence material must be an insulator or semiconductor. The second one is that it should absorb some energy such as radiation. The third one is that material must be stimulated by heating process. One should differ thermoluminescence light from the light spontaneously emitted from a substance when it is heated to incandescence. At higher temperatures (especially above 200°C), a solid material give off infrared radiation and its magnitude increases with increases temperature. This kind of radiation is known as black body radiation and different from thermoluminescence light. The thermoluminescence light cannot be observed without storing some energy before stimulation. That is answer of why thermoluminescence substance does not give off thermoluminescence light again without reexposed to any radiation source.

The storage capacity of a thermoluminescence sample plays an important role in dosimetric applications. Thermoluminescence has been extensively applied in radiation dosimetry, archeological dating, geology and academic studies [1].

Annealing is one of the most wanted necessities for dosimeter applications. This process aims to remove all knowledges in thermoluminescence materials and obtain the best reproducibility. In addition to this, annealing operation brings enhancement or decline in the sensitivity of thermoluminescence glow peaks of many TL samples. Furthermore, new glow peaks can take place in the TL glow curve. The crystal structure may transform one from the other at different temperatures.

In this thesis, some thermoluminescence techniques, methods and instrumentations were used to find the effects of pre-irradiation annealing procedures on thermoluminescence dosimetric properties of different natural samples. The chosen natural minerals are calcite extracted from natural sand used in making roasted chickpea, fluorapatite mineral ($\text{Ca}_5\text{F}(\text{PO}_4)_3$) in tooth enamel, biogenic minerals present in the seashells and plagioclase minerals in basaltic rocks.

In the first study of the thesis, the effects of different thermal treatments on thermoluminescence (TL) properties of the calcite extracted from natural sand which is used in making roasted chickpeas were observed. This sand is extracted from a cave located in Ağın region of Elazığ, Turkey and is an important agent during making of Ağın leblebi. Ağın leblebi is one type of a roasted chickpea and a famous snack in the east of Turkey. It differs from other roasted chickpeas by flavor due to use of special sand. The results of this study were published in Journal of Luminescence with doi number; <http://dx.doi.org/10.1016/j.jlumin.2014.03.061>.

In the second study, the handling of fluorapatite mineral ($\text{Ca}_5\text{F}(\text{PO}_4)_3$) in tooth enamel under the different thermal conditions were investigated. Fluorapatite $\text{Ca}_5\text{F}(\text{PO}_4)_3$ is a kind of important thermoluminescence dosimeter (TLD) substance, because the effective atomic number of fluorapatite is close to that human bones and teeth. The tooth enamel samples used in this study were taken from a dentist who is Özlem Özbiçki Akbaba. She helped us about separating enamel from dentine. The results of this study were published in Thermochemica Acta with doi number; <http://dx.doi.org/10.1016/j.tca.2014.12.009>.

In the third study, the effects of thermal treatments on the thermoluminescence properties of biogenic minerals present in the seashells collected from the shores of the Mediterranean were investigated. Seashell is used in lime-stone to acquire, animal feed mixtures, road construction, some chemical treatments, and the manufacture of the prosthesis and implant dentistry. The results of this study were published in *Radiation Effects and Defects in Solids* with doi number; <http://dx.doi.org/10.1080/10420150.2016.1259623>

In the fourth study, the influences of the pre-irradiation thermal process on the thermoluminescence properties of the plagioclase minerals in basaltic rocks were investigated. The basaltic rock samples were collected in Karataş region of Gaziantep which located in southeastern region of Turkey. Basalt is well known as an extrusive igneous rock erupts on land by volcanic eruption. It is darker, denser and finer grained compared to the familiar granite of the continents. The results of this study were published in *Applied Radiation and Isotopes* with doi number; <http://dx.doi.org/10.1016/j.apradiso.2016.12.051>

The thesis consists of five main chapters. In the chapter 1, an overview of my thesis was given. In the chapter 2, a literature survey has been done. It summarizes the subject of luminescence and the thermoluminescence. Following subject sums up well-known types of the defects and color centers. These serve the types of defect centers can behave as traps and recombination centers. The description of the conventional models of TL goes on in this chapter. The most important kinetic models which are the Randall-Wilkins, the Garlick-Gibson, the May-Partridge and the advanced kinetics are summarized. The chapter then takes up the cycle of measurement (reproducibility) and annealing. The following subject explains natural minerals used in experiments.

Chapter 3 introduces the used equipments for experiments in the laboratory, the follow subjects presenting preparations of four different natural minerals for applied procedure in all experiments. The XRD analysis of the samples are were given in this chapter. Finally, all procedures for experiments were summarized.

Chapter 4 includes the experimental results under four cases for four natural minerals. In the first case, the effects of different grain sizes of the samples on the shape of thermoluminescence glow curve and the TL glow curve area were given, respectively. The second case includes the figures to see the effect of different annealing

temperature on the shape of thermoluminescence glow curve, the glow curve area, TL peak intensity, and peak temperature of the natural minerals. In the third case of chapter 4, we concluded that how the different annealing time affects the TL glow curve shape, area under the curve, thermoluminescence peak intensity, and peak temperature. In the last case of chapter 4, the reproducibilities of the samples at different annealing temperatures at fixed annealing times (30 min) before irradiated 36 Gy and standard deviations of each experiment were given in figures.

In the chapter 5, we concluded all results and gave all physics behind of them with using literature. And also, we tried to find a common relation between four natural minerals for four studies which were effects of grain size, different annealing temperatures, different annealing times and cycle of measurements (reproducibility) at different annealing temperatures.

CHAPTER 2

LITERATURE SURVEY

In this chapter of the thesis, a literature survey of the theory of luminescence, thermoluminescence, defects and color center, models in thermoluminescence, cycle of measurement (reproducibility), annealing processes and the samples used for the experiments are given below in details.

2.1 Luminescence

Luminescence is a light phenomenon which is observed when an irradiated insulator or wide band-gap semiconductor is stimulated by an excitation energy. This excitation energy classifies the luminescence. Some sorts of luminescence and their excitations are given in Table 2.1.

The description of wide band gap materials is based on a band model that concerns absorption and storage of ionizing radiation energy and release of the stored energy as the emission of photon by thermally or optically stimulation. In the band model, absorption of radiation energy means creation of electron-hole pairs. The property of storing energy is due to the presence of crystal defects such as vacancies and impurities. The defects are able to capture the electrons and holes generated in the irradiation process.

A crystal defect is classified as a trap center if the defect is able to capture a charge carrier and reemit it back to the band it comes from. A crystal defect where carriers of opposite sign can be captured, resulting in an electron-hole recombination, is classified as a recombination center. For the trap center, we assume that only transition between the center and the conduction band and valence band are possible. For recombination centers, we assume that only recombination of electron and hole is possible. Finally, an electron-hole pair is assumed initially to consist of an electron and a hole. Exchange of charge carriers between the crystal defects are assumed to take place through the conduction and valence band [2, 3]. Figure 2.1 shows the typical transitions used in simulations presented in the dissertation. During the ionizing irradiation of the crystal,

electron–hole pairs are generated by stimulation of electron from the valence band(V.B) to the conduction band(C.B). The excited electrons are freely moving in the crystal until they are captured by an electron trap center T_s and T_t , or by a recombination center R . A hole generated in the valence band is captured into either a hole trap center H or the recombination center R . Recombinations are assumed to be accompanied by emission of photons, i.e. luminescence. However, nonradiative recombinations are also possible.

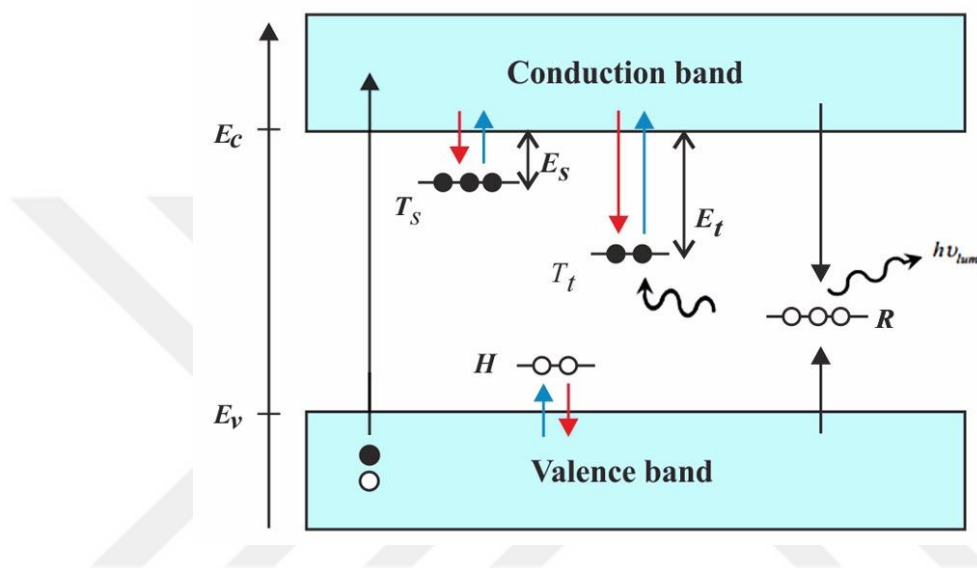


Figure 2.1 Basic concepts of irradiation, thermally and optically process between trap centers and recombination centers in a simple phenomenological band model. The transitions define whether a defect is a trap center **T** or a recombination center **R**. A recombination of an electron into a **R** center is assumed to be followed by photon emission [4].

By heating the crystal, captured electrons and holes may be freed by thermal energy into the conduction or valence band and make a transition to the radiative recombination center R . This process is termed thermoluminescence. Alternatively, external light exposure of the crystal can release captured electrons from a trap center to the conduction band from where they can recombine into the recombination center R . This phenomenon is termed optically stimulated luminescence (OSL).

The optically or thermally freed charge carriers in the conduction/valance band can be measured as electrical current when a voltage source is applied across the crystal.

These measurements are termed thermally and optically stimulated conductivity (TSC, OSC), respectively.

There are many luminescence phenomena seen naturally or synthetically in the world. The luminescence types can be named as their excitation mechanisms. The list of the luminescence phenomena and the methods of stimulation are given below table.

Table 2.1 List of the luminescence phenomena and the methods of excitation.

LUMINESCENCE PHENOMENA	METHODS OF EXCITATION
Bioluminescence	Biochemical reactions
Cathodoluminescence	Electron beam
Chemiluminescence	Chemical reactions
Electroluminescence	Electric field
Photoluminescence	U.V. and infrared light
Piezoluminescence	Pressure
Triboluminescence	Friction
Radioluminescence	Ionising radiation
Sonoluminescence	Sound waves
Fluorescence Phosphorescence Thermoluminescence Lyoluminescence	Ionizing radiation, U.V. and visible light

2.2 Thermoluminescence

Thermally stimulated luminescence or thermoluminescence (TL) is a kind of luminescence and has been used in the radiation dose measurement for seventy years[5]. This light phenomenon has also been used in archaeological dating for sixty years [6-8] and to geological dating for forty years [9]. Thermoluminescence is typically detected by heating a sample from room temperature to the finite temperature (e.g. 400°C) and recording its intensity as function of temperature. The thermoluminescence output is characterized by a computer to get a curve called TL glow curve. A glow curve includes distinct peaks occurring at different temperatures.

Each one relates to the electron traps existing in the material. The traps are the defects in the structure.

A kind of defect is a negative ion vacancy formed by the displacement of a negative ion and behaves as an electron trap. When an electron is trapped, it is possible that the trapped electron may escape from the trap by thermal energy causing lattice vibrations. The magnitude of these vibrations increase by increase temperature and the escaping chance of electron will be bigger. Some electrons recombine with trapped holes with radiative recombination and TL light is produced. A classic thermoluminescence glow curve obtained from sedimentary feldspar is given in Figure 2.2. As shown in figure each temperature peak corresponding to different electron trap depths.

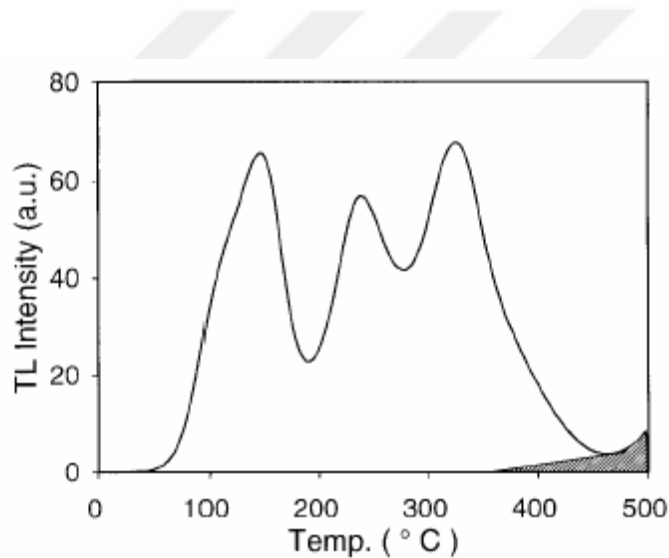


Figure 2.2 Typical thermoluminescence glow curve from a sedimentary K-feldspar substance exposed by a beta dose (8 Gy) plus the natural dose (~200 Gy). The peak located 150°C peak in this figure has been created by the recent beta dose. The shaded part is the black body radiation [4].

As seen in figure there are only three peaks, it does not mean the sample includes only three traps. Indeed, the glow curve may consist of a number of overlapping peaks from different traps. The shallow traps have smaller lifetime than deep traps. The traps whose peak temperature lower than 200°C are not useful for dosimetry. Because electrons can be exhausted from these traps at environmental temperatures. The traps usually found at 300°C or higher temperature give stable glow peaks suitable for dosimetry. But unexpected fading, known as anomalous fading, of high temperature

glow peaks at room temperature has been noted in some feldspars. This is explained as a quantum mechanical tunneling effect [10]. Another obstacle in thermoluminescence methods is thermal quenching. It means that higher temperatures cause the bigger probability of non-radiative recombination [11].

2.3 Defects and Color centers

Thermoluminescence depends on the band structure of solids and especially impurities known as centers inside it. The centers may arise as positive and negative ions move away from their original positions, therefore leaving vacancy states. These states can interact with free charge carriers (electrons and holes) and trap them. The other way is that ions can diffuse in interstitial sites and disturb the lattice order because of their sizes and valences. Additionally, these extrinsic defects can interact with the intrinsic ones, and ultimately both of them can gather in more multifaceted formations. The defects are characterized as locations positioned at different depths found in the forbidden gap.

Creation states inside the energy gap of the host material is essential because there are the defects and impurities within them and these states may be the type of electron and hole. And these states which are created have the ability for light absorption from some spectrum of the visible part. The crystal seems colorful and, thus, described these centers also as the color centers.

The presence of lattice defects (impurities, radiation damage centers, vacancies, interstitials...etc.) which disturb the translational symmetry of the crystal line structure results in localized energy states which might be found in the band gap.

The localized energy states, upon capturing free charge carriers may behave as traps or recombination centers shown in Figure 2.3. Traps and recombination centers can be differentiated by the probabilities of thermal release and recombination. At finite temperature, a carrier can escape from the trap by the probability:

$$p = s \exp\left(-\frac{\Delta E}{kT}\right) \quad (2.1)$$

In the formula, ΔE is the energy depth, or trap depth (i.e. energy difference between the center and the bottom of the conduction band (C.B) for the electron localized level, or the top of the valence band (V.B) for the hole localized level); k is Boltzmann's

constant, and s , frequency factor, is a constant. As seen in equation (2.1), the probability of releasing electron (or hole) is bigger for small trap depth. Therefore, the centers with small ΔE are more likely to behave as traps than recombination localized levels. Generally, the traps locate close to the conduction or valance bands although the recombination localized levels are found near the midmost of the bandgap. There is a reference delocalized level with an energy depth (D). At this delocalized level, both of trap process and recombination have same probabilities.

This kind of level is known as demarcation level and a boundary between the traps and the recombination localized level. It means that centers with $E < D$ behave as a trap, in other case they become recombination localized level given in Figure 2.3.

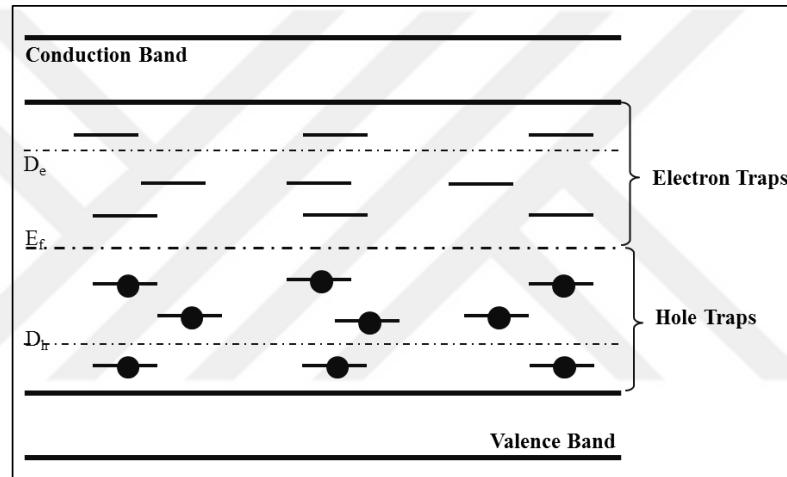


Figure.2.3 Energy levels in an insulator in equilibrium at absolute zero.

It should be mentioned that discrimination between traps and recombination centers is not solely depend on the trap depth (ΔE). The cross-section area of charge carrier has an important role in the probability of the recombination and depends upon the potential allocation in the zone of the defect. The probability of recombination is given;

$$A = v\sigma \quad (2.2)$$

Where \mathbf{v} is the carrier thermal velocity ($\propto T^{1/2}$) and σ is the capture cross-section.

2.4 Models in Thermoluminescence

The goal of a mathematical analysis about the TL light is to get knowledge of the kinetic parameters of the traps found in the TL sample. These kinetic parameters are, for each trap, the activation energy or trap depth (E), a frequency factor (s) and a kinetic order (b) manufacturing the superiority of the involved phenomena. The kinetic order varies from 1 to 2.

2.4.1 Randall-Wilkins Model (First Order Kinetics)

In 1945, the first treatment was proposed by Randall and Wilkins [12] who broadly used a mathematical depiction for each peak in a glow curve on phosphorescence. Their mathematical studies were constructed on the energy band model and results were summarized as the first order expression. In the figure 2.4, the basic model in thermoluminescence is given.

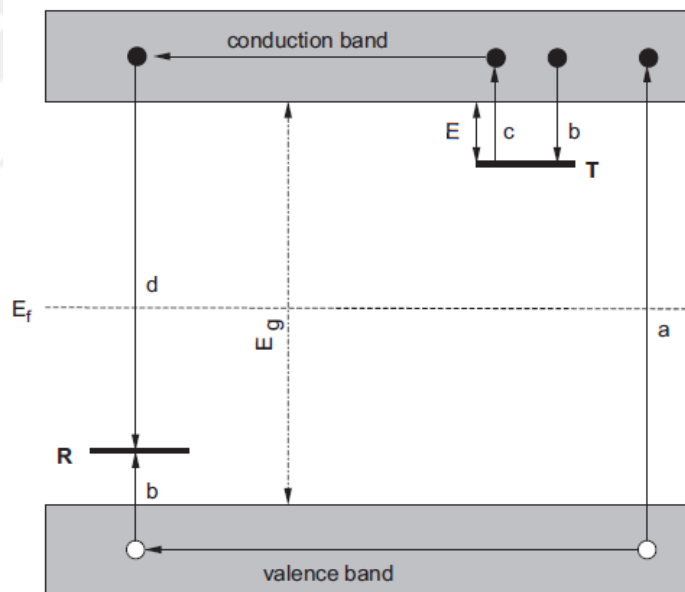


Figure 2.4 Energy band model showing the electronic transitions in a thermoluminescence material according to a simple two-level model (a) generation of electrons and holes; (b) electron and hole trapping; (c) electron release due to thermal stimulation; (d) recombination. (●) shows electrons, (○) shows holes. Level T is an electron trap, level R is a recombination center, E_f is Fermi level [1].

In the simple model, two centers which are a trap (T) and a recombination center (R) are found between conduction band (CB), and valence band (VB). The gap between the trap T and the edge of the CB is called activation energy (E_a) or trap depth E . This energy is the minimum necessary energy to escape a charge trapped in T . The term “ p ” gives the probability per unit of time of escaping of electron in a trap. It is given by the Arrhenius equation;

$$p = s \exp\left(-\frac{E}{kT}\right) \quad (2.1)$$

where E is the trap depth (eV), k is the Boltzmann’s constant, T is the temperature (K), s is the frequency factor (s^{-1}), depending on the frequency of the number of hits of an electron in the trap, seen as a potential well. The life time, τ , of the charge carrier in the localized level at temperature T , given by

$$\tau = p^{-1} \quad (2.3)$$

If n is the number of electrons in T , and for constant temperature n reduces with time t according to the given equation:

$$\frac{dn}{dt} = -np \quad (2.4)$$

Integrating this equation

$$\int_{n_0}^n \frac{dn}{n} = - \int_{t_0}^t p \cdot dt \quad (2.5)$$

$$n = n_0 \exp\left[-s \exp\left(-\frac{E}{kT}\right) t\right] \quad (2.6)$$

where n_0 is the initial number of electrons in trap at $t_0 = 0$.

Assume:

- electrons cannot escape from trap at low temperature,
- the electrons in the C.B has small life time,
- the escaped charges from trap will completely recombine in recombination site,
- the temperature should not affect the luminescence efficiency of the recombination sites, the concentrations of traps and recombination sites
- the retrapping probability is zero

As said by the above assumptions, the intensity, $I(t)$, of thermoluminescence in photons/second at any time t depends on the proportion of recombination of holes and electrons at R . If m (m^{-3}) is the number of holes at recombination center, the thermoluminescence intensity becomes;

$$I(t) = -\frac{dm}{dt} \quad (2.7)$$

Here it is assumed that a photon is generated at the end of each recombination and that all generated photons are counted. The number of free electrons in the conduction band n_c and the number of holes m affect the rate of recombination;

$$I(t) = -\frac{dm}{dt} = n_c m A \quad (2.7a)$$

with the constant A , the temperature does not affect the recombination probability.

The rate of change of the number of electrons n in the trap is given by;

$$-\frac{dn}{dt} = n p - n_c(N - n)A_r \quad (2.7b)$$

The first term of right side of the equation is the rate of thermal release and second term is of retrapping. In the equation, N is the number of electron traps and A_r is the probability of retrapping (m^3/s). Similarly, the rate change of the number of electrons in C.B given as;

$$\frac{dn_c}{dt} = n p - n_c(N - n)A_r - n_c m A \quad (2.7c)$$

The third term in the right side of the equation is the rate of recombination. Eqns. (2.7a) – (2.7c) give the traffic of charge carrier for the release of an electron from a single-electron trap and recombination in a single center. Eqns. (2.7a) – (2.7c) can be written for the generated thermoluminescence by the release of holes. these equations do not give overall analytical solution. Therefore, some assumptions must be made. One of the assumptions is the quasi-equilibrium assumption called by Chen and McKeever [13]

$$\left| \frac{dn_c}{dt} \right| \ll \left| \frac{dn}{dt} \right|, \quad \left| \frac{dn_c}{dt} \right| \ll \left| \frac{dm}{dt} \right| \quad (2.8)$$

In this assumption, the number of electrons in the conduction band is considered as quasi-stationary. The electrons and holes in traps are generated in pairs during the ionization (absorbing radiation energy). Charge neutrality is written as;

$$n_c + n = m \quad (2.9)$$

where n_c is almost zero at any time that means that $n \approx m$ and

$$I(t) = -\frac{dm}{dt} \approx -\frac{dn}{dt} \quad (2.10)$$

As $dn_c/dt \approx 0$ the below formula is derived from Eqns (2.7a) and (2.7b):

$$I(t) = \frac{m A n s \exp\left(-\frac{E}{kT}\right)}{(N - n)A_r + m A} \quad (2.11)$$

But Eqn. (2.11) needs extra assumptions to be solved analytically. Randall and Wilkins [12, 13] omitted retrapping during the stimulating part. They assumed $m A \gg (N - n)A_r$. After this assumption, Eqn. (2.11) becomes;

$$I(t) = -\frac{dn}{dt} = n p = s n \exp\left(-\frac{E}{kT}\right) \quad (2.12)$$

Eqn. (2.12) represents an exponential decay of phosphorescence. Using Eqn. (2.5) in Eqn. (2.12) one obtains:

$$I(t) = n_0 s \exp\left(-\frac{E}{kT}\right) \exp\left[-s t \exp\left(-\frac{E}{kT}\right)\right] \quad (2.13)$$

Usually the TL material is heated with a linear function of time by

$$T(t) = T_0 + \beta t \quad (2.14)$$

with the constant heating rate (β) and the temperature (T_0) at $t = 0$. With using Eqn. (2.14), heating rate can be written as $\beta = dT/dt$ and introducing it into Eqn. (2.4)

$$\int_{n_0}^n \frac{dn}{n} = -\left(\frac{s}{\beta}\right) \int_{T_0}^T \exp\left(-\frac{E}{kT'}\right) dT' \quad (2.15)$$

And the number of trapped electrons (n) in term of β

$$n = n_0 \exp\left[-\left(\frac{s}{\beta}\right) \int_{T_0}^T \exp\left(-\frac{E}{kT'}\right) dT'\right] \quad (2.16)$$

Then, using Eqn. (2.12) becomes

$$I(T) = -\frac{1}{\beta} \frac{dn}{dt} = n_0 \frac{s}{\beta} \exp\left(-\frac{E}{kT}\right) \exp\left(-\left(\frac{s}{\beta}\right) \int_{T_0}^T \exp\left(-\frac{E}{kT'}\right) dT'\right) \quad (2.17)$$

Eqn. (2.17) is assessed by mean of numerical integration, and it results a bell-shaped curve, as in Figure 2.5. the bell-shaped curve is characterized by peak intensity at a maximum temperature T_m .

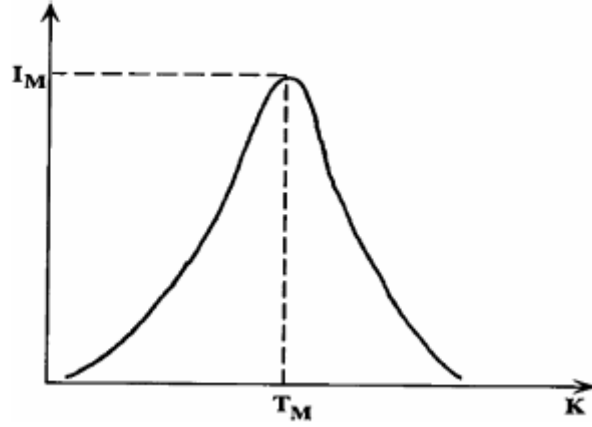


Figure 2.5 A bell shaped glow curve as a result of Randall-Wilkins model.

2.4.2 Garlick-Gibson Model (Second Order Kinetics)

In the mid of 20th century, Garlick and Gibson [14], carried out phosphorescence, considered that an electron (or hole) has probability of either being trapped or recombining within a recombination center. The term second order kinetics is used to describe a case that includes retrapping part. They assumed that the released electron from the trap has equal probability of either being retrapped or of recombining with hole in a recombination center. They considered the possibility that retrapping is bigger, i.e. $mA \ll (N - n)A_r$. They also assume that the trap is far from saturation ($\gg n$ and $n = m$) and Eqn. (2.11) becomes

$$I(t) = -\frac{dn}{dt} = s \frac{A}{NA_r} n^2 \exp\left(-\frac{E}{kT}\right) \quad (2.18)$$

It is seen that TL intensity ($-dn/dt$) is proportional to n^2 which represents second-order. If equal probabilities of recombination and retrapping are present, $A = A_r$, and one can get the Garlick-Gibson thermoluminescence expression for second-order kinetics from Eqn. (2.18)

$$I(t) = \frac{n_0^2 s}{N \beta} \exp\left(-\frac{E}{kT}\right) \left[1 + \frac{n_0 s}{N \beta} \int_{T_0}^T \exp\left(-\frac{E}{kT'}\right) dT' \right]^{-2} \quad (2.19)$$

The Garlick–Gibson thermoluminescence expression produces a nearly symmetric. In this curve, the half of the curve which lies on the high temperature part is marginally broader than the other half of the curve which lies on the low temperature part. In a second-order reaction significant concentrations of released electrons are retrapped before they recombine. That cause a delay in the luminescence light and it is seen in a broad temperature region.

2.4.3 May-Partridge Model (General Order Kinetics)

The derivation of first and second order TL equations are obtained by making some assumptions mentioned before. But sometimes these assumptions cannot be done and TL peak does not fit both first and second order kinetics. May and Partridge [15] developed an empirical expression for general order thermoluminescence kinetics:

$$I(t) = -\frac{dn}{dt} = n^b s' \exp\left(-\frac{E}{kT}\right) \quad (2.20)$$

Where s' is $m^{3(b-1)} s^{-1}$ and b is the general order parameter varies between 1 or 2. Eqn. (2.20) for $b \neq 1$ gives

$$I(t) = \frac{s''}{\beta} n_0 \exp\left(-\frac{E}{kT}\right) \left[1 + (b-1) \frac{s''}{\beta} \int_{T_0}^T \exp\left(-\frac{E}{kT'}\right) dT' \right]^{-b/(b-1)} \quad (2.21)$$

where $s'' = s' n_0^{b-1}$ with unit s^{-1} . Eqn. (2.21) has the second order situation ($b = 2$) and drops to Eqn. (2.17) when $b \rightarrow 1$. The general order situation is valuable because it can be dealt with medium situations and it slickly goes to first and second orders when $b \rightarrow 1$ and $b \rightarrow 2$, respectively as shown Figure 2.6.

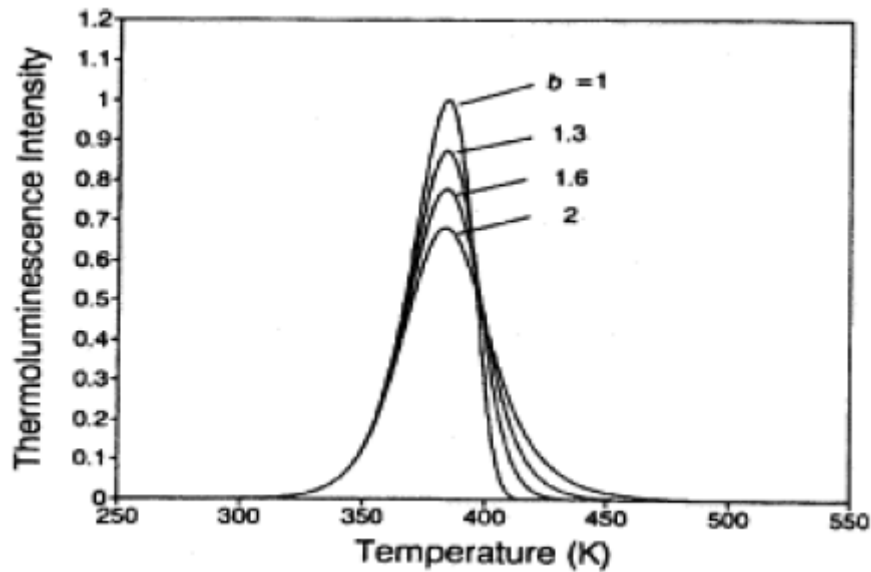


Figure 2.6 Comparison of first order ($b = 1$), second order ($b = 2$) and intermediate order ($b = 1.3$ and 1.6) thermoluminescence peaks, with $E = 1\text{eV}$, $s = 1 \times 10^{12} \text{ s}^{-1}$, $n_0 = N = 1 \text{ m}^{-3}$, and $\beta = 1 \text{ K/s}$ [16].

2.4.4 Advanced Models

Although the simple model gives all the characteristics of the thermoluminescence glow curve and can help us in the interpretation of many features which can be considered as variations of the one trap–one center model, thermoluminescence material can not exactly be explained by the simple model. All the advanced (more realistic) models in detail is referred to the text book of Chen and McKeever [13].

Generally, a real thermoluminescence material has more than one single electron trap. In TL process, when sample is heated, it does not mean all traps will be affected. A thermally disconnected trap is located in the deep positions and its trap depth is bigger than active traps though it can be filled with carriers during absorbing energy. When the TL material is stimulated thermally, only carriers trapped in the active trap (AT) and the shallow trap (ST) shown in Figure 2.7(a) are escaped. Carriers in the deeper traps are not affected and therefore this is called as deep electron (or hole) trap (DET) shown in Figure 2.7(a). The deep trap is said to be thermally disconnected [17].

It was assumed that the electrons in traps are freed during heating whilst the holes are stable in the recombination center. On the contrary, the holes are freed and recombine

at a localized level where the electrons are steady during heating is mathematically identical. But, the case will change if both electrons and holes are released from their traps at the same time at the same temperature region and the holes are being thermally released from the same centers are acting as recombination sites for the thermally released electrons and vice versa as seen Figure 2.7b.

Another possible process seen in Figure.2.7(c) is the center to center transition. In this transition, electron in a center recombines with hole in another center without going to the conduction band. The transition probability may intensely depend on the distance between the two centers.

The last transition is shown in Figure 2.7(d) and mentions the possibility that the defect which has trapped the electron is not stable and interact with an adjacent defect.

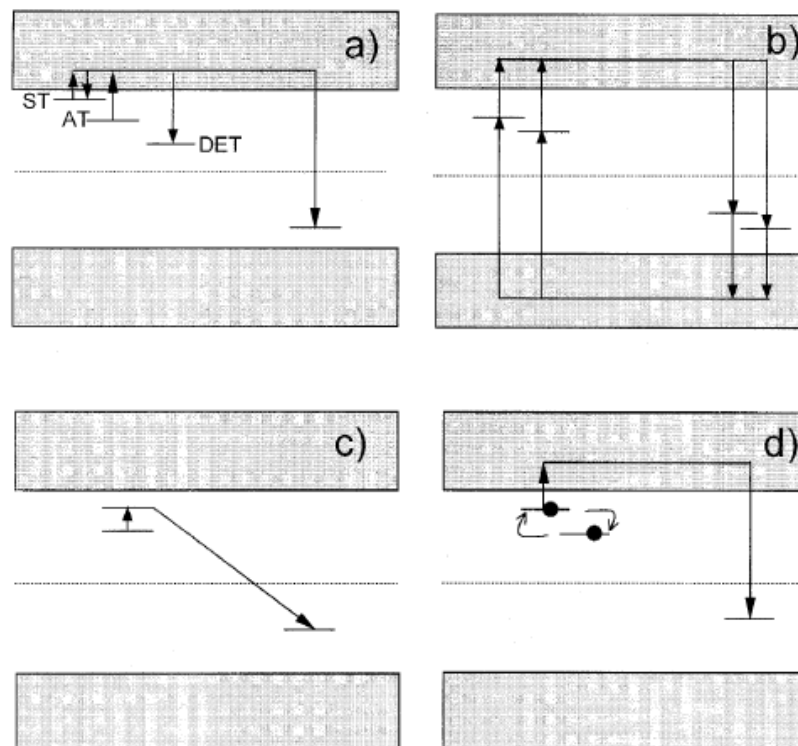


Figure 2.7 Advanced models describing the thermally stimulated release of trapped charged carriers including: (a) a shallow trap (ST), a deep electron trap (DET), and a active trap (AT); (b) two active traps and two recombination centers; (c) localized transitions; (d) defect interaction (trapping center interacts with another defect).

At low temperature, the position of trap varies though the electron concentration in the trap is stable. At higher temperatures, transition electron to the C.B and defect interactions may be observed. Piters and Boss [18] used defect interactions incorporated into the rate expressions and glow curves simulated. In their studies, the computer-generated glow curves can be exactly fitted by Eqn. (2.17).

2.5 Cycle of Measurements (Reproducibility)

One of the most necessity in dosimetry is reproducibility which also called as cycle of measurement. This needs to get same results after each repeat of experiment. It is known that the intensity and glow curve may change with the repeat of experiment. This may be due to the alteration or unclearing of traps in the sample at the end of each repeat. Such an alteration may be harmful to the simple evaluation of the measured effect; but, a variation of sensitivity in detail may enhance knowledge about the studied substance. During dose measurement by a dosimeter, variation of TL intensity may hamper the correct results [19]. A standard deviation of $\pm 2\%$ or less is the index for a good reproducibility [20].

2.6 Annealing

Annealing is a kind of thermal process that generally used to delete all information from irradiated dosimetric sample. In dosimetric applications, there may be some enduring charge carriers in the traps of the dosimetric material after each TL reading. Therefore, these cause an undesired signal which increases the background noise. This problem can be eliminated by the annealing of the sample at higher temperature. In contrast, annealing of the sample at lower temperature may make stable and gather low temperature traps to improve the sensitivity of the major dosimetric traps and to diminish dissipations of signal caused by radiation. This reason can arise because of fading thermally or optically through usage. The usage of these two annealing at the same time is known as standard annealing process [21].

In the dosimetric applications, the preparation of TL material is important to get good and healthful results. Firstly, the previous dose must be deleted. That means some information may stay in traps after reading of TL material. And the preparation is done for getting stable the trap structure.

These preparations can be done by using thermal process, generally named as annealing [22, 23]. The annealing is done for three aims during usage of new thermoluminescence material. Firstly, it is to remove any residual signals from previous irradiation. Secondly, it is to reset the sensitivity to a known value. Thirdly, it is to reduce fading of the stored signal after irradiation (i.e. post irradiation anneal). There are two basic ways of annealing. One of them, reader anneals usually for low dose measurements, e.g. less than a few cGy and another, external anneal for high doses or long intervals before irradiation and readout. Different annealing temperatures and times for a TL material may change the TL properties of the material. For this reason, they change the shape of the glow curve during readout after irradiation.

The cooling rate immediately after annealing may also affect the response (light output) of TL materials. Some TL materials e.g. LiF:Mg,Ti are very much affected by the annealing and cooling rate while others may not be affected at all. Hence, for TL substances such as LiF:Mg,Ti a fixed thermal treatment and cooling regime should be applied in order to achieve consistent and accurate results.

The annealing for the thermoluminescence dosimeter is considered in three parts;

Initialization Treatments: This process is used for unused TL materials or for a prolonged unused dosimeter. In this thermal process, the stabilization of trap positions can be provided. With this initialization, the producibility of the sample is achieved.

Erasing process (Standard Annealing) (Pre-irradiation Annealing or Post-readout Annealing): This process is also known as pre-irradiation annealing and deletes prior rest irradiation effect. It is done before usage of the TL dosimeter. The usual goal of this treatment is to reset the localized level form. It may include one or more thermal treatments.

Post-irradiation (Pre-readout Annealing): This thermal process is used to remove the peaks at lower temperature region. Low temperature peaks are generally faded and not useful for the dosimetric applications.

In all conditions, the cooling rate after the annealing has an important role in the performance of a thermoluminescence dosimeter system. Typically, the usage of rapid cooling increases the thermoluminescence dosimeter sensitivity. The biggest

sensitivity is observed at a cooling rate of 50-100 °C/s. In the cooling process, the sample is putted on a cooler metal after completing annealing process.

Most thermoluminescence materials which used in personal dosimeter branch are covered by plastics. Due to this reason, the plastics which store thermoluminescence materials do not have ability to eliminate high temperatures. Sometimes the annealing process is done in thermoluminescence reader, termed as in-reader annealing, instead of any oven or furnace. But, the efficiency is not good when higher dose values are subjected to dosimeter. The in-reader thermal process should be used only if the absorbed dose is smaller than 10 to 20 mGy. In the study of Driscoll [22], annealing was performed in oven during 20 hours at 80 °C for cards including LiF:Mg,Ti. At this temperature, the plastic coverage does not suffer any deformation. Therefore, the annealing must be done in a furnace for naked TL solid samples or TL materials in powder cases excluding cards.

2.7 Natural Minerals Used in Experiments

Four natural minerals were used for the experiments in this dissertation. These natural minerals are:

- **Calcite Extracted from Natural Sand Used in Making Roasted Chickpea:** This sand samples were extracted from a cave located in Ağın region of Elazığ.
- **Fluorapatite Mineral ($\text{Ca}_5\text{F}(\text{P}_4\text{O}_{13})_3$) in Tooth Enamel:** The tooth enamel samples were taken from a dentist who separated enamel from dentine.
- **Biogenic Minerals Present in the Seashells:** The seashell samples which were collected from the shores of the Mediterranean
- **Plagioclase Minerals in Basaltic Rocks:** Basaltic rock samples were collected in Karataş region of Gaziantep which located in southeastern region of Turkey

2.7.1 Calcite Extracted from Natural Sand Used in Making Roasted Chickpea (Leblebi)

Leblebi, a Turkish word, is a kind of a snack made from roasted chickpeas, very common and popular in Turkey. Ağın Leblebi is one type of a roasted chickpea and a famous snack in the east of Turkey. It differs from other roasted chickpeas by flavor due to use of special sand. This sand is extracted from a cave located in Ağın region of Elazığ, Turkey and is an important agent during making of Ağın leblebi. Sand is a

natural material and its chemical composition depends on the local region where the sand is extracted. The melting point of sand, which consists mainly of silicon dioxide or silica, is approximately 1610 °C. It may be a candidate of a dosimeter during nuclear emergencies. The personal radiation dose measurement is another application of sand while handling highly radioactive material [1, 24, 25]. Silica (SiO₂) in the form of quartz and feldspar is a well-known major ingredient of the sand. Some researchers and scientists [6-8, 24, 25] were interested in the thermoluminescence properties of quartz and feldspar extracted from sand as a high dose dosimetry. And also, some researchers in Brazil have studied dosimetric properties of commercial glasses made of sand for high doses using different techniques [9, 26, 27].

Another major mineral of sand is calcite. Calcite crystal is a major ingredient of limestone, speleothem, coral, etc. and normally integrate various impurities (magnesium, copper, cobalt, iron, etc.) during crystal formation [28]. Natural calcite is generally used in the industry. It is a main material for production of cement and white washing powder. Another usage areas of natural calcite are wall painting and measuring of industrial pollution level [2].

In some studies [3, 4, 10-12], thermoluminescence properties of calcite have been investigated in geological dating, dosimetric applications and in the measuring of γ -doses used for food preservation. Soliman et al. [13] studied TL properties of the green radiation of calcite and concluded that it has worthy TL response in the dose region of 0.01-10⁴ Gy. Effects of annealing on natural calcite crystals were investigated by Ponnusamy et al [2, 28]. They concluded that thermal treatment does not alter the localized levels but TL intensities of low temperature peaks were affected by increase annealing temperature up to 600 °C.

2.7.2 Fluorapatite Mineral (Ca₅F(PO₄)₃) In Tooth Enamel

Tooth enamel is the hardest part of tooth and protects the dentine. In terms of its weight, it consists of 95% inorganic minerals, 1% organic minerals, and 3% water [29-31] It is complicated biomaterial, a compound of elongated mineral crystallites in the form of biological apatite bonded by polymeric proteins and peptide chains saturated with water [32]. It has an ordered structure with crystals of hexagonal cross-section firmly packed into rods (prisms) (width ~5 μ m) [33] and surrounded by polymeric sheaths (width 0.1 mm) [32]. In 1964 about twenty inorganic elements except oxygen,

hydrogen and carbon were found in tooth enamel. Hydroxyapatite [$\text{Ca}_{10}(\text{PO}_4)_6(\text{OH})_2$] and fluorapatite [$\text{Ca}_5\text{F}(\text{PO}_4)_3$] are two major inorganic apatite minerals in tooth enamel. Apatite is a kind of compounds identified by an alike structure, albeit with unlike configurations. When fluor (F) ions substitute with OH in hydroxyapatite ($\text{Ca}_{10}(\text{PO}_4)_6(\text{OH})_2$), fluorapatite minerals ($\text{Ca}_5\text{F}(\text{PO}_4)_3$) are formed [29-31, 34]. The melting point of fluorapatite minerals in tooth enamel, is approximately 1200 °C. Most of the present information related the enamel apatite were obtained from performing of associated synthetic or natural compounds. Biological apatite contains some ions such as CO_3^{2-} , PO_4^{3-} , OH^- and Ca^{2+} and different forms of apatite may form with substituting of present ions [35] P, CO_3 , Mg, Cl, and K are the major and Fe, Zn, Sr, F, Ca and Na are the minor constituents in tooth enamel [36]. For all that, Zn, Sr, Si, F, S, Al and Fe are the trace elements in tooth enamel. Minor ingredients and trace elements are found in tooth enamel during mineralization. Trace elements and minor ingredients can affect the stability of apatite [37].

A few researches [38-45] have investigated the thermoluminescence properties of synthetic and biological apatites. In the study of Secu et al. [39], they pointed out the tooth enamel exhibits a wide glow curve from 100 °C to 450 °C and thermoluminescence intensity in the 250 °C-450 °C temperature region raises with irradiation dose. They supposed that the impurities such as Mn^{+2} and trivalent rare earth impurities are responsible from the thermoluminescence peaks lower than 300°C. The occurrence of a few paramagnetic types such as CO_2^- , CO_3^- and CO^- revealed by EPR spectra of biological and synthetic apatite may cause higher TL peaks especially in the range of 300 °C and 400 °. Also, they concluded the complicated structure of the thermoluminescence glow curve in tooth enamel had been ascribed to the recombination of radiation induced CO_2^- radicals produced from surface CO_2 and or bulk CO_3 impurities. The radiation induced signal in tooth enamel may consist of several CO_2^- species located in different sites [44] Fukuda [46] investigated some thermoluminescence properties of synthetic fluorapatite since the effective atomic number of synthetic fluorapatite is about 14 [47] and nearly same with human bones and tooth. A thermoluminescence glow curve with two main peaks centered at 100 °C and 235 °C was obtained.

Tooth enamel has been used as a detector for in vivo dosimetry for more than three decades [48]. The accumulated dose in tooth enamel was investigated by some

researchers [10, 21-26] using electro paramagnetic resonance (EPR) technique based on the measurement of stable radiation induced radicals [38]. On the other hand, thermoluminescence retrospective dosimeter using tooth enamel is an alternative to EPR retrospective dosimetry since it needs significantly small quantity of material (only few mg) that may be safely taken by dentist without tooth removal [39]. A few researchers [38, 40-44] have investigated the thermoluminescence properties of two major inorganic minerals which are hydroxyl-apatite and fluorapatite. Alvarez et al. [49] carried out the thermoluminescent characteristics of synthetic hydroxyapatite which is one of the most important ingredient in tooth enamel. Two main peaks centered around 200 °C and 300 °C are seen and good TL properties such as wide linearity range and good reproducibility is observed.

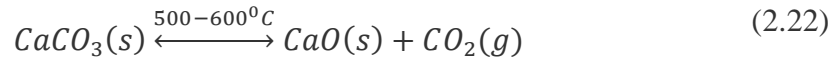
2.7.3 Biogenic Minerals Present in the Seashells

Shell, soft-bodied marine with the creatures of the molluscs that surrounds their bodies protective hard a layered outer shell. Usually the offspring of molluscs hatch as thin-shelled. Material for formation of the shell of mollusc is secreted from its body. When the secreted material is increased, the shell grows. The calcium is the main material used in the formation of the shell. There are plenty of calcium in the blood of molluscs. The bottom of the crust and the soft tissue that surrounds the internal organs is called the mantle. Calcium is comprised from its blood. Calcium carbonate crystals form secreted from certain points of the mantle. The shell stores calcium carbonate in this crystal layers of various thicknesses. Thus, the size and the thickness of it increase with accumulation of calcium carbonate in the mantle.

Shell of mollusc consists three different layers. The outermost layer is a thin layer that does not contain calcium. Below this one contains the calcium carbonate crystals. In the interior parts of some shells, they include nacre which is the raw material of pearl. The 95% of the shell's structure is composed of calcium carbonate crystals and 5% of it takes place about 30 different proteins. These proteins keep together the calcium carbonate crystals. Seashell is used in the acquiring of lime-stone, animal feed mixtures, materials of road construction, some chemical treatments, and the manufacturing of the prosthesis and implant dentistry.

The most important mineral of the seashell is calcium carbonate (CaCO_3) seen as aragonite in its nature form. Another important mineral in the seashell is calcium oxide

(CaO). It is a white crystalline solid with a melting point of 2572 °C. It is produced by heating limestone, coral, sea shells, or chalk, which are mainly calcium carbonate to drive off CaO.



This reaction is revocable; CaO reacts with CO₂ (carbon dioxide) to form calcium carbonate. The reaction is driven to the right by flushing CO₂ from the mixture.

Calcium oxide is generally found in limestone which is one of the most sophisticated chemicals in the world with a wide range of industrial, environmental and chemical uses. In addition, calcium oxide plays an important role in the manufacturing of hydrated lime [Ca(OH)₂] [50].

Some researchers have studied radiation effects, luminescence and EPR properties of minerals found in the seashells. Johnson and Blanchard [51] have studied radiation dosimetry from natural thermoluminescence of fossil shells and evaluated the problems peculiar to natural thermoluminescence dosimetry such as post-irradiation calibration techniques, dose equivalency factors, and secular equilibrium effects. They have suggested solutions by a study of naturally thermoluminescent mollusc shells. Köseoğlu et al. [52] have investigated gamma-irradiated marine mollusc by EPR at any temperature. Aydaş et al [53] studied aragonitic marine fossil shell samples from northwestern part of Turkey for the purpose of ESR dating. The studies of luminescence and EPR properties of calcium carbonate (CaCO₃) and calcium oxide (CaO) which are profoundly found in the seashell have been done [54-59].

2.7.4 Plagioclase Minerals in Basaltic Rocks

Basalt is the rock that is the most founded in the crust of the Earth. It is a dense-looking, black, frequently weathering to a brown, and is the commonest of all lavas. It is estimated that the basalt flows of the world have five times the volume of all other extrusive rocks together [60]. Nearly all oceanic crust is made of basalt and is a usual extrusion from many volcanic areas in the world. It is shaped as the volcanic magma erupts onto the surface or even in the water and experiences a fast cooling process. Its appearance varies from grey to black. In the rapid cooling, the minerals

almost invisible, making it a fine-grained substance were created. Basalt can be present in the Moon, Venus, Mars and several asteroids, as well. The ocean ground is largely formed by basaltic rock. In addition, basalt comes from wide lava flows. Basalt lava can easily flow and quickly across huge distances delivering great volumes of basalt rock. Some of these extrusions covered great areas of the Earth.

Basalt has no harmful properties, non-explosive and noncombustible. The melting point of basaltic rock, is approximately 1460-1500 °C. It is used for a lot of purposes such as road base, concrete aggregate, asphalt pavement aggregate, railroad ballast, filter stone in drain fields and other purposes. Essential minerals in the basalt are plagioclase and augite. The basalt samples used in the study of Canakci et al. [61] involving of a ~50% to ~60% plagioclase, ~25% to ~30% olivin and ~2% to ~25% calcite. The region of basalt samples used in our study is same with Canakci et al [61]. In figure 2.8, photomicrograph of the tested vesicular basalt showing a mixture of plagioclase, pyroxene and vesicles [61]. Plagioclase is the name of the collection feldspar minerals from albite (sodium aluminum silicate) to anorthite (calcium aluminum silicate). The normal feldspar of basalts is labradorite, but andesine, oliogclase, or albite may occur in different varieties. Several studies [61-67] about engineering applications of basalt have been done except for luminescence studies [68-73].

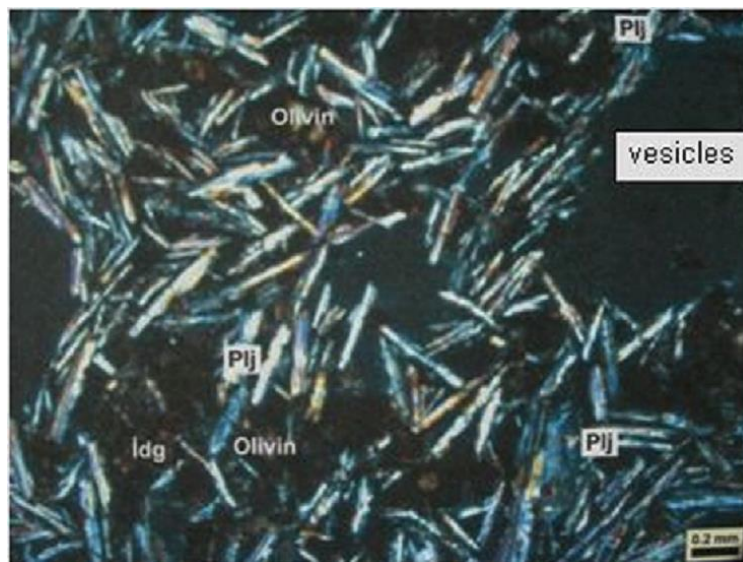


Figure 2.8 Photomicrograph of the tested vesicular basalt showing a mixture of plagioclase, pyroxene and vesicles [61].

Correcher et al. [73] used basaltic samples of a lava flow from Poas volcano (Costa Rica) in their study to obtain the trap parameters of both natural and induced thermoluminescence curves of a basaltic rock (polymineral phase) because of uniform distribution of traps.

Morthekai et al. [68] have been studied that the anomalous fading phenomena in basalt and andesite rock substances. They concluded that OSL signals exhibit fast fading (between ~4% and ~27% per decade). According to their results, small fading rates were observed for high temperature peaks.

Another study concerned of basaltic sample has been done by Tsukamoto et al. [70]. Their study was about the fading rates (g-values) of luminescence signals using four different specimens of basaltic rock. It was obtained that the fading rate was bigger in the specimens containing olivine, pyroxene and plagioclase phenocrysts and small value in glassy specimens. Fading rates of plagioclases and alkali feldspars was studied by Huntley et al. [71] and concluded that the fading rate is proportional with calcium(Ca) content for plagioclase feldspars. Besides, Akber and Prescott [74] detailed the plagioclases with bigger-Ca content usually exhibits anomalous fading. A study about cathodoluminescence of plagioclase was done by Kayama et al. [72] to see effects of He⁺ ion insertion and electron irradiation. In their results, electron irradiation triggers Na⁺ relocation in plagioclase, and then a substantial diminution in luminescence signal allocated to impurities, which are responsible for a variation in the energy state or a reduction in luminescence efficiency following the variation of trap depth.

Large volume of basalt deposits dominantly exists in few areas of the Gaziantep, especially Karataş region seen in figure 2.9.



Figure 2.9 The original basaltic rocks in the Karataş region of Gaziantep, Turkey.

Geological map of the Gaziantep and its near vicinity is shown in Fig. 2.10. The map was arranged by General Directorate of Mineral Research and Exploration (MTA), Turkey.

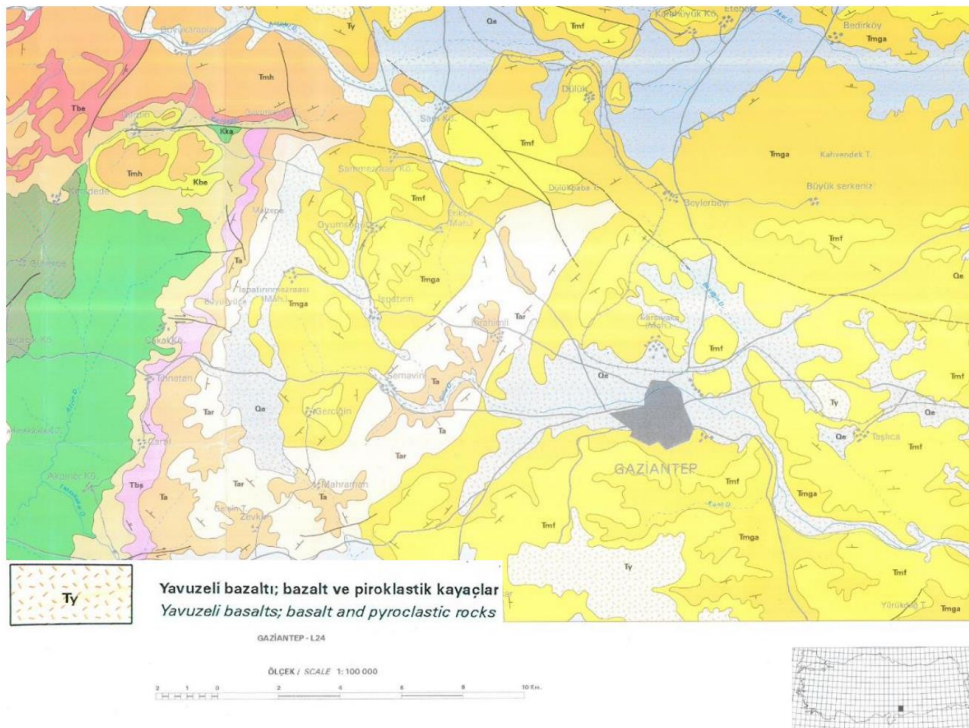


Figure 2.10 Geological map of Gaziantep city and near its vicinity (MTA 1994) [61].

The basalt used in this study was generally formed by flow of lava. There are different ideas about the formation of this lava. Some groups explain this lava flow with the East Anatolian Fault and other faults related to main fault. Others explain it with the tectonic movements activated during Middle Miocene [75]. Basalt extracted from the region is called as Yavuzeli basalt by Yoldemir [76].



CHAPTER 3

EXPERIMENTAL EQUIPMENT AND PROCEDURES

3.1 Equipment in the Laboratory

The thermoluminescence laboratory has three main rooms. There is a furnace in the first room. In the second room, there are sieves, a digital balance and, etc. They were used to prepare the samples to the experimental applications. The irradiation and reading process were applied in the third room where called as darkroom. Radiation source and TL reader are present in this room.



Figure 3.1 Thermoluminescence Laboratory

The equipment, materials and experimental procedures utilized in this study are described below in details.

3.1.1 Radiation Source and Irradiator

The samples were irradiated at room temperature with a point beta source (^{90}Sr - ^{90}Y), given in figure 3.2, which delivers 0.040 Gy/s before reading process. The beta source installed in a 9010-optical dating system which is interfaced to a PC using a serial RS-232 port the control irradiation time and its activity is about 3.7 GBq (100 mCi). It was calibrated by manufacturer on March, 10, 1994. Strontium-90 emits high energy beta particles from their daughter products (^{90}S β -0.546 MeV together with ^{90}Y β -2.27 MeV). Beta radiation is absorbed by air, so its intensity declines with distance much more rapidly than inverse square law calculations would indicate. The irradiation equipment shown in figure 3.3 is an additional part of the 9010 Optical Dating System which is purchased from Little More Scientific Engineering, UK.

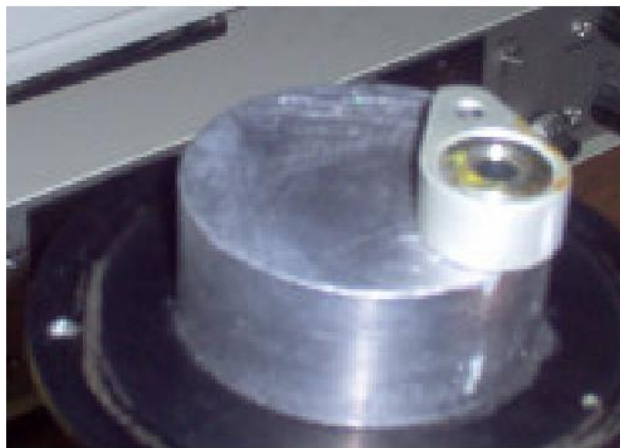


Figure 3.2 ^{90}Sr - ^{90}Y β -source

Feature of the 9010 Optical Dating System:

- Precision on paleo dose determination typically 3-5%, often better (90-125 micrometer quartz)
- System design remove the need to handle sample disc after they are first placed in the tray.
- 64 disc positions enable large numbers of dose points to be well defined.
- Temperature control of samples during illumination

- Reproducible and precise sample positioning
- High speed operation. A short exposure (≤ 1 second) to all samples takes only ten minutes



Figure 3.3 Irradiator.

3.1.2 TL Reader and Peak Analyzer

The glow curve measurements for samples were made using a Harshaw TLD System 3500 Manual TL Reader shown in Figure 3.4. The technical architecture of the system includes both the Reader and a personal computer connected through a standard RS-232 serial communication port to control the 3500 Reader.



Figure 3.4 Harshaw TLD System 3500 Manual TL Reader

The Harshaw 3500 includes a sample drawer for a single element TLD dosimeter, a linear, programmable heating system and a cooled photomultiplier tube with associated electronics to measure the thermoluminescence light output. It is the device where the irradiated materials are heated and the intensity of the light output measured. Using the software program Winrems, we can set the starting and ending temperatures of the heating process, and the temperature increments. Search Response Database (RSP) is used to view the results. Temperature settings are made with the Time Temperature Profile (TTP). The glow curves were obtained by using a Harshaw QS 3500 Manual type thermoluminescence reader interfaced to a PC, where the thermoluminescence signals were analyzed. The basic block diagram of reader is shown in Figure 3.5.

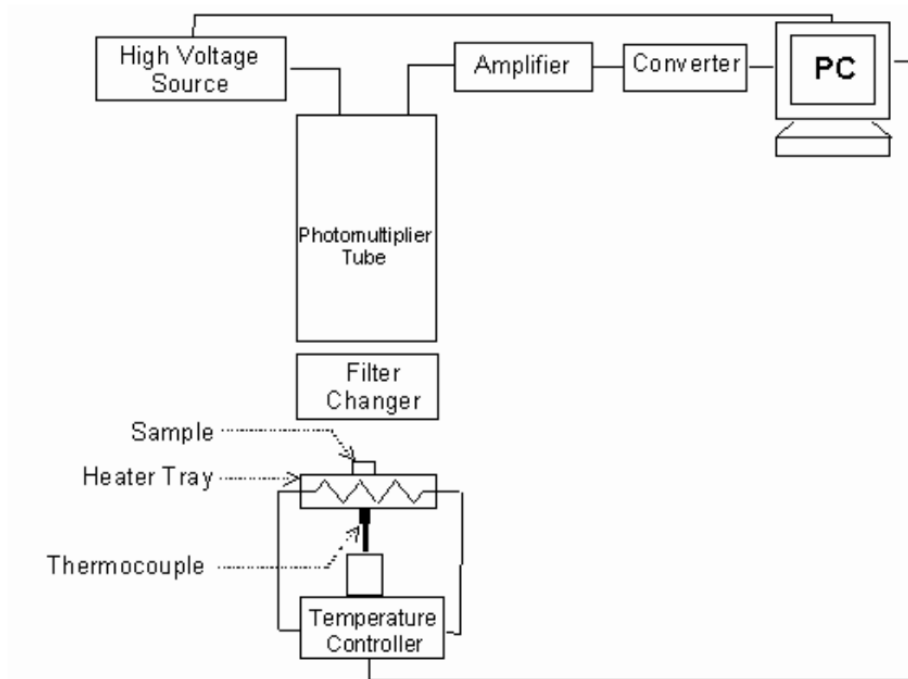


Figure 3.5. Basic block diagram of TL reader.

3.1.3 Microprocessor Controlled Electrical Oven

In the given work shown in figure 3.6, a microprocessor controlled electrical oven were used to anneal the samples at different temperature. The temperature range of oven change room temperature up to 1100 °C and its sensitivity was estimated ± 1 °C.



Figure 3.6 Microprocessor controlled Electrical Oven

3.1.4 Equipment Used Before Irradiation Process

Some chemicals were used to decontaminate undesired residuals and organic materials from each sample. Sieves were used to determine the dimensions (grain sizes) of the particles that vary from 50 μm to 400 μm . A digital balance was used to weight samples for desired measures.



Figure 3.7 Some of the used equipment; chemicals, sieves and digital balance

3.2 Material and Preparation

In all experiments, four different natural samples have been used for this thesis;

3.2.1 Calcite Extracted from Natural Sand Used in Making Roasted Chickpea

The sample preparation is done by following steps. (1) The extracted sand from the cave is washed in HCl acid to eliminate organic residues and is kept in diluted HF (1M) to eliminate remaining clay materials [24, 25, 78] (2) It is washed with pure water several times. (3) It is then dried in an oven at room temperature. (4) Then it is sieved using fine sieves which have different dimensions. (5) Each sample is weighted to be 20 mg for each measurement.

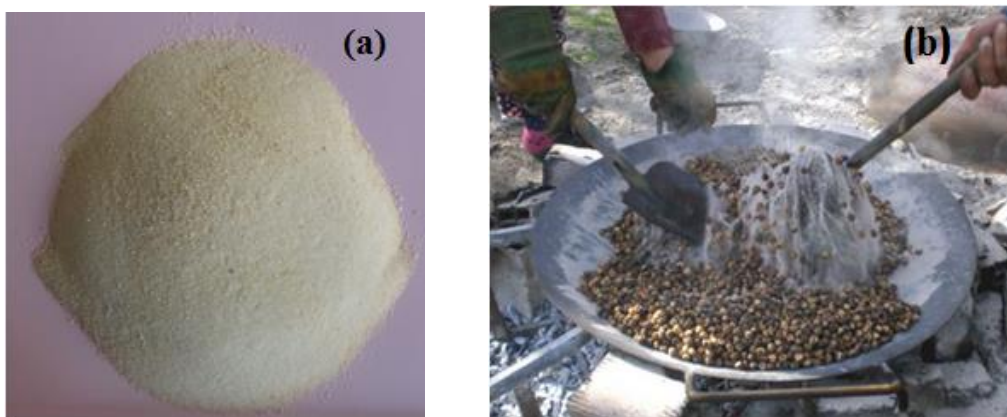


Figure 3.8 (a) Natural sand used in making roasted chickpea, (b) usage of sand sample during making roasted chickpea

3.2.2 Fluorapatite Mineral ($\text{Ca}_5\text{F}(\text{PO}_4)_3$) in Tooth Enamel

The tooth enamel samples were taken from a dentist who separated enamel from dentine. The samples were crushed in the agate mortar to get powder form. The powdered tooth enamel sample was etched for 5 min a 20% acetic acid water solution followed by drying [39]. It is sieved using fine sieves which have different dimensions and the samples whose grain sizes are between 100 μm and 120 μm are used in all TL measurements. Due to lack of sample, each experiment was performed with 10 mg aliquot samples instead of 20 mg.

3.2.3 Biogenic Minerals Present in the Seashells

The seashell samples which were collected from the shores of the Mediterranean seen in Figure 3.9a. All these samples were crushed and ground carefully with agate mortar and pestle seen in Figure 3.9b. After milling, the samples were washed with acetic acid ($\text{C}_2\text{H}_4\text{O}_2$) solution to remove any organic materials. Finally, the samples were again washed with distilled water and then dried in room temperature. Then they were sieved to the grain sizes between 50 -400 μm . Each sample was weighted to be 20 mg for each measurement.

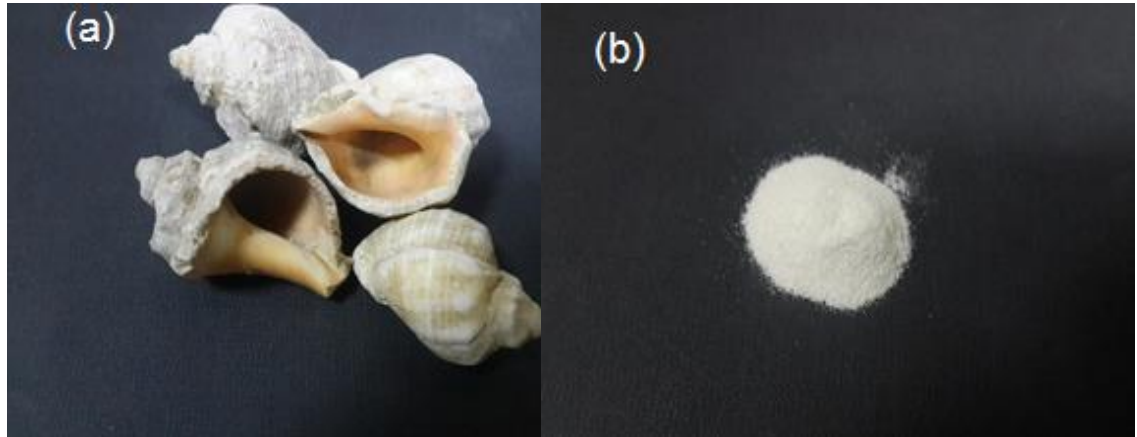


Figure 3.9 The seashells which were collected from the shores of the Mediterranean (a) as bulk form (b) as powder form

3.2.4 Plagioclase Minerals in Basaltic Rocks

The collected basaltic rocks in the field were crushed using agate mortar and washed in HCl acid to eliminate organic residues [79-81]. Then, they were washed with pure water several times and dried at room temperature. They were sieved with using fine sieves whose have different dimensions from 50 to 400 μm . Finally, each sample was weighted 20 mg for each measurement.

3.3 XRD Analysis of the Samples

The XRD results of all samples obtained from XRD Facility of Boğaziçi University Advanced Technologies R&D Center, a Rigaku D/MAX-Ultima+/PC X-ray diffraction equipment. The Rigaku D/MAX-Ultima+/PC X-ray diffraction equipment is engineered to create a multiple purpose configuration. The X-ray generator is a part of Rigaku D/MAX-Ultima+/PC X-ray diffraction equipment and operates at 20–60 kV rated voltage, 2–80 mA rated current and 3 kW maximum rated output with SCR phase control. The focal spot size in the X-ray generator is $1 \times 10 \text{ mm}^2$.

3.3.1 Calcite Extracted from Natural Sand Used in Making Roasted Chickpea

The main mineral of sand used in making Ağın leblebi is Magnesium calcite ($Mg_{0.03}Ca_{0.97}CO_3$).

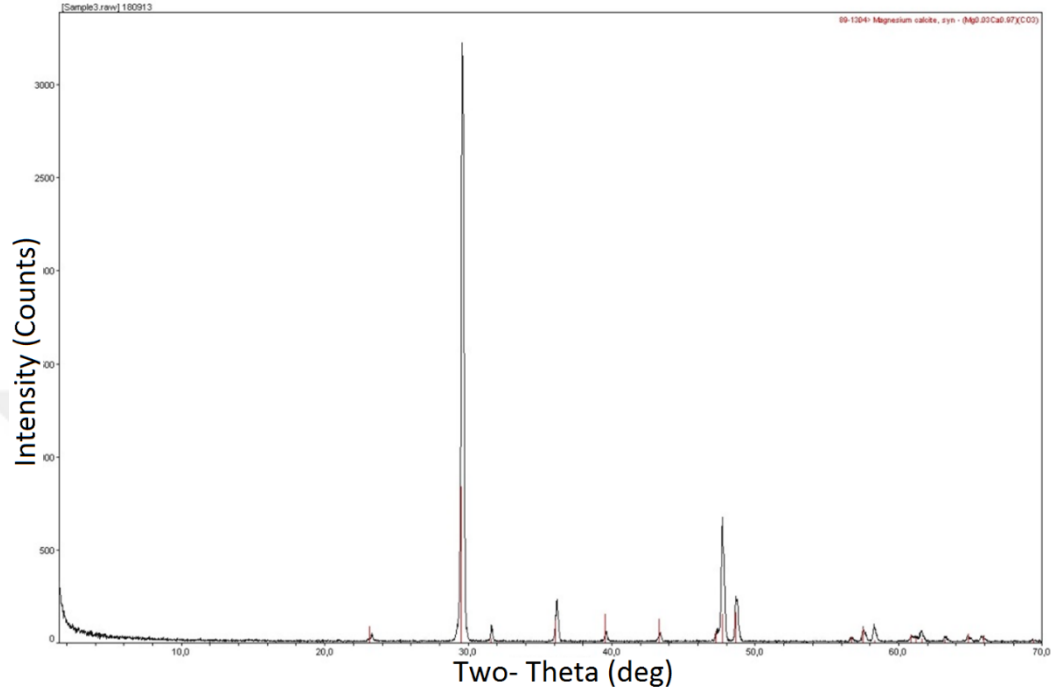


Figure 3.10 The XRD measurement of sand used in making Ağın leblebi.

Table 3.1 The analysis of XRD measurement of the sand sample

2 θ	d(Å)	Height %	Phase ID	Hkl
23,301	3,8144	1.4	Magnesium calcite, syn	(0 1 2)
29,602	3,0152	100.0	Magnesium calcite, syn	(1 0 4)
36,217	2,4783	7.0	Magnesium calcite, syn	(1 1 0)
47,740	1,9035	20.4	Magnesium calcite, syn	(0 1 8)
48,700	1,8682	7.5	Magnesium calcite, syn	(1 1 6)

3.3.2 Fluorapatite Mineral ($\text{Ca}_5\text{F}(\text{PO}_4)_3$) in Tooth Enamel

The main mineral of tooth enamel is fluorapatite mineral ($\text{Ca}_5\text{F}(\text{PO}_4)_3$).

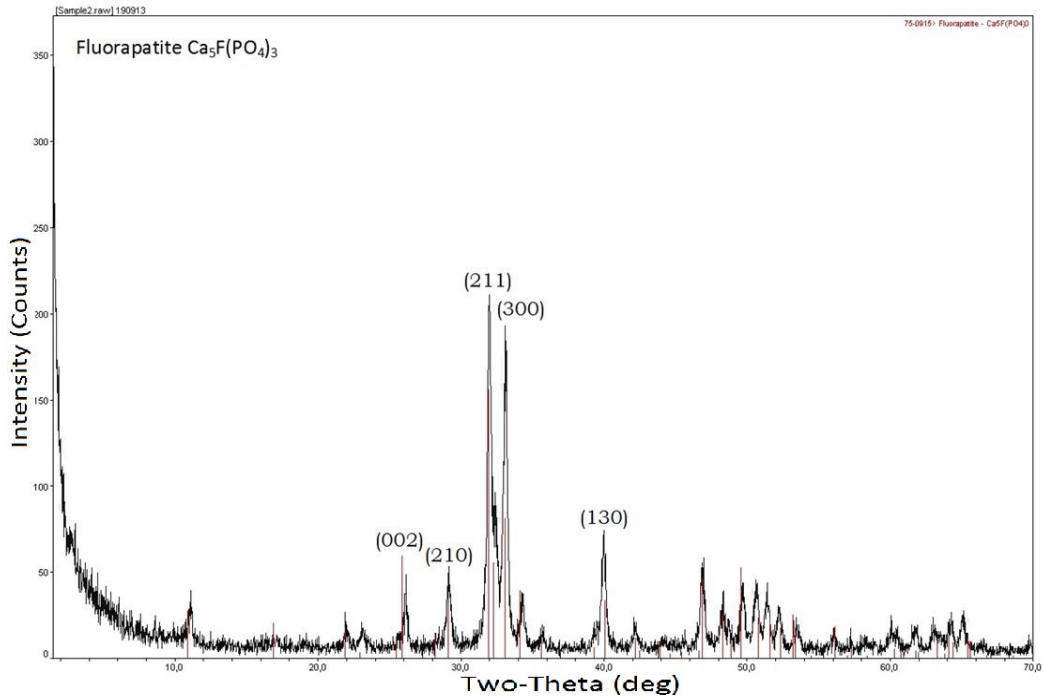


Figure 3.11 X-ray diffraction (XRD) pattern of tooth enamel

Table 3.2 The Peak ID Extended Report of tooth enamel

2 θ	d(\AA)	Height %	Phase ID	hkl
26,175	3,4018	21,5	Fluorapatite	(0 0 2)
29,177	3,0582	23,5	Fluorapatite	(2 1 0)
32,019	2,7929	100,0	Fluorapatite	(2 1 1)
33,122	2,7024	92,0	Fluorapatite	(3 0 0)
40,035	2,2503	34,5	Fluorapatite	(1 3 0)

3.3.3 Biogenic Minerals Present in the Seashells

The main mineral of unannealed seashell sample is Aragonite whose composition is identical with calcite or carbonate of lime shown in Table 3.3, but differing from it in its crystalline form and some of its physical characters whereas of annealed seashell is calcium carbonate (CaCO₃ and lime (CaO) shown in Table 3.4.

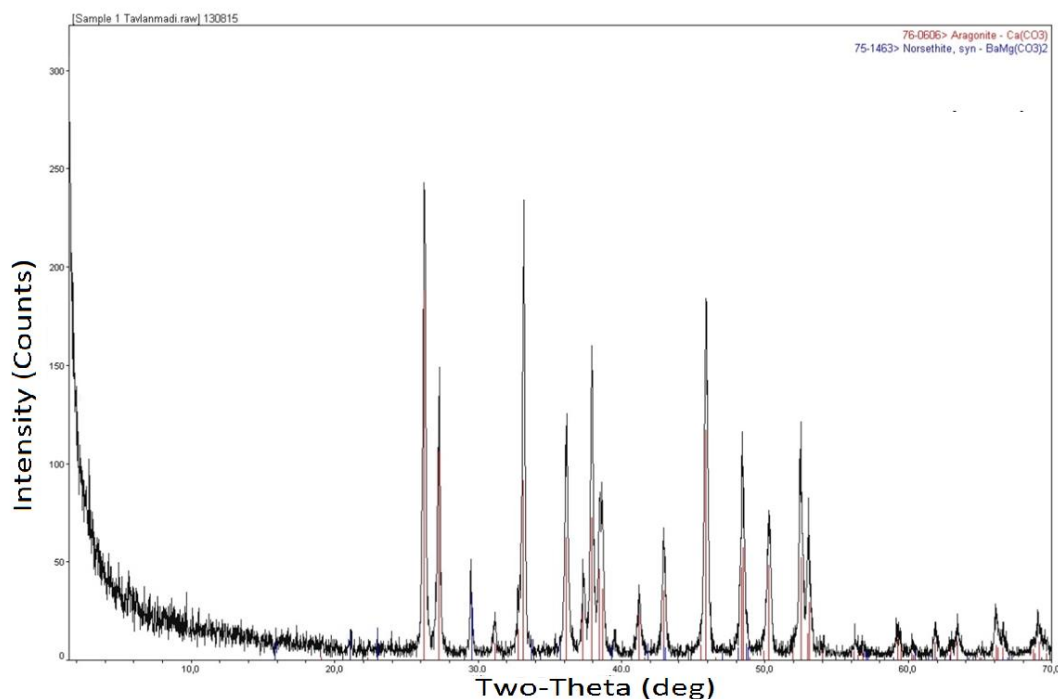


Figure 3.12 The XRD measurement of un-annealed seashell as powder form.

Table 3.3 The analysis of XRD measurement of the un-annealed seashell

2 θ	d(Å)	Height %	Phase ID	hkl
26,262	3,3907	100,0	Aragonite	(1 1 1)
27,319	3,2619	61,4	Aragonite	(0 2 1)
29,535	3,0219	20,2	Norsethite, syn	(1 0 4)
33,219	2,6947	98,3	Aragonite	(0 1 2)
37,959	2,3684	64,8	Aragonite	(1 1 2)
42,959	2,1036	27,0	Norsethite, syn	(2 0 2)
45,921	1,9746	76,8	Aragonite	(2 2 1)
50,302	1,8124	30,5	Aragonite	(1 3 2)

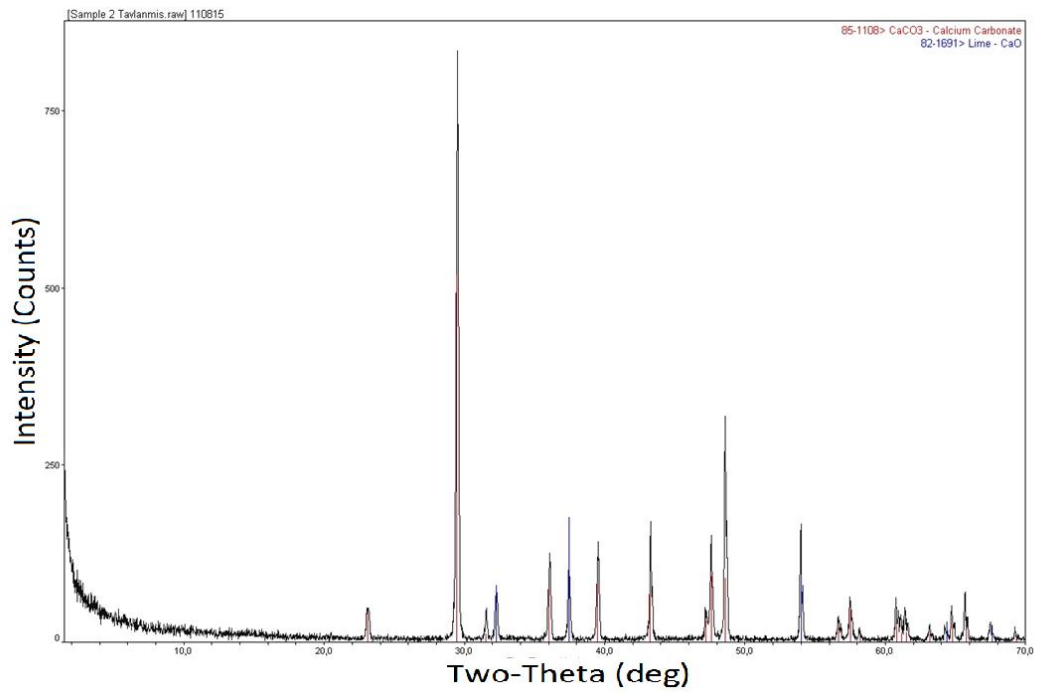


Figure 3.13 The XRD measurement of annealed seashell at 700 °C as powder form.

Table 3.4 The analysis of XRD measurement of the annealed seashell at 700 °C.

2 θ	d(Å)	Height %	Phase ID	hkl
23,179	3,8341	5,2	CaCO ₃	(0 1 2)
29,541	3,0214	100,0	CaCO ₃	(1 0 4)
32,321	2,7675	8,4	Lime(CaO)	(1 1 1)
36,101	2,4859	14,5	CaCO ₃	(1 1 0)
43,301	2,0878	19,8	CaCO ₃	(2 0 2)
48,618	1,8712	37,5	CaCO ₃	(1 1 6)
54,012	1,6964	19,5	Lime(CaO)	(2 2 0)
65,714	1,4198	7,9	CaCO ₃	(0 0 12)

3.3.4 Plagioclase Minerals in Basaltic Rocks

The main minerals of the powdered basaltic rock are anorhtite sodian ($\text{Na}_{0.48}\text{Ca}_{0.52}\text{Al}_{1.52}\text{Si}_{2.48}$), cristobalite (syn, SiO_2) and quartz (SiO_2).

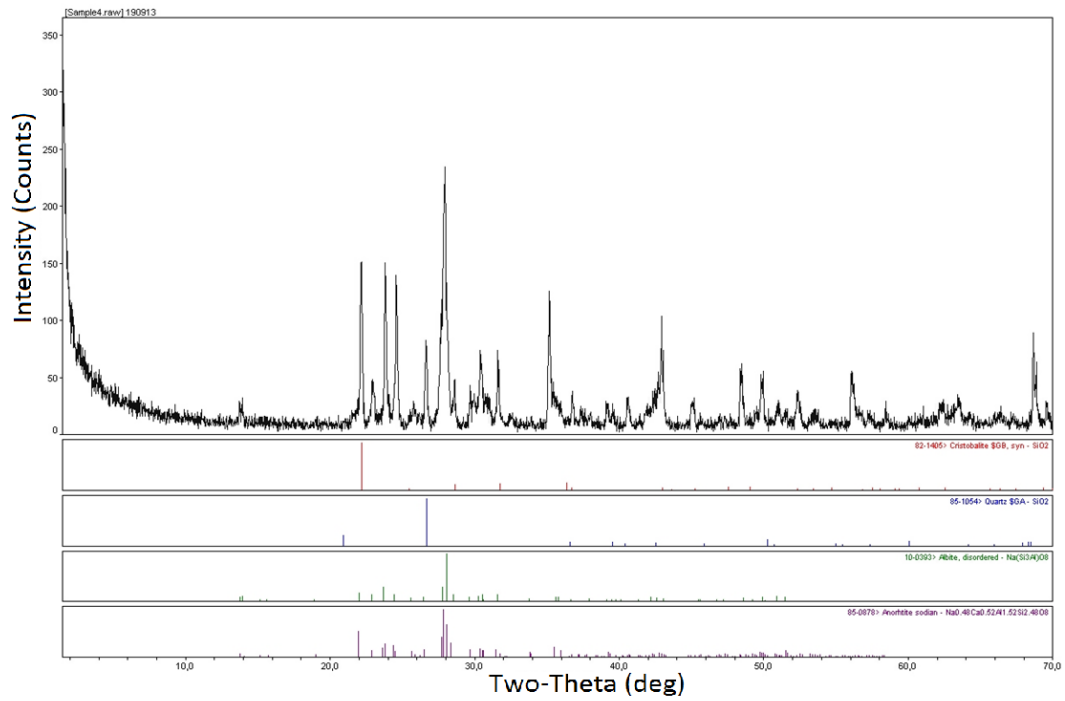


Figure 3.14 The XRD measurement of powdered basaltic rock

Table 3.5 The analysis of XRD measurement of the powdered basaltic rock

2 θ	d(\AA)	Height %	Phase ID	hkl
22,983	3,8664	15,5	Albite	(1-1 1)
23,840	3,7293	59,3	Anorhtite sodian	(-1 3 0)
24,603	3,6154	56,6	Anorhtite sodian	(-1-3 2)
26,660	3,3409	32,3	Quartz	(0 1 1)
27,995	3,1845	100,0	Anorhtite sodian	(0 0 4)
28,636	3,1148	17,7	Cristobalite	(1 1 1)
35,200	2,5475	51,8	Anorhtite sodian	(-2-4 2)
42,958	2,1037	39,8	Cristobalite	(2 1 1)
56,100	1,6381	20,8	Anorhtite sodian	(4 2 1)
68,680	1,3655	35,0	Quartz	(0 3 1)

3.4 Procedure

All examples were irradiated at room temperature with a point beta source (^{90}Sr - ^{90}Y) which delivers 0.040 Gy/s. Glow curve measurements were made using a Harshaw TLD System 3500 Manual TLD Reader at 1 °C/s heating rate in experiments. The irradiated samples were read out in N_2 atmosphere in order to avoid undesired signals. A standard clear glass filter was always installed in the reader between the planchet and photomultiplier tube. Each experiment was repeated three times for different aliquots.

The four main headlines in this work were performed;

- At different grain sizes from 50 to 400 μm , 20 mg samples were irradiated with beta source about 36 Gy and read out to see the effects of grain size on TL glow curve and obtain glow curve by the TLD reader to get best grain size whose TL signal is the biggest.
- 20 mg samples were annealed at different annealing temperatures (from 200°C to 1100 °C) and read out to see the effects of pre-irradiation annealing at different annealing temperatures on the TL glow curves.
- 20 mg samples were annealed at different annealing times (from 15 minutes to 360 minutes) and read out to see the effects of pre-irradiation annealing at different annealing times on the TL glow curves.
- Reproducibility (cycle of measurement) were performed at different annealing temperatures (from 200°C to 1100 °C). In this stage, a 20 mg sample was annealed, irradiated 36 Gy before reading process and read out. This process was repeated six times for ten different annealing temperatures.

Due to the lack of tooth enamel samples, the same procedure could not be applied. Seven aliquots weighted 10 mg were used to see the effects of different annealing temperature (from 500 °C to 1100 °C) at fixed annealing time (30min). Five aliquots were annealed at 1000 °C for different annealing times (15, 30, 60, 90 and 120 min) to

see the effects of different annealing time at fixed annealing temperature before irradiation process. The aliquots were irradiated 36 Gy before reading process.



CHAPTER 4

EXPERIMENTAL RESULTS

In this chapter, we examined the experimental results under four cases which are:

- Grain Size Effect (excepting tooth enamel)
- Annealing effects at different annealing temperatures
- Annealing effects at different annealing times
- Reproducibility (Cycle of Measurement) at different annealing temperatures

4.1 Grain Size Effect

In the grain-size experiment, we used three natural minerals. Due to lack of tooth enamel, we didn't carry out the grain size experiment of tooth enamel.

4.1.1 Calcite Extracted from Natural Sand Used in Making Roasted Chickpea

Fig.4.1 and 4.2 show the effect of different grain sizes of the sample on the shape of TL glow curve and the area under the TL glow curve, respectively. The grain size varies from 50 μm to 400 μm . The shape of TL glow curve doesn't change with changing grain size shown in fig. 4.1. As seen in Fig. 4.2, each sample at different grain sizes gives different areas and the largest area is observed at $\sim 100 \mu\text{m}$. Therefore, we used samples whose grain size is $\sim 100 \mu\text{m}$ in all experiments on account of better result.

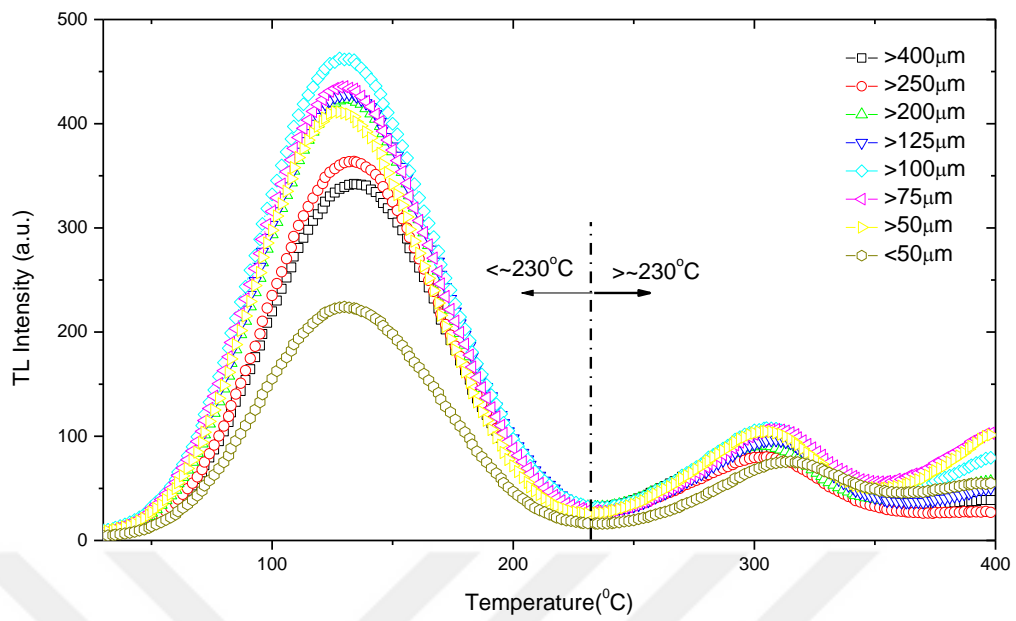


Figure 4.1 Effect of different grain size of sand sample on the shape of TL glow curve

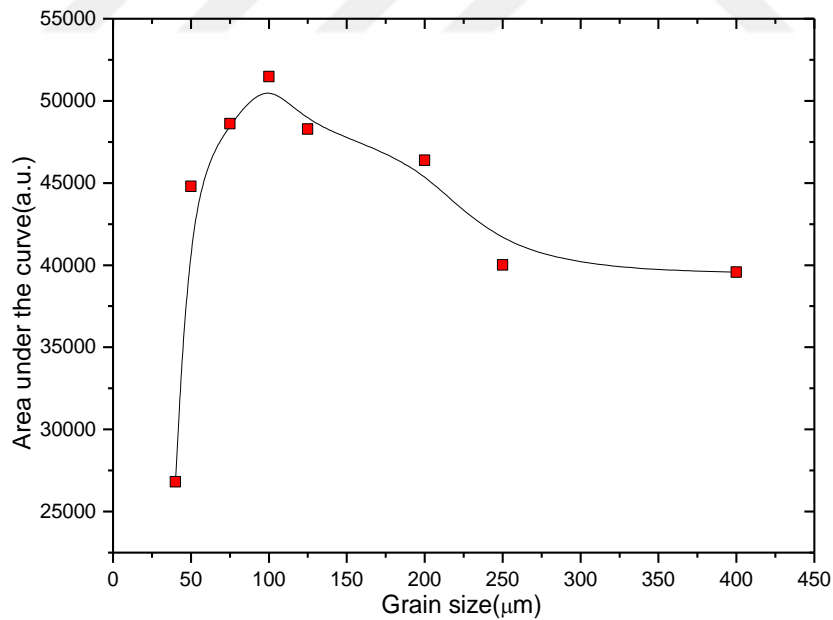


Figure 4.2 Effect of different grain size of sand sample on the area under the glow curve

4.1.2 Biogenic Minerals Present in the Seashells

During grain size experiment, all samples whose particle size varies from 50 μm to 400 μm were annealed at 700 $^{\circ}\text{C}$ for 30 minutes before irradiating. Fig. 4.3 and 4.4 show the effect of different grain sizes of the sample on glow curve shape, area under the TL glow curves. As seen in Fig. 4.3 and 4.4, each sample at different grain sizes gives different results and the largest area was observed at about 250 μm . Therefore, we used samples whose grain size is 250 μm in all experiments on account of better result.

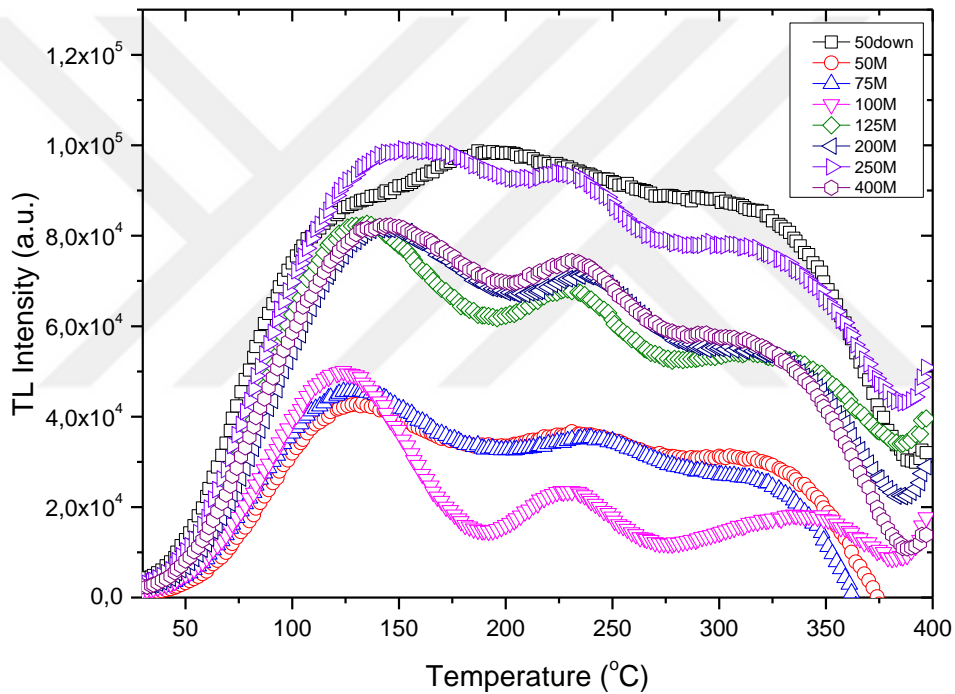


Figure 4.3 The effect of different grain sizes of the seashell sample on glow curve shape

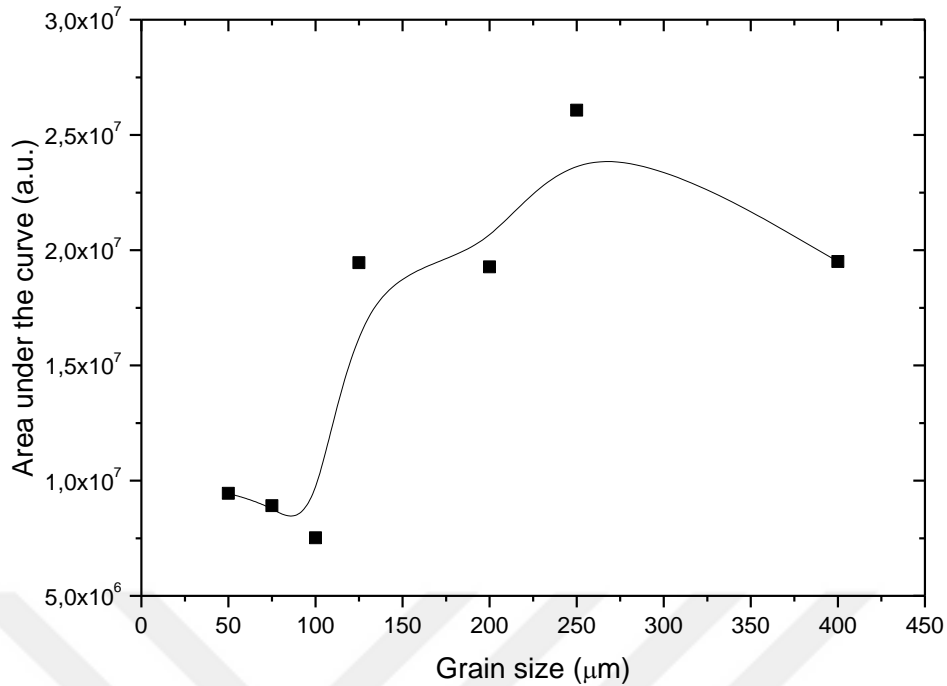


Figure 4.4 The effect of different grain sizes of the seashell sample on the area under the TL glow curves

4.1.3 Plagioclase Minerals in Basaltic Rocks

In figure 4.5 and 4.6, variation of TL glow curve and area under the glow curve at different grain sizes (from 50μm to 400μm) of sample are seen. Each of eight samples weighted 20mg was irradiated 36 Gy and read out. According to the results of fig. 4.5 and 4.6, the biggest area and TL intensity are observed between ~100μm and ~200μm, especially at ~100μm. Therefore, we used samples whose grain size is ~100μm in all experiment on account of better result. The TL glow curve shape doesn't change at different grain sizes shown in fig. 4.5.

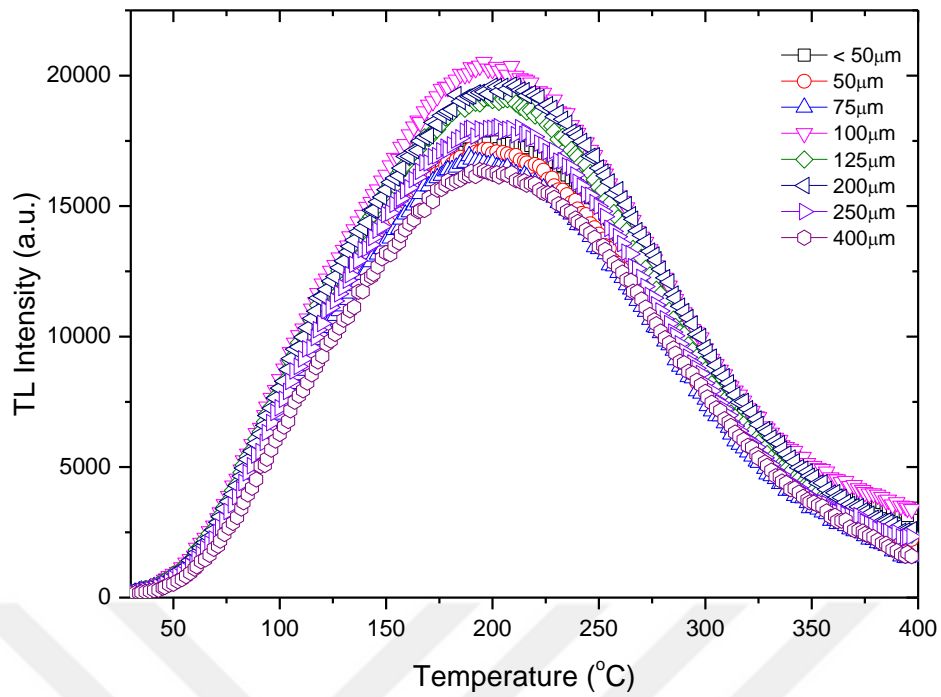


Figure 4.5 Variation of TL glow curve at different grain sizes of basalt sample.

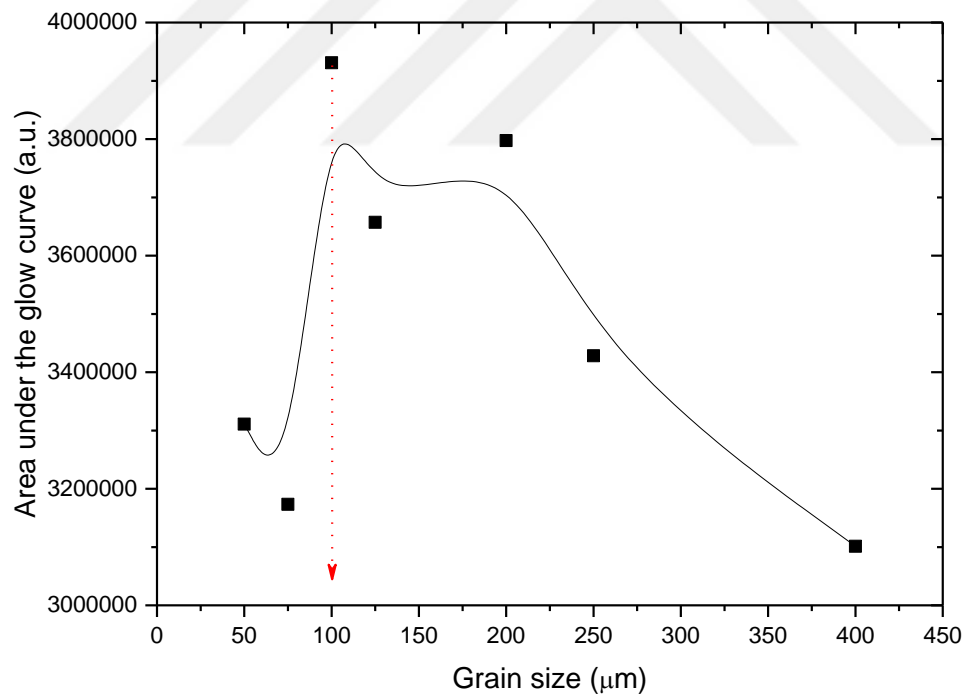


Figure 4.6 Variation of area under the glow curve at different grain sizes of basalt sample.

4.2 Annealing Effects at Different Annealing Temperatures

This part of the work was done to see the effect of different annealing temperature on the shape of TL glow curve, area under the glow curve, TL peak intensity, and peak temperature of the natural minerals used in this thesis.

4.2.1 Calcite Extracted from Natural Sand Used in Making Roasted Chickpea

The effect of different annealing temperature on the shape of TL glow curve, area under the glow curve, TL peak intensity, and peak temperature of the calcite extracted from natural sand used in making roasted chickpea (Leblebi) shown in Fig. 4.7, 4.8, 4.9, and 4.10, respectively. At a first glance, the glow curve shape varies at each annealing temperature shown in Fig. 4.7. At higher annealing temperatures two peaks are distinguishable and separated from each other. When the area under the glow curve and TL peak intensity are analyzed at different annealing temperatures, as shown in Fig. 4.8 and 4.9, the area and TL peak intensity increase tremendously beyond 600 °C annealing temperature and the biggest area and TL peak intensity are seen at 900 °C. Annealing at this temperature causes an enhancement in the area under the curve and TL peak intensity of about 70 times when it is compared with no-annealed sample. As seen in Fig. 4.10, peak temperature of low temperature peak (110 °C) shifts to higher temperature region about 60 °C between no-annealed sample and annealed sample at 800 °C. But a sharp decrease is observed beyond annealing temperature 800 °C. A shifting of about 30 °C is observed between peak temperature of intermediate temperature peak (230 °C) of annealed sample at 200 °C and no-annealed sample. However, no significant change is seen in the peak temperature of intermediate temperature peak for annealing temperature between 200 °C and 1100 °C.

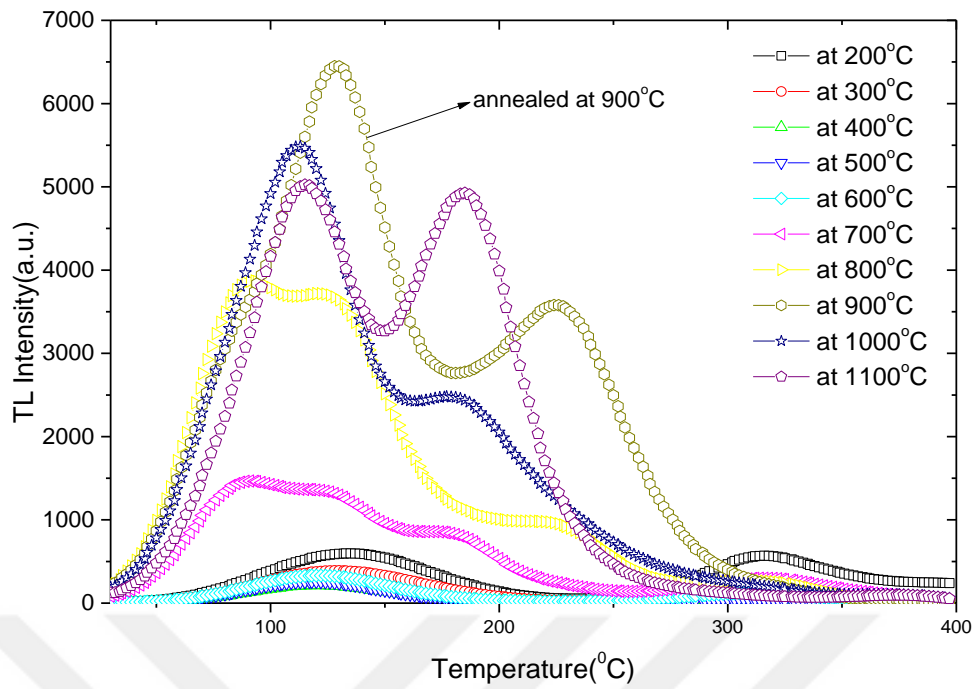


Figure 4.7 Variation of TL glow curve shape as a function of annealing temperature.

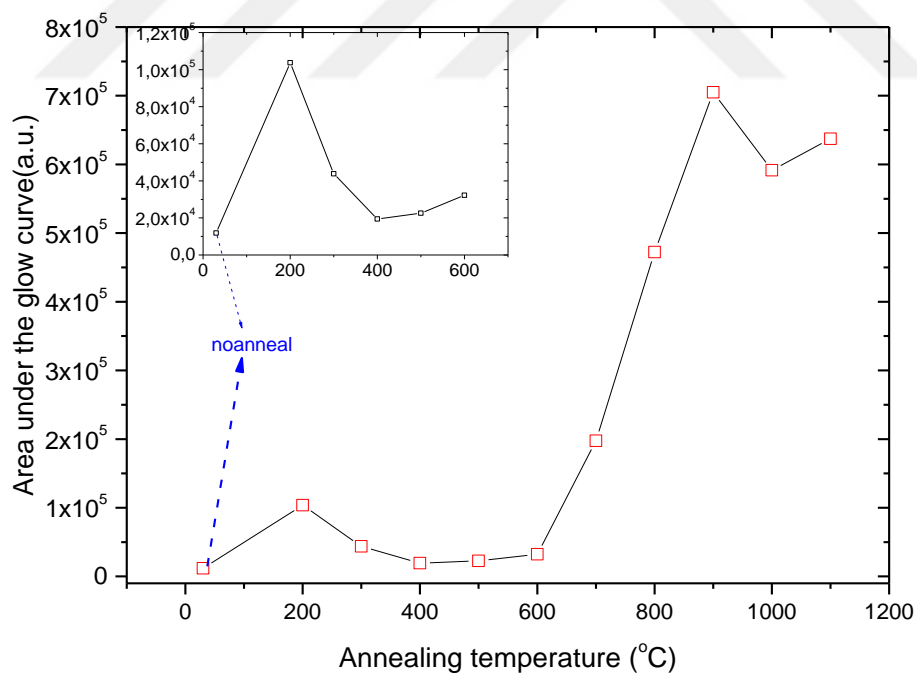


Figure 4.8 Variation of area under the curve as a function of annealing temperature.

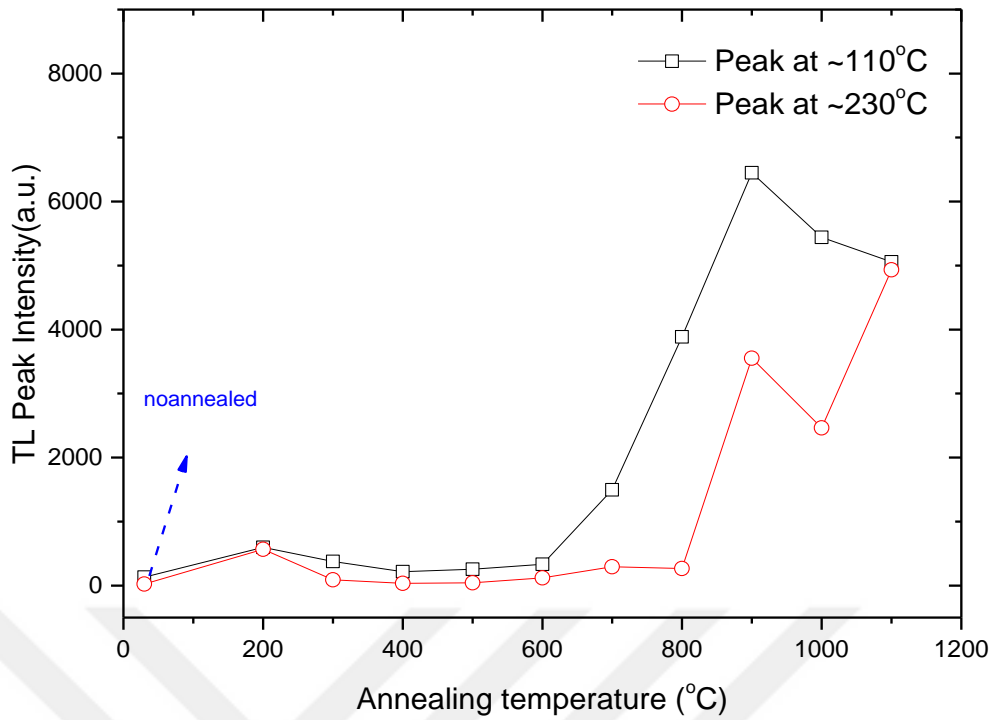


Figure 4.9 Variation of TL peak intensities as a function of annealing temperature.

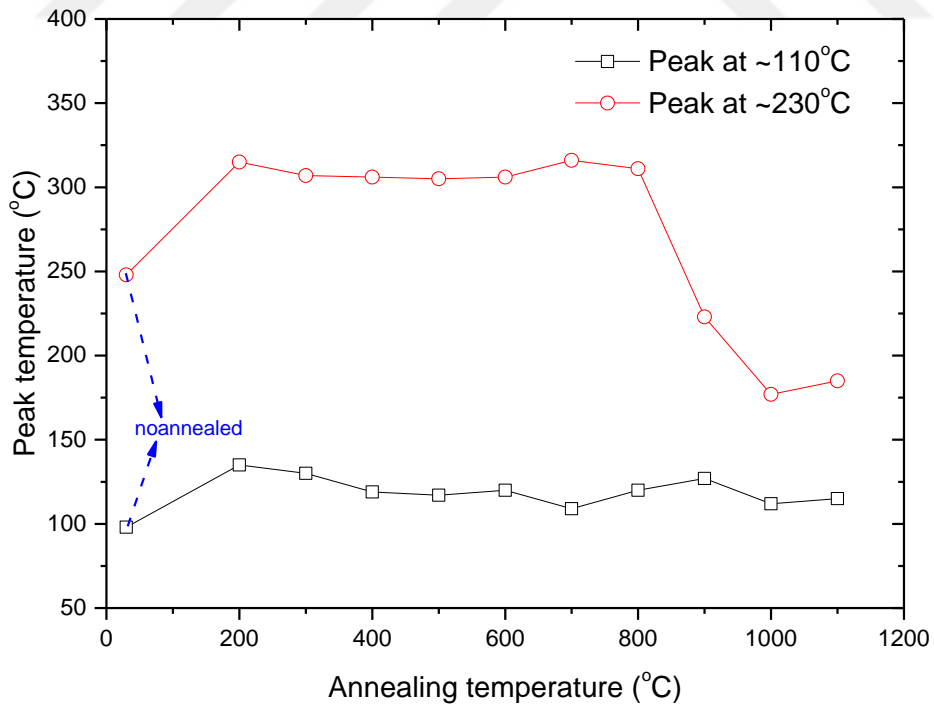


Figure 4.10 Variation of peak temperatures as a function of annealing temperature.

4.2.2 Fluorapatite Mineral ($\text{Ca}_5\text{F}(\text{PO}_4)_3$) in Tooth Enamel

Fig. 4.11 and 4.12 show the variation of the shape of TL glow curve as a function of annealing temperature at (a) 500-800 °C and (b) 900-1100 °C. For each annealing temperature, the samples were annealed about 30 min. It is seen that the different glow curves were obtained for each annealing temperature. Annealing of the sample at higher temperatures causes an increase in TL peak intensities and a decrease in the number of peak in the glow curve to single peak which is located around 200-230 C shown in fig.4.11 and 4.12.

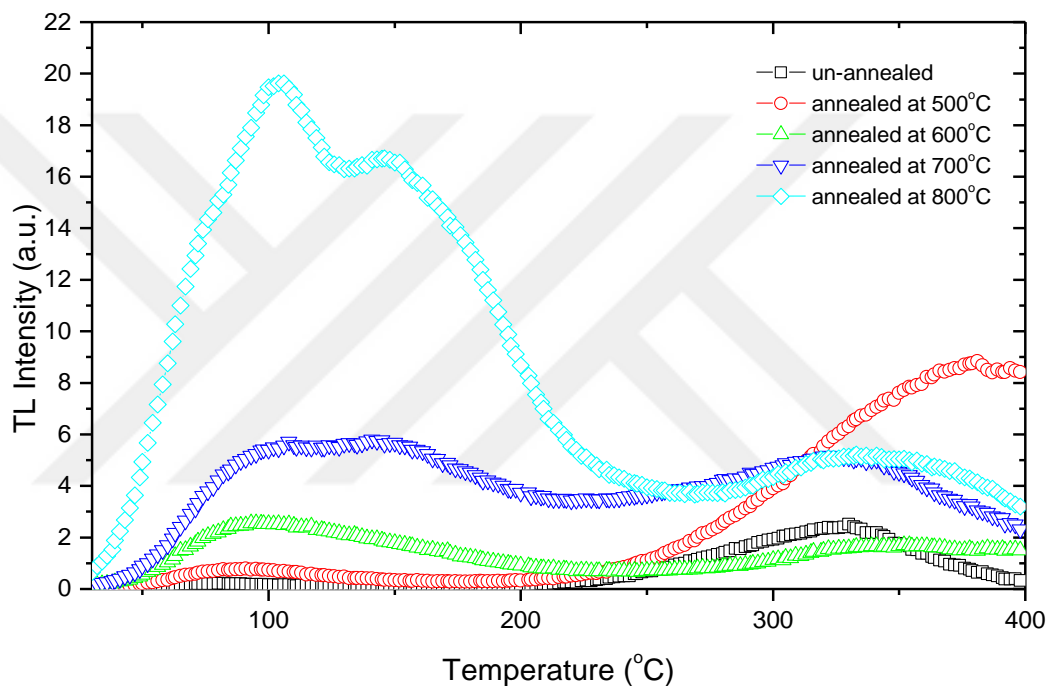


Figure 4.11 The variation of the shape of TL glow curve as a function of annealed temperatures at 500-800 °C and about 30 min.

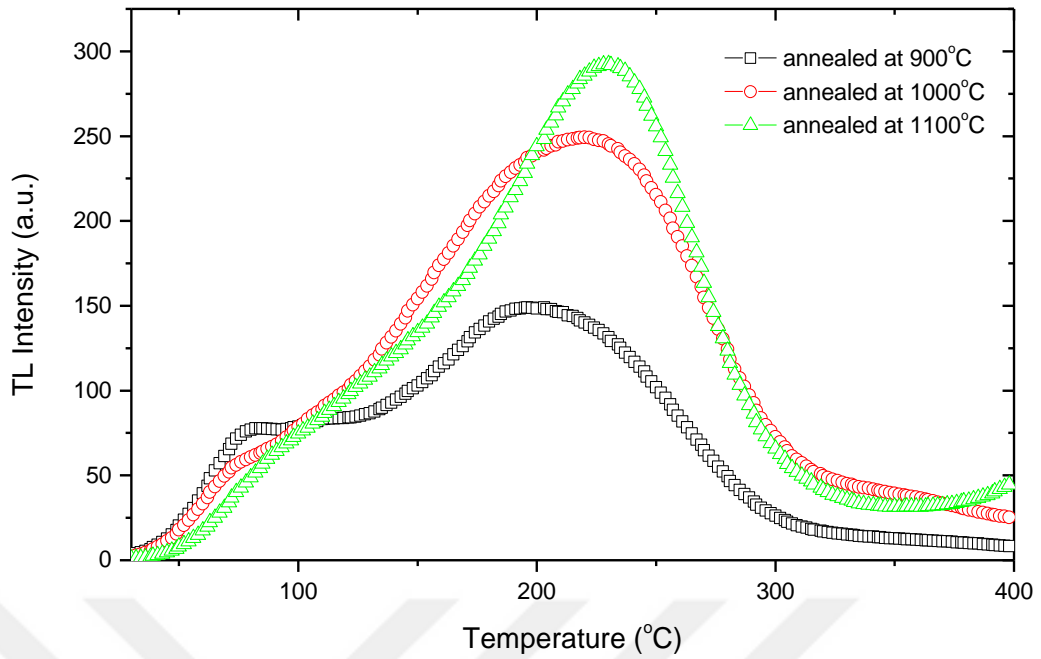


Figure 4.12 The variation of TL glow curve as a function of annealed temperatures at 900-1100 °C about 30 min.

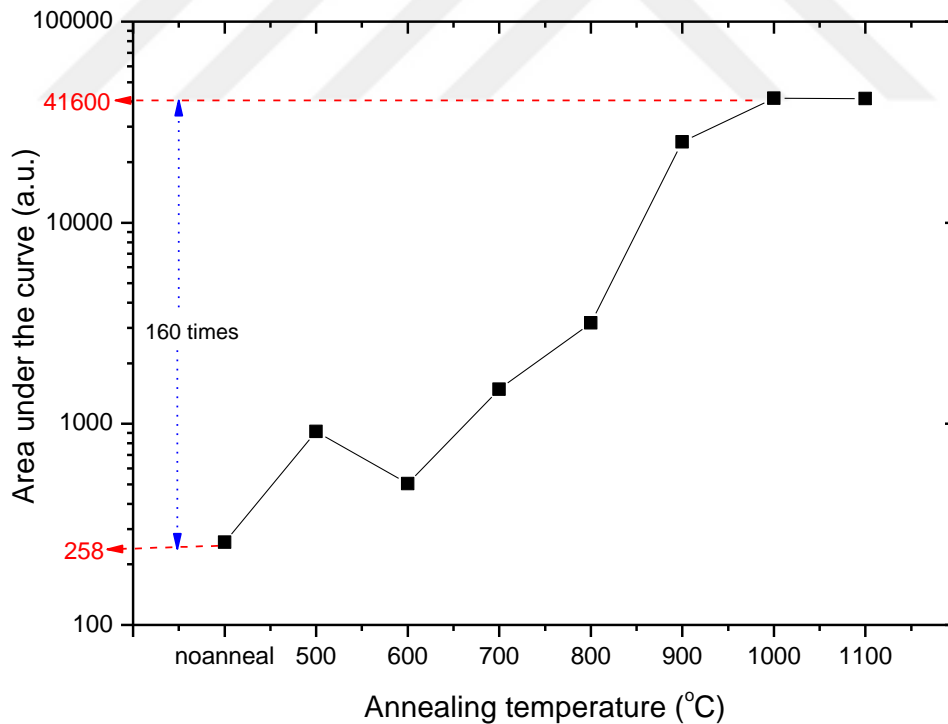


Figure 4.13 The variation of area under the glow curve as a function of annealing temperatures at 500°C -1100°C about 30 minutes.

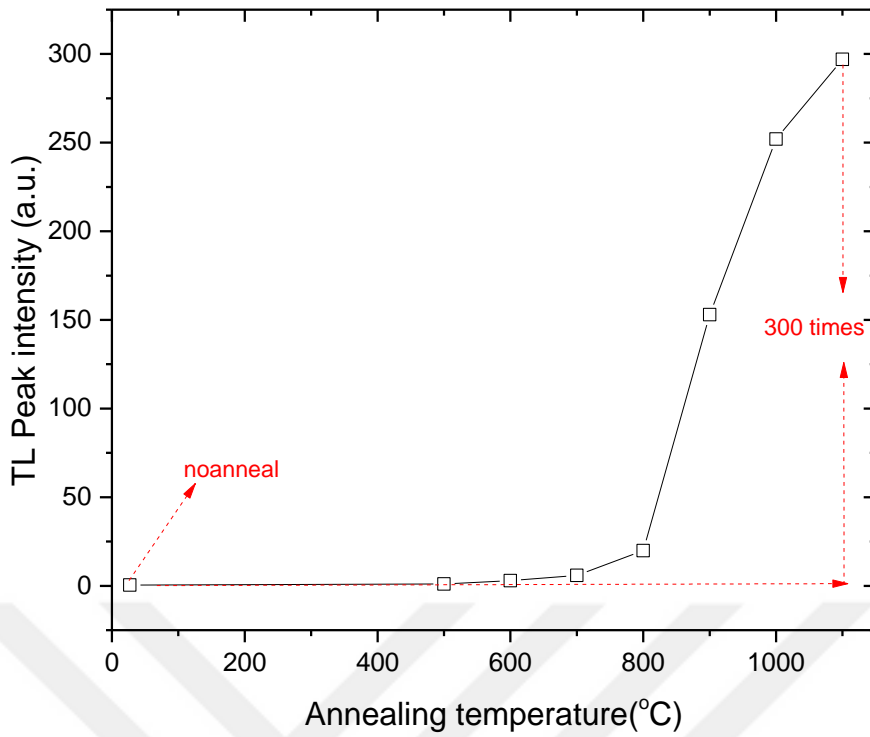


Figure 4.14 The variation of TL peak intensity as a function of annealing temperatures at 500°C -1100°C about 30 minutes.

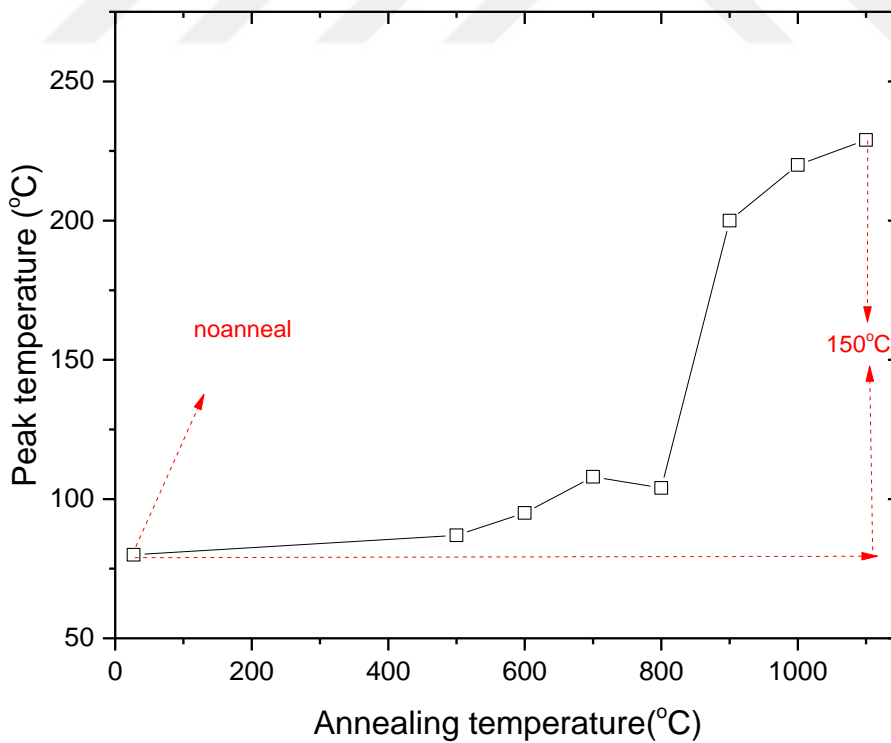


Figure 4.15 The variation of peak temperature as a function of annealing temperatures at 500°C -1100°C about 30 minutes.

The effect of annealing of the sample is seen clearly in Fig.4.13 and 4.14. In Fig. 4.13, the variation of area under the glow curve as a function of annealing temperatures at 500-1100 °C is seen. The area under the curve increases with increasing annealing temperature up to 1000 °C then reaches to its saturation value. In short, the area under the curve of the sample annealed at 1000 °C is bigger than un-annealed sample about 160 times. As in Fig. 4.14, a huge increase about 300 times was observed in TL peak intensity when annealed sample at 1100 °C is compared with the un-annealed sample shown in Fig.4.14. The similar effect and enhancement were observed in the study of calcite extracted from natural sand used in making roasted chickpea given in section 4.2.1. Increasing of annealing temperature affects also the peak temperature. As seen in fig. 4.15, peak temperature shifts to higher temperature region about 150°C at 1100°C.

4.2.3 Biogenic Minerals Present in the Seashells

The samples were annealed at different temperatures in the range 200–1100 °C by step for 100 °C for 30 minutes in a furnace. The annealed samples were then irradiated with the beta source. The irradiated samples were read out at TL reader system.

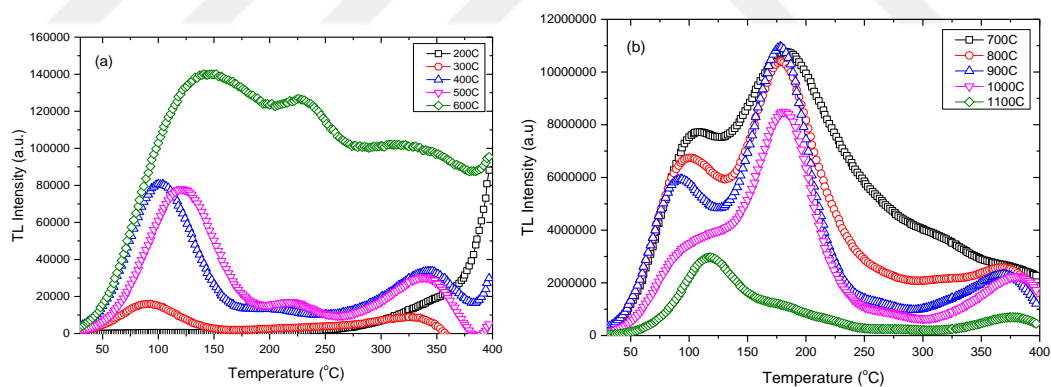


Figure 4.16 The effects of different annealing temperatures on TL glow curve (a) between 200 and 600 °C, (b) between 700 and 1100 °C.

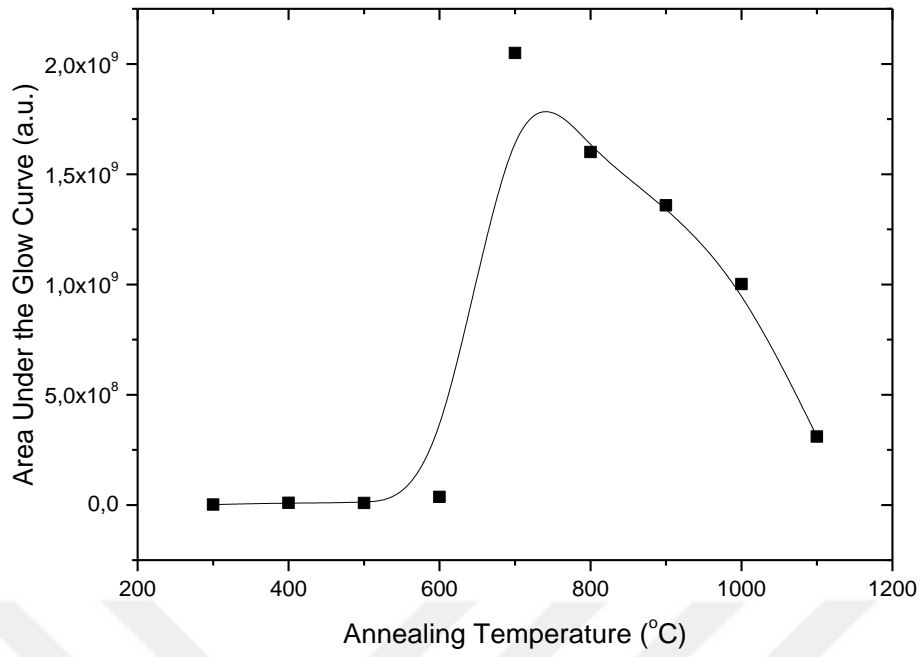


Figure 4.17 The effects of different annealing temperatures on the area under the glow curve

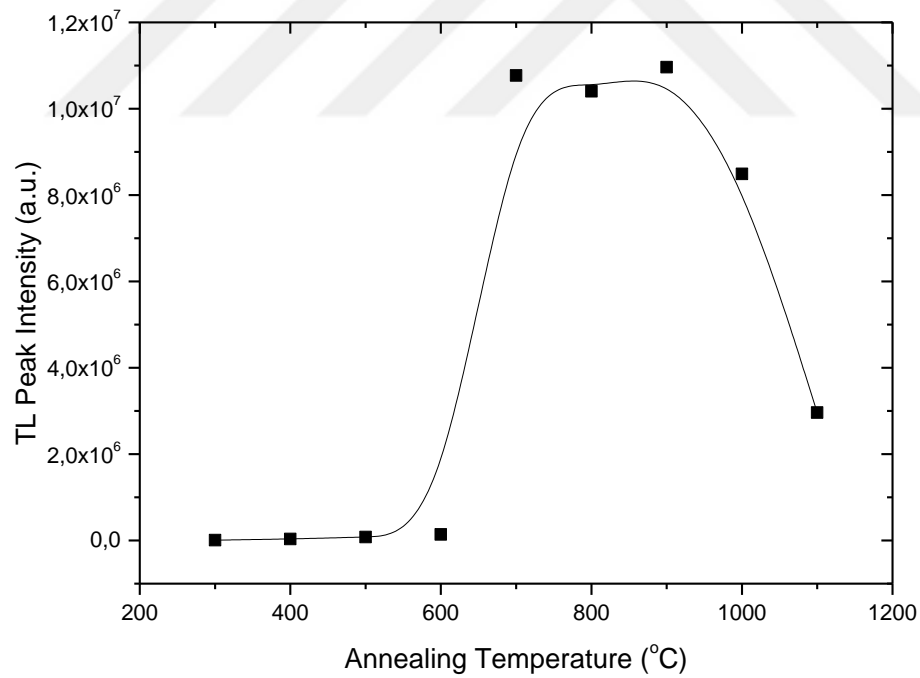


Figure 4.18 The effects of different annealing temperatures on the TL peak intensity

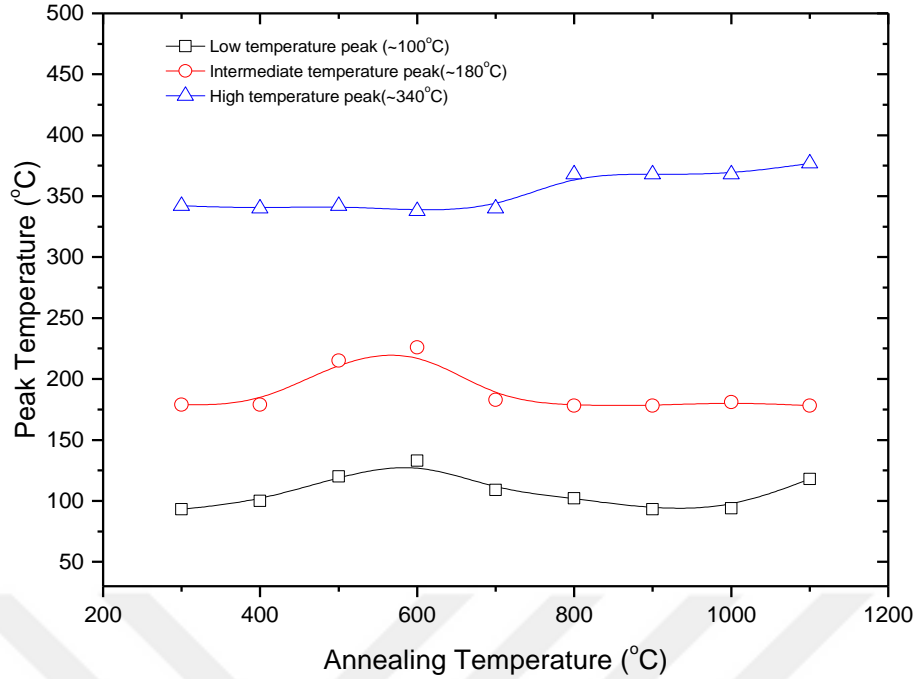


Figure 4.19 The effects of different annealing temperatures on the peak temperatures

The effects of different annealing temperature on the TL glow curve between 200 and 600 °C, between 700 and 1100 °C, area under the curve, TL peak intensity, and peak temperatures are shown in Fig. 4.16-4.19.

At first view, the glow curve shape varies at each annealing temperature seen in fig 4.16a and 4.16b. The biggest area under the curve and TL peak intensity were seen at 700 °C annealing temperature shown in fig 4.17 and 4.18. Annealing between 200 and 500 °C does not affect significantly the glow curve shape and area under the curve. But a visible change in the glow curve shape and area under the curve was observed at 600 °C annealing temperature. Especially, a fabulous change was observed at 700 °C annealing temperature. In the range of 700 °C and 1000 °C annealing temperatures, two peaks are distinguishable and separated from each other. Between 700 and 1100 °C annealing temperatures, unless no change in glow curve shape is not observed the area under the curve and TL peak intensity decrease. As seen in figure 4.19, low and intermediate peak temperatures are affected by the annealing temperatures in the range of 400 °C and 600 °C while high temperature peak is affected beyond 700 °C.

4.2.4. Plagioclase Minerals in Basaltic Rocks

In the figure 4.20-4.23, the effects of annealing at different temperatures on the shape of TL glow curve, area under the curve, TL peak intensity and peak temperature were given, respectively. Although no important change is seen in the shape of TL glow curve (in figure 4.20), area under the curve and TL peak intensity decrease to one-third of the value of annealing at 200 °C (in figure 4.21 and 4.22). The largest area under the curve and TL peak intensity were observed at 200 °C of annealing. Increasing in annealing temperature causes a shifting peak position to higher temperature region. About 60°C shifting in peak temperature is observed between 200 °C and 1100 °C (in figure 4.23).

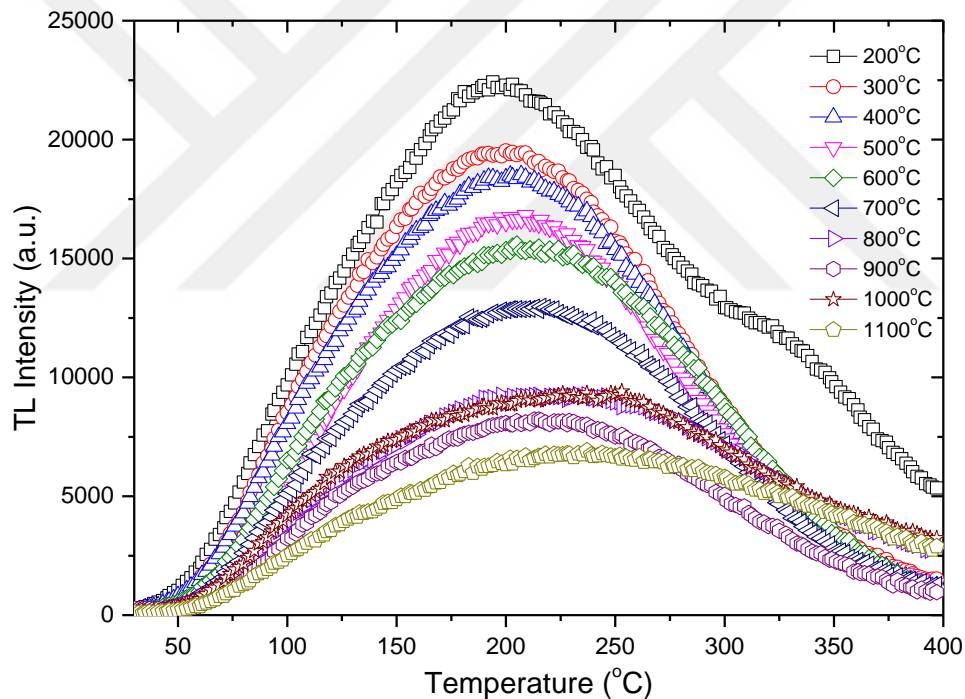


Figure 4.20 Variation of TL glow curve as a function of annealing temperature.

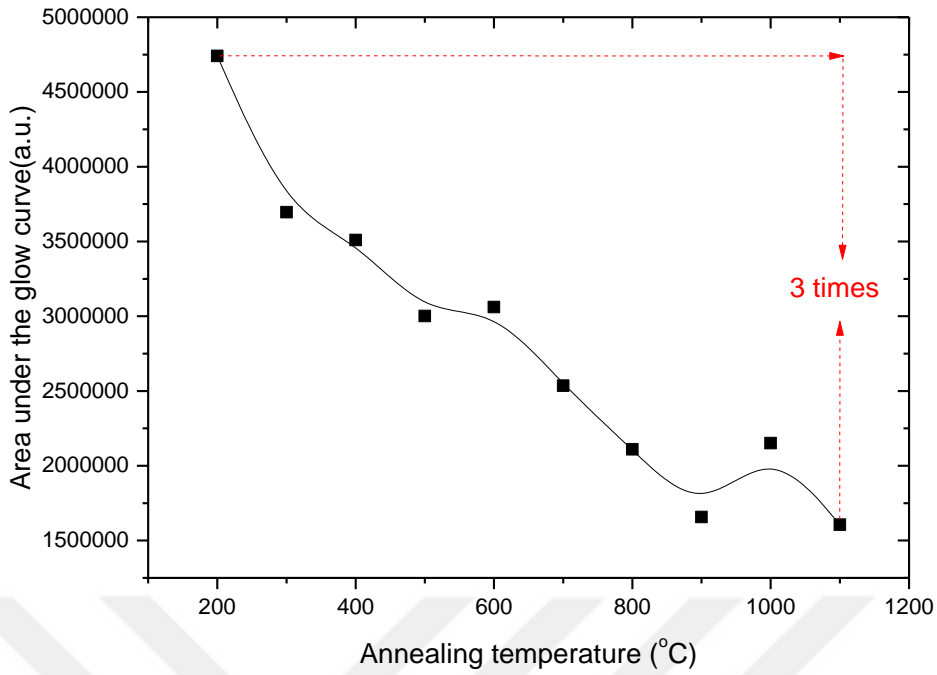


Figure 4.21 Variation of area under the curve as a function of annealing temperature.

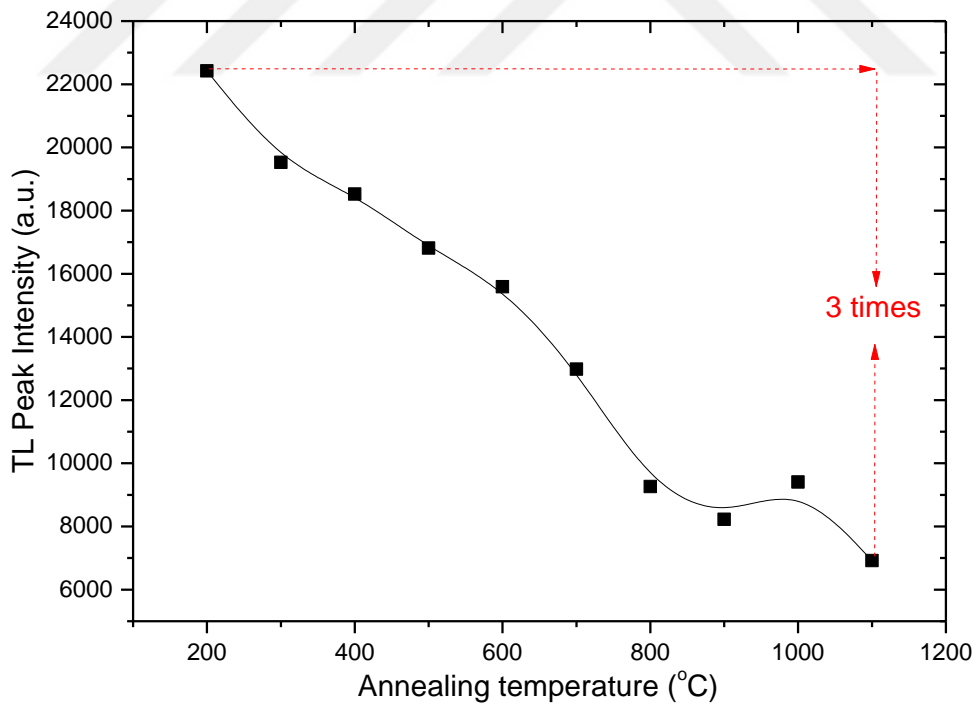


Figure 4.22 Variation of TL peak intensity as a function of annealing temperature.

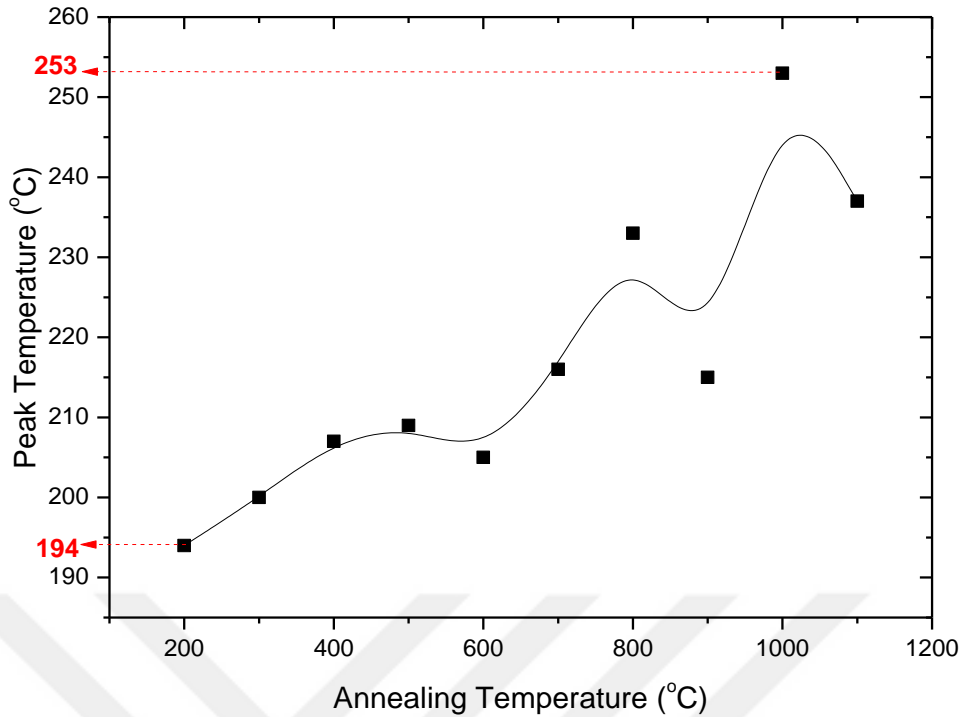


Figure 4.23 Variation of peak temperature as a function of annealing temperature.

4.3 Annealing Effects at Different Annealing Times

The second part of the thermal treatment in this work is to see that how the annealing time affects the shape of TL glow curve, area under the curve, TL peak intensity, and peak temperature for different values of it.

4.3.1 Calcite Extracted from Natural Sand Used in Making Roasted Chickpea

The effects of different annealing time at 900 °C on the the shape of TL glow curve, area under the curve, TL peak intensity, and peak temperature of calcite extracted from natural sand used in making roasted chickpea were shown in Fig. 4.24, 4.25, 4.26 and 4.27, respectively. As seen in Fig. 4.24, glow curve of samples which are annealed at 900 °C for about 15 min and 60 min have different shapes from the others. Especially at 15 min annealing, the intermediate peak (~230 °C) becomes distinct. There is no appreciable variation in glow curve shape for annealing time between 60 min and 360 min. As shown in Fig. 4.25 and 4.26, the largest area under the curve and TL peak intensities are seen at 15 min annealing time. In addition, the peak temperatures for ~110 °C peak and ~230 °C peak do not vary with increasing annealing time in Fig. 4.27.

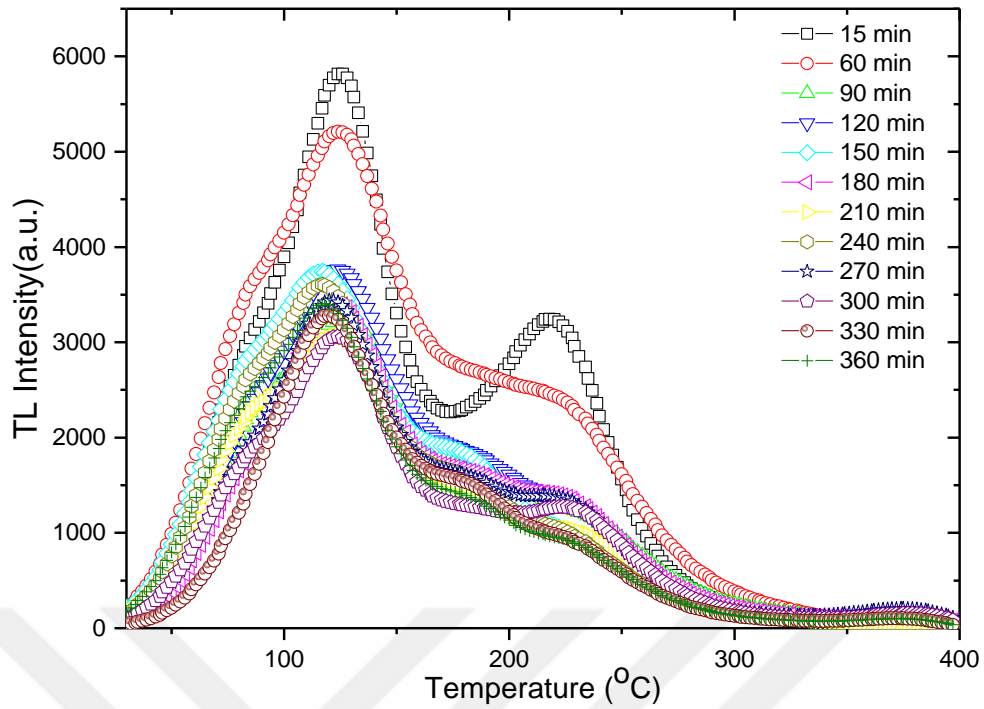


Figure 4.24 Variation of shape of TL glow curve as a function of annealing time at 900 °C.

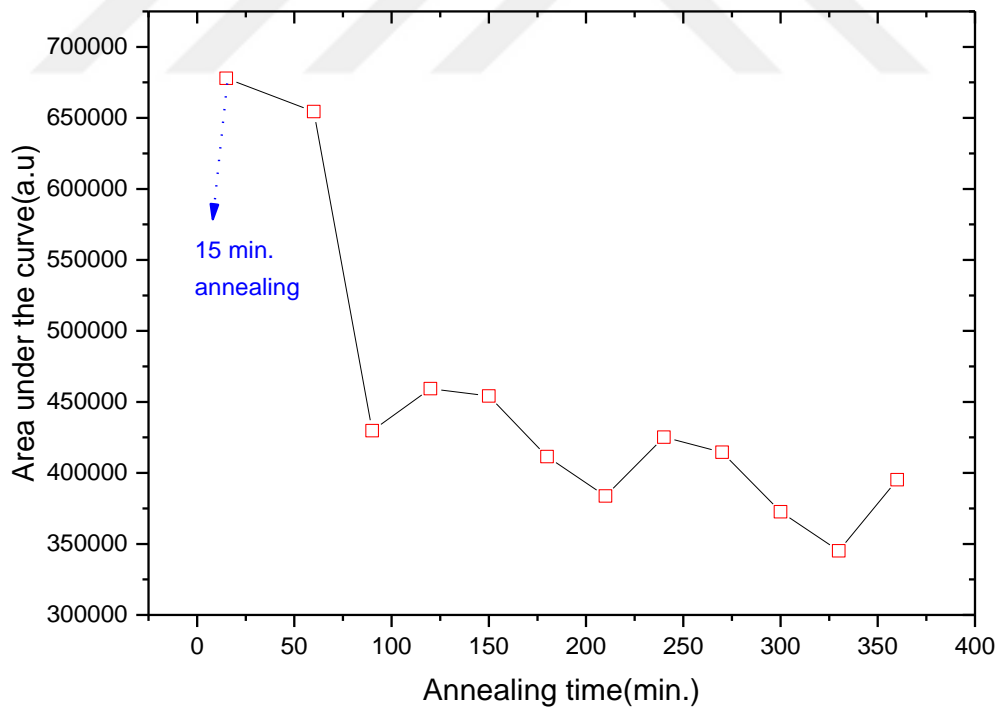


Figure 4.25 Variation of area under the glow curve as a function of annealing time at 900 °C.

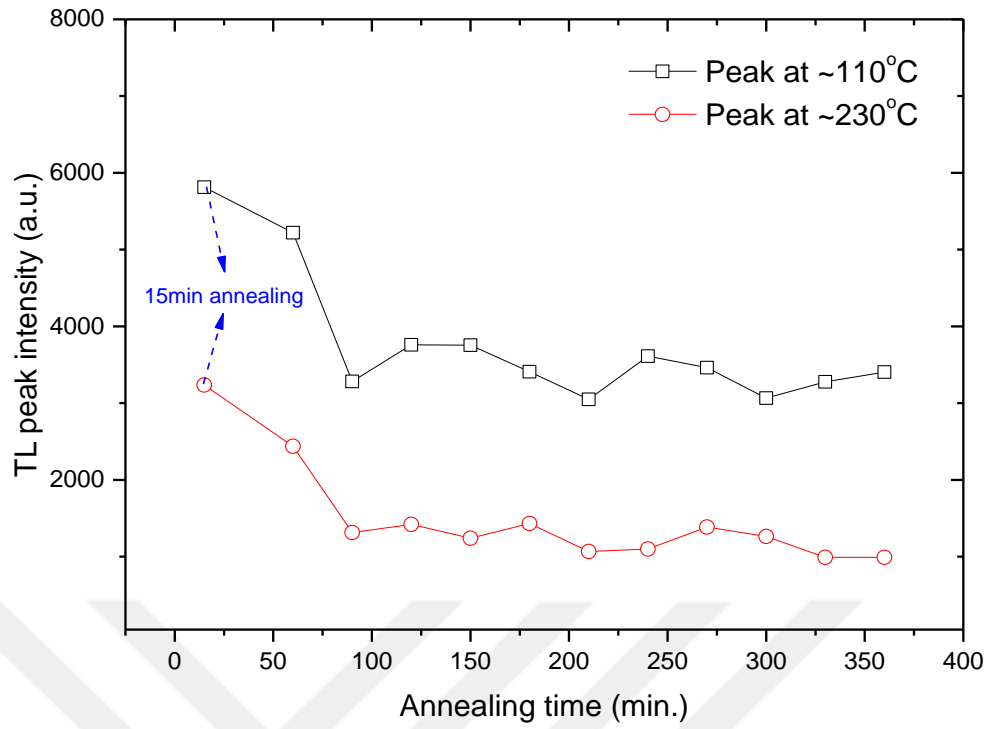


Figure 4.26 Variation of TL peak intensity as a function of annealing time at 900 °C.

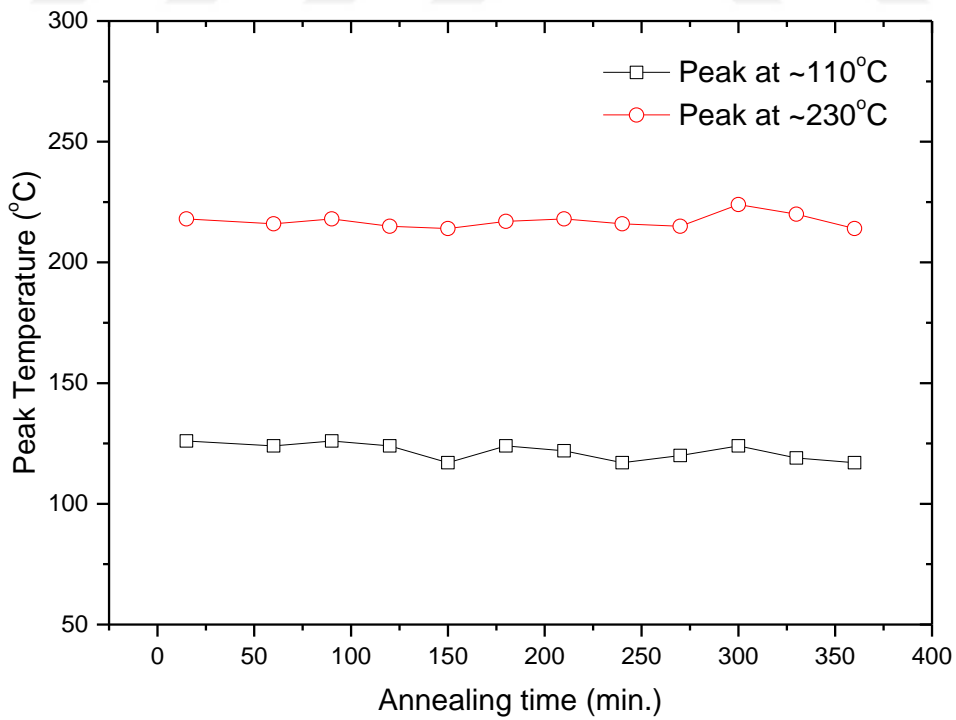


Figure 4.27 Variation of peak temperatures as a function of annealing time at 900 °C.

4.3.2 Fluorapatite Mineral ($\text{Ca}_5\text{F}(\text{PO}_4)_3$) in Tooth Enamel

The effects of different annealing times at fixed annealing temperature ($1000\text{ }^\circ\text{C}$) were carried out and shown in Fig. 4.28, 4.29, 4.30, and 4.31. In Fig. 4.28 and 4.31, it is seen that there is no important change in the shape of glow curve and TL peak temperature with the variation of annealing time except for 120 min. When the sample is annealed about 120 min, the peak temperature shifts to higher temperature region about $60\text{ }^\circ\text{C}$ and glow curve becomes wider. An increase is observed in the area under the curve with increasing annealing time, shown in Fig. 4.29. Especially, an incredible increase (about 660 times) is seen in the area under the curve when the result of un-annealed sample is compared with the sample annealed at $1000\text{ }^\circ\text{C}$ about 120 minutes. Furthermore, TL peak intensity increases with increasing annealing time shown in fig. 4.30.

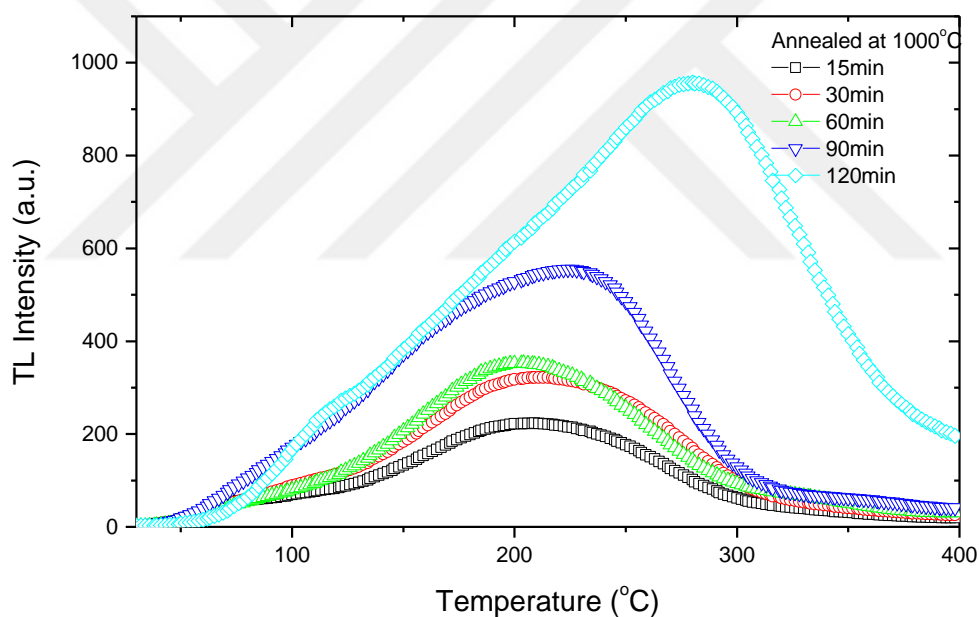


Figure 4.28 Effects of different annealing times at fixed annealing temperature ($1000\text{ }^\circ\text{C}$) on the glow curve.

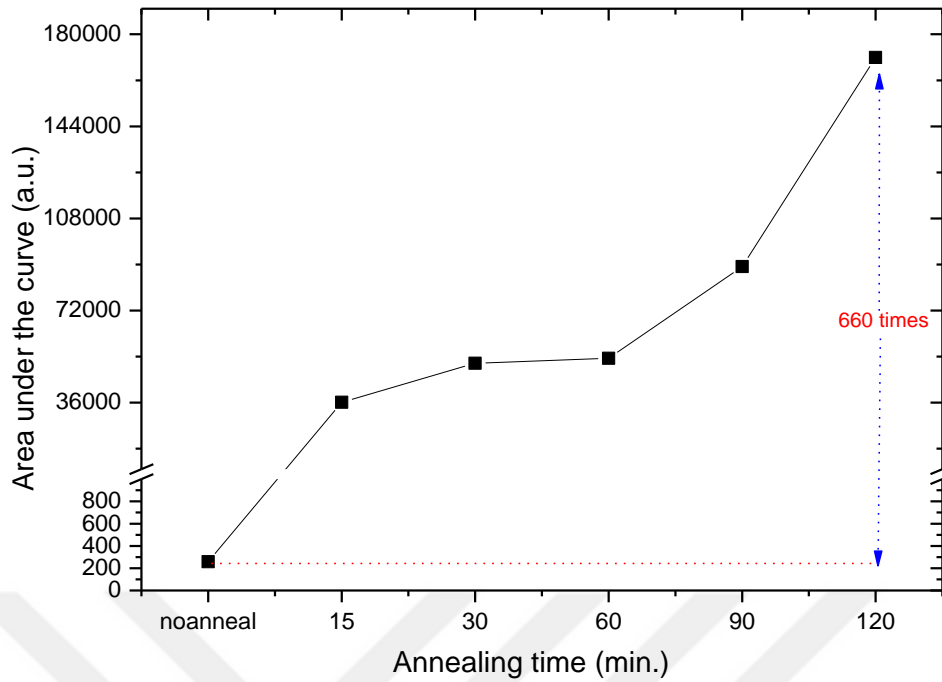


Figure 4.29 Effects of different annealing times at fixed annealing temperature (1000°C) on the area under the curve.

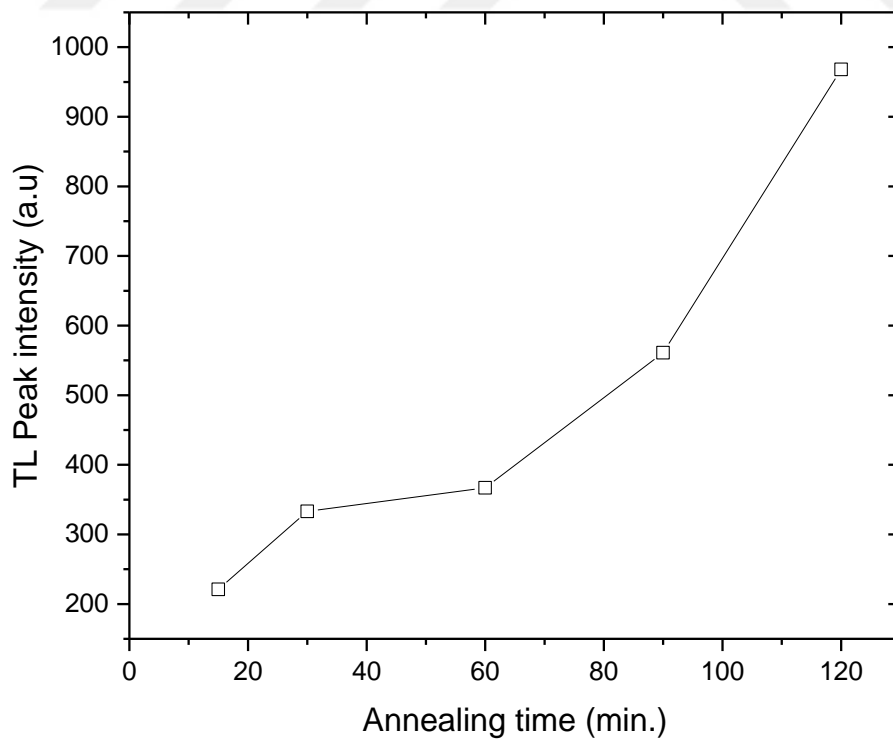


Figure 4.30 Effects of different annealing times at fixed annealing temperature (1000°C) on the TL peak intensity.

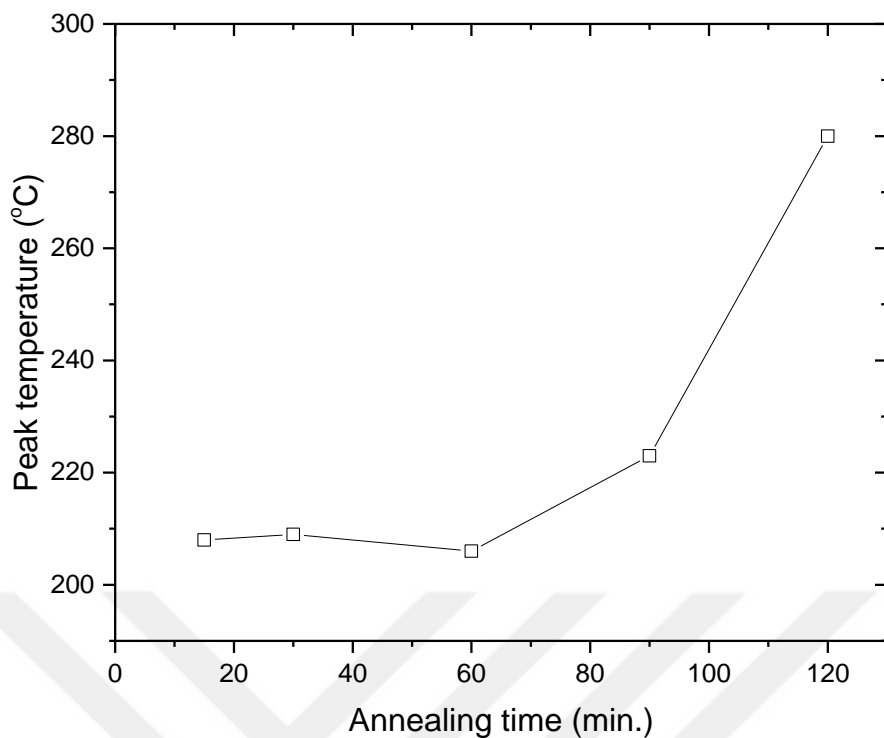


Figure 4.31 Effects of different annealing times at fixed annealing temperature (1000°C) on the TL peak intensity.

4.3.3 Biogenic Minerals Present in the Seashells

The effect of different annealing time on the TL glow curve for annealing time between 30 min-180 min and 240 min-360 min, area under the curve, TL peak intensity, and peak temperature of biogenic minerals present in the seashells are shown in Fig. 4.32-4.35. During these experiments, the samples were annealed at 700 °C. No appreciable variation in glow curve shape for annealing time has been observed between 60 min and 360 min annealing times seen in fig. 4.32a and 4.32b. As shown in Fig. 4.33 and 4.34, the largest area under the curve and TL peak intensities are seen at 180 min annealing time. Furthermore, the peak temperatures for low and intermediate peaks do not vary with increasing annealing time. But beyond 270 minutes annealing time, an increase is seen in the peak temperature of high temperature peak, as shown in Fig. 4.35.

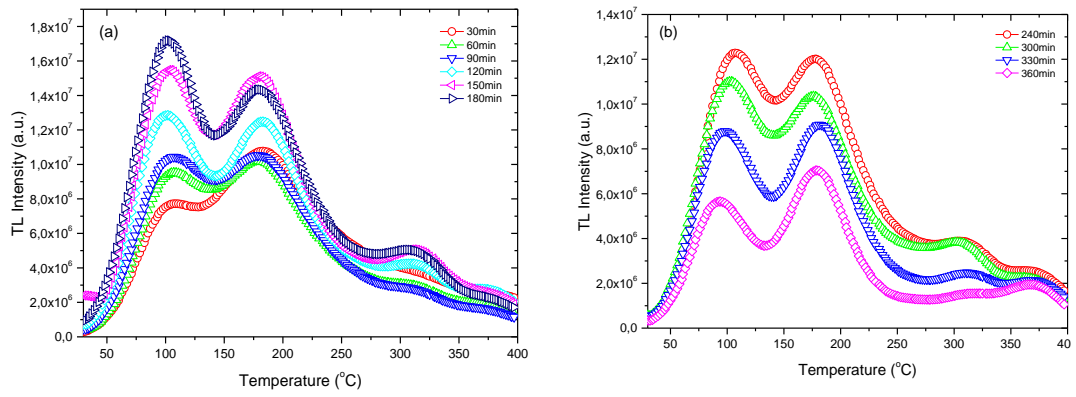


Figure 4.32 Effect of different annealing time on the TL glow curve for annealing time between (a) 30min-180min and (b) 240min-360min

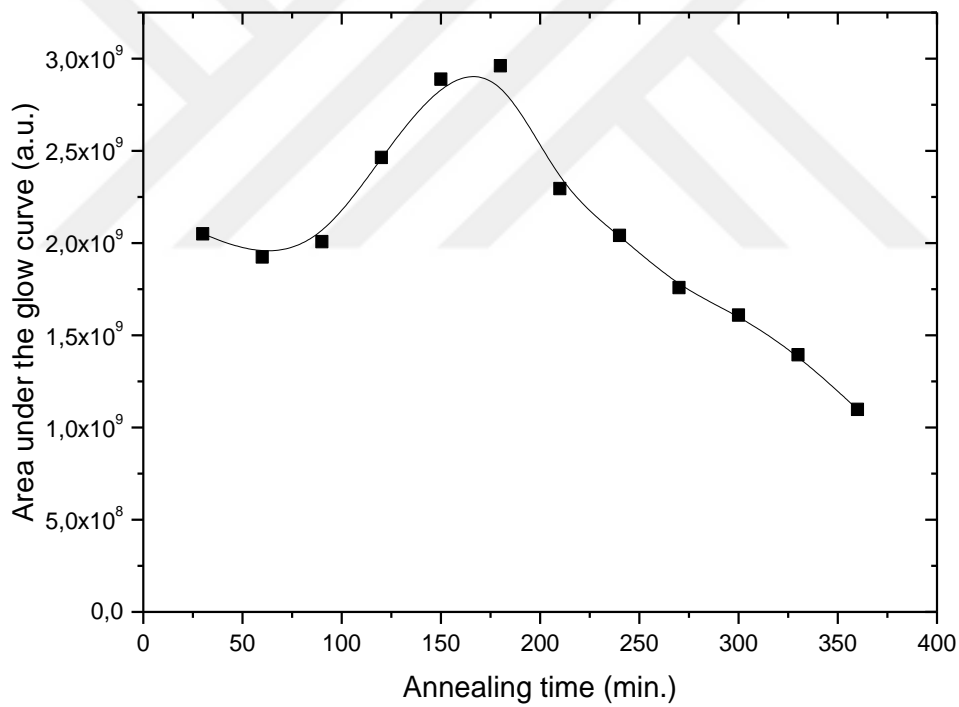


Figure 4.33 Effect of different annealing time on the area under the curve.

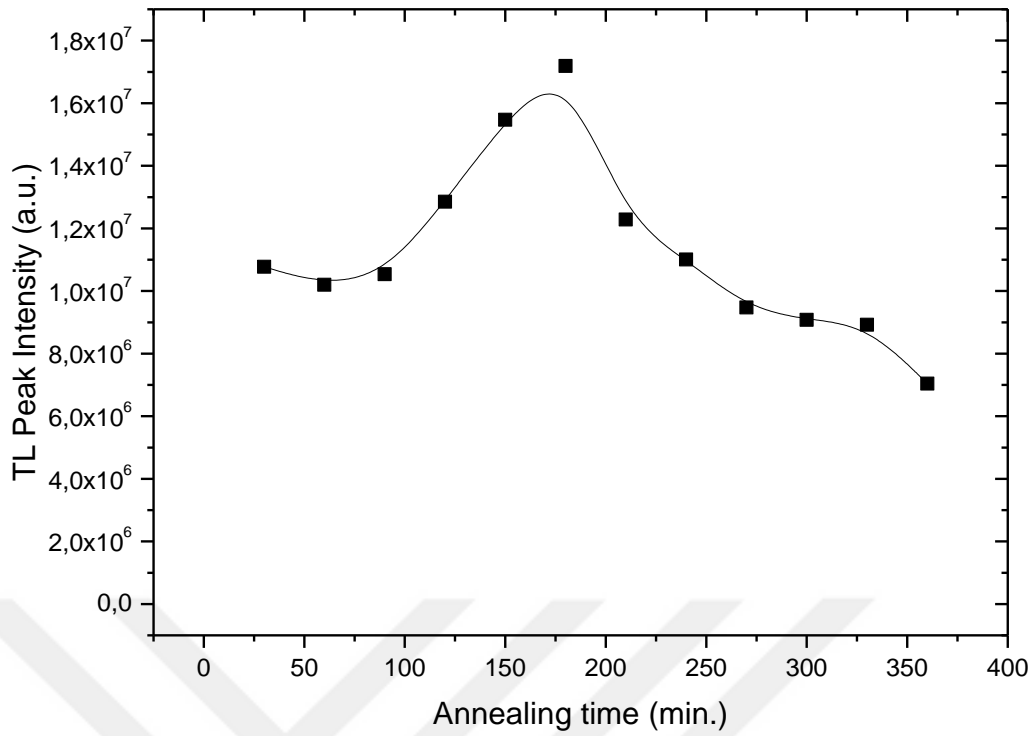


Figure 4.34 Effect of different annealing time on the TL peak intensity.

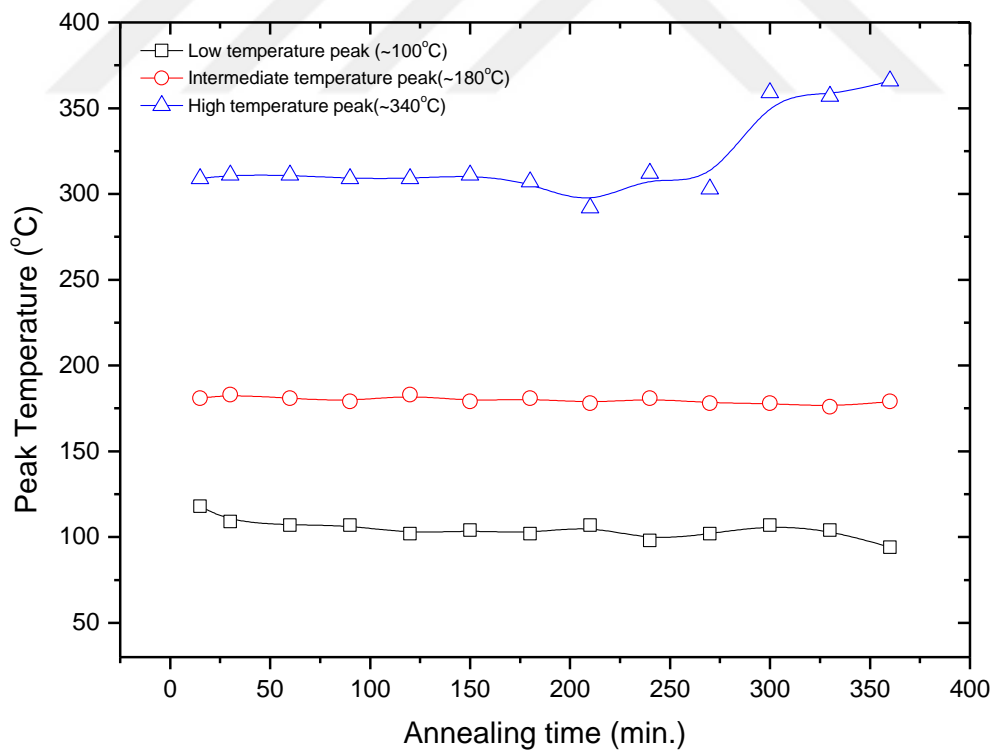


Figure 4.35 Effect of different annealing time on the peak temperature.

4.3.4 Plagioclase Minerals in Basaltic Rocks

It has been investigated that how annealing of sample at different annealing times affects TL glow curve, area under the curve, TL peak intensity, and peak temperature of plagioclase minerals in basaltic rocks given in figure 4.36-4.39, respectively. The all samples were annealed at 200 °C because the biggest value of area and TL peak intensity were observed at that annealing value. Annealing at different times does not affect the shape of TL glow curve shown in figure 4.36. Area under the curve and TL peak intensity show different behavior at different annealing time shown in figure 4.37 and 4.38. Firstly, they increase until 120 minutes and become stable between 120 and 240 minutes of annealing time. Then an abrupt decrease is seen at 270 minutes of annealing time. Again, they increase between 270 and 360 minutes of annealing times. But best TL sensitivity is observed between 120 and 240 minutes of annealing times. In the annealing time experiment, the peak temperature fluctuates between 196 and 207°C shown in figure 4.39.

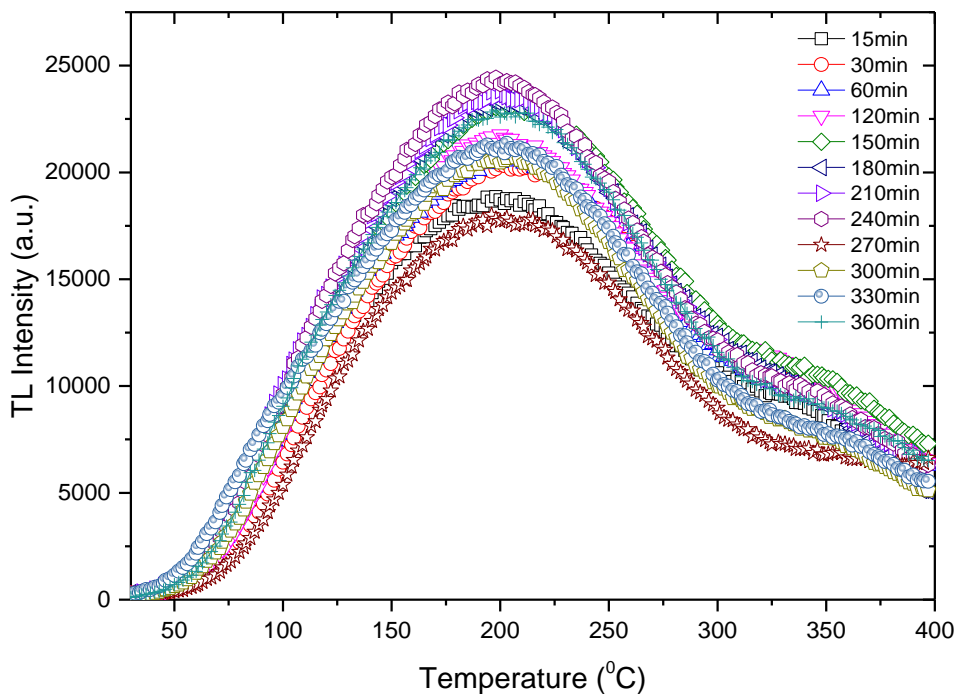


Figure 4.36 Variation of TL glow curve as a function of annealing time at 200 °C.

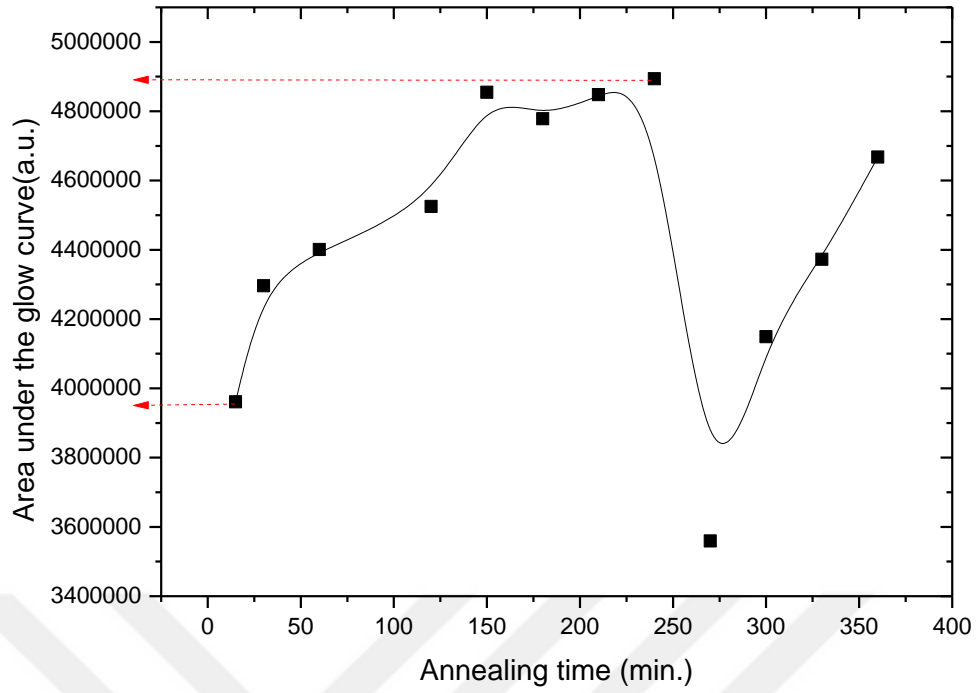


Figure 4.37 Variation of area under the curve as a function of annealing time at 200°C.

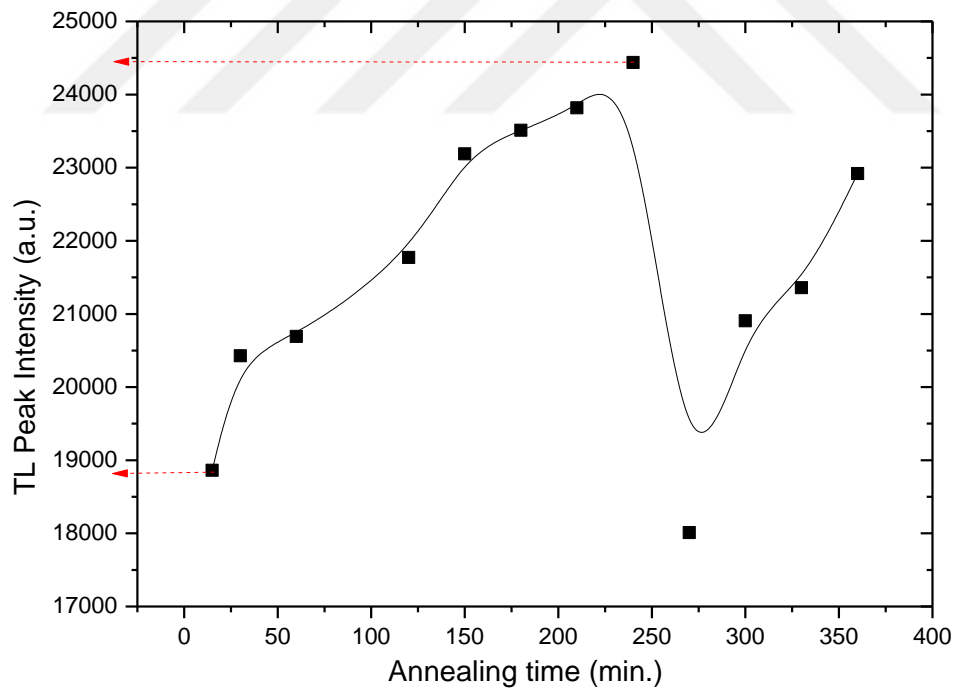


Figure 4.38 Variation of TL peak intensity as a function of annealing time at 200°C.

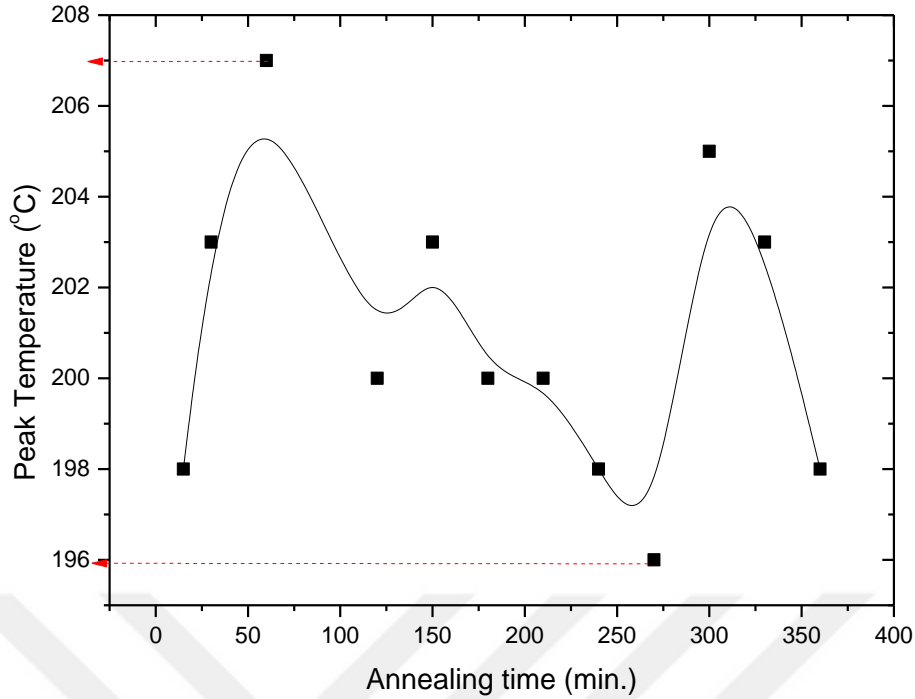


Figure 4.39 Variation of peak temperature as a function of annealing time at 200 °C.

4.4 Reproducibility at Different Annealing Temperatures

Reproducibility (Cycle of Measurement) is an important parameter for a dosimeter. For each cycle of measurement, the same result is wanted for a good dosimeter. Standard deviations in all figures were calculated by using the following equation:

$$\sigma = \sqrt{\frac{\sum_i (X_i - M)^2}{n-1}} \quad (4.1)$$

where X is individual experiment, M is mean of measurement and n is number of measurements.

4.4.1 Calcite Extracted from Natural Sand Used in Making Roasted Chickpea

Fig. 4.40, 4.41, and 4.42 show the normalized area under the glow curve versus cycle of measurement for annealed sample between 200 and 400 °C, 500 and 700 °C and 800 and 1100 °C for 30minutes duration. Especially, at higher annealing temperature between 900 and 1100 °C the worst reproducibility is obtained.

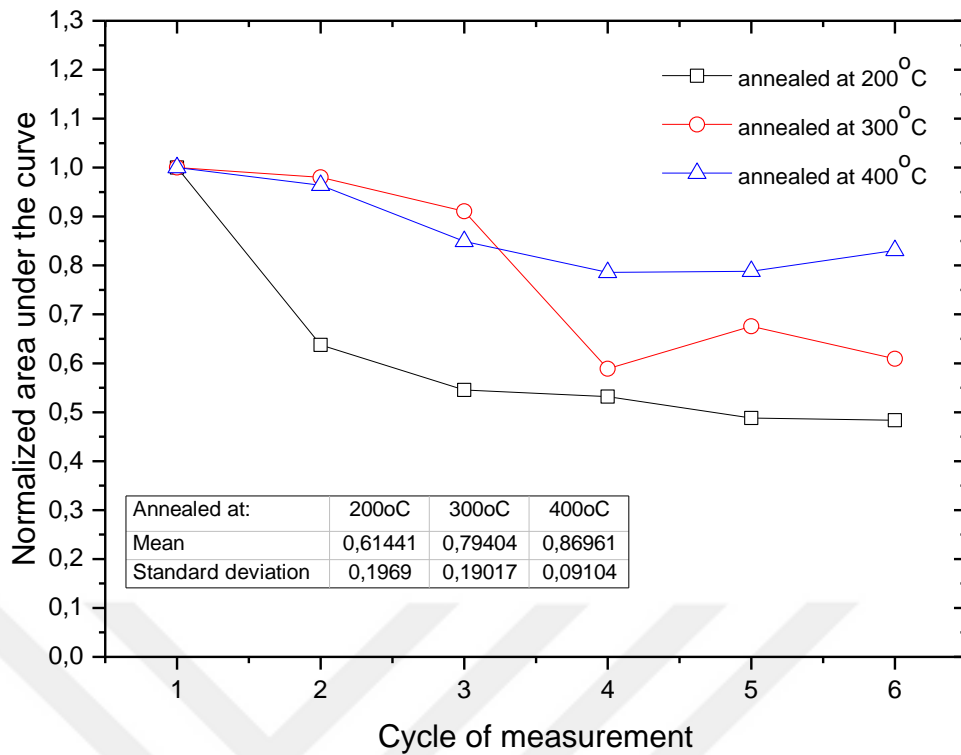


Figure 4.40 Normalized area under the glow curve versus cycle of measurement for annealed samples between 200°C-400°C.

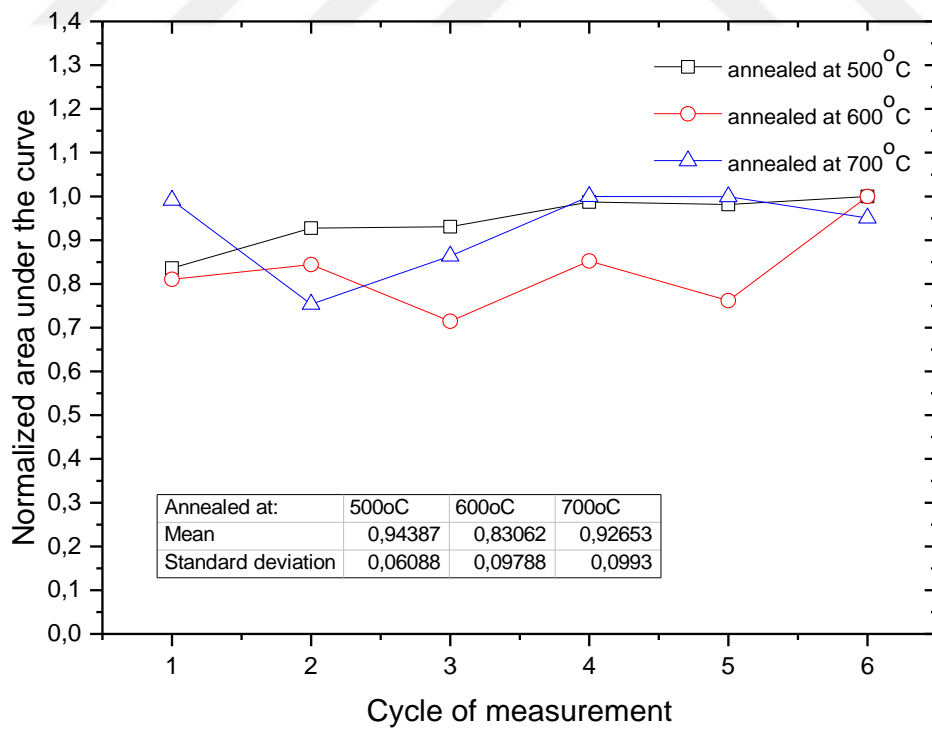


Figure 4.41 Normalized area under the glow curve versus cycle of measurement for annealed samples between 500°C-700°C.

At the end of sixth cycle of experiment, the area under the curve decreases by about 80% from its initial value shown in Fig.4.42. On the other hand, the best reproducibility is seen when the samples are annealed between 400 and 600 °C shown in Fig. 4.40 and 4.41. The area under the glow curve varies only 10% from its initial value.

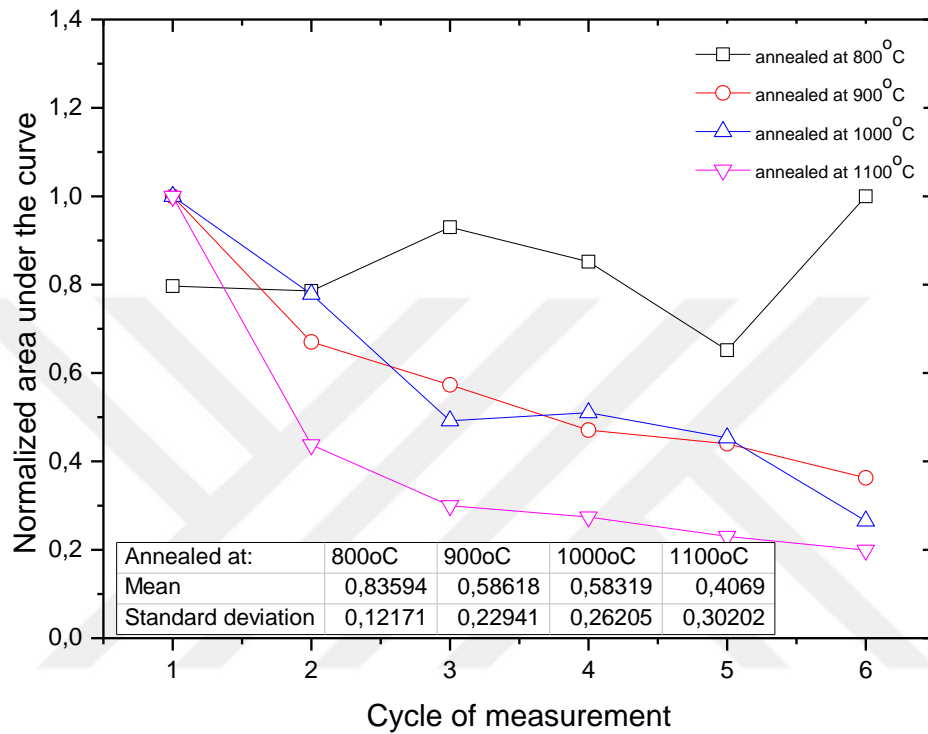


Figure 4.42 Normalized area under the glow curve versus cycle of measurement for annealed samples between 800°C-1100°C.

4.4.2 Fluorapatite Mineral (Ca₅F(PO₄)₃) in Tooth Enamel

Fig. 4.43-4.48 show the reproducibility of the sample at different annealing temperature at fixed annealing time (30 min) before irradiated 36 Gy and standard deviation of each experiment. It is seen that the best reproducibility is obtained when the sample is annealed at 1000 °C whereas the worst reproducibility is obtained at 900 °C. However, the reproducibility of the sample annealed at 700 °C is good but no satisfying results are obtained in the reproducibility of sample annealed at 600 °C, 800 °C and 900 °C.

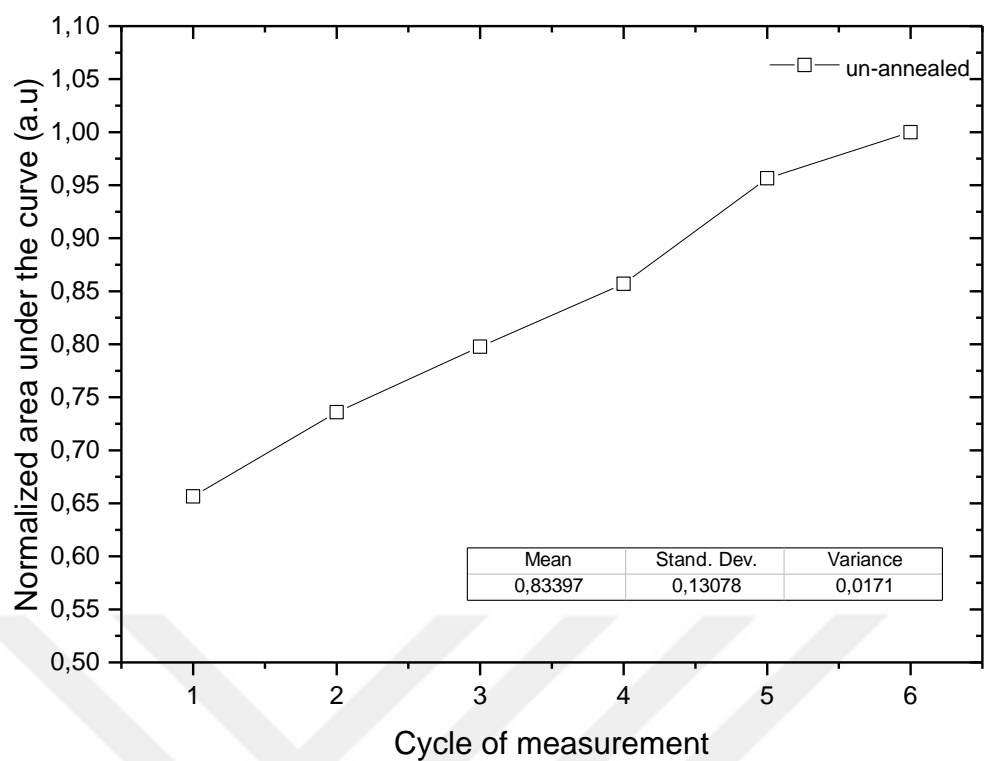


Figure 4.43 Reproducibility of the un-annealed sample at fixed annealing time (30 min) and standard deviation.

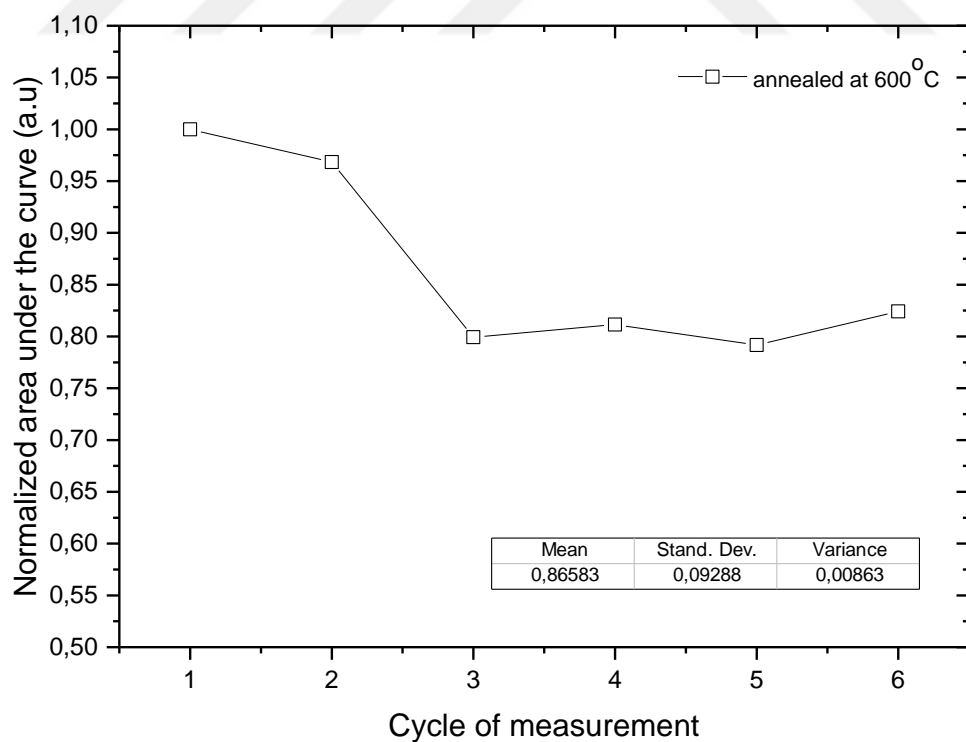


Figure 4.44 Reproducibility of the sample annealed at 600°C at fixed annealing time (30 min) and standard deviation.

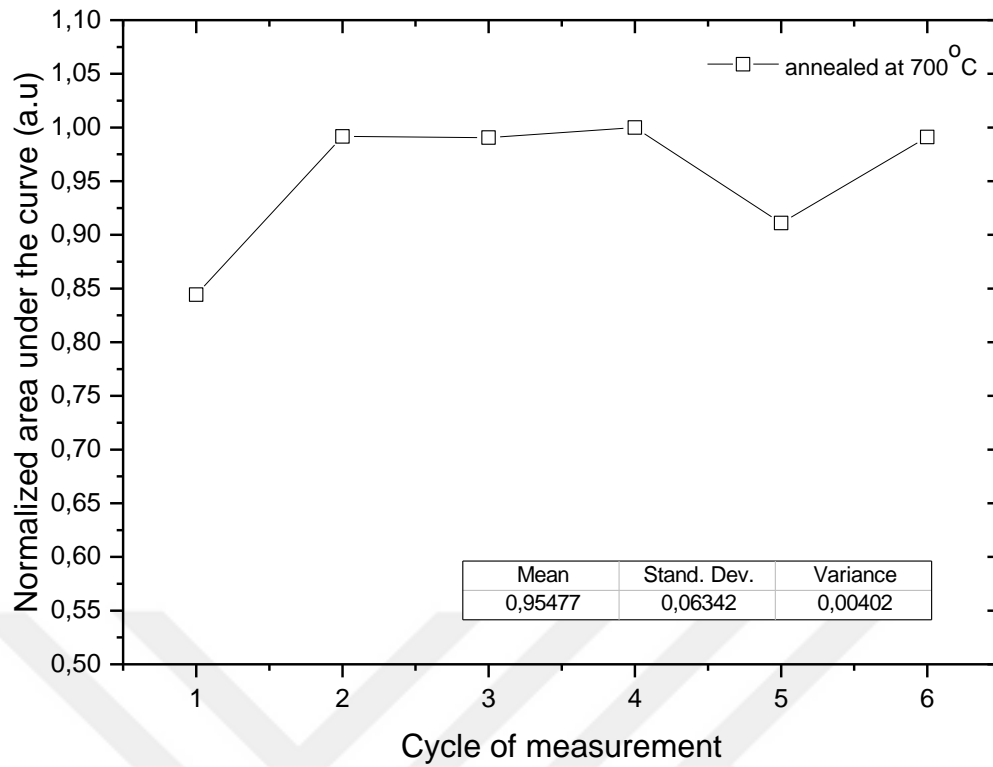


Figure 4.45 Reproducibility of the sample annealed at 700°C at fixed annealing time (30 min) and standard deviation.

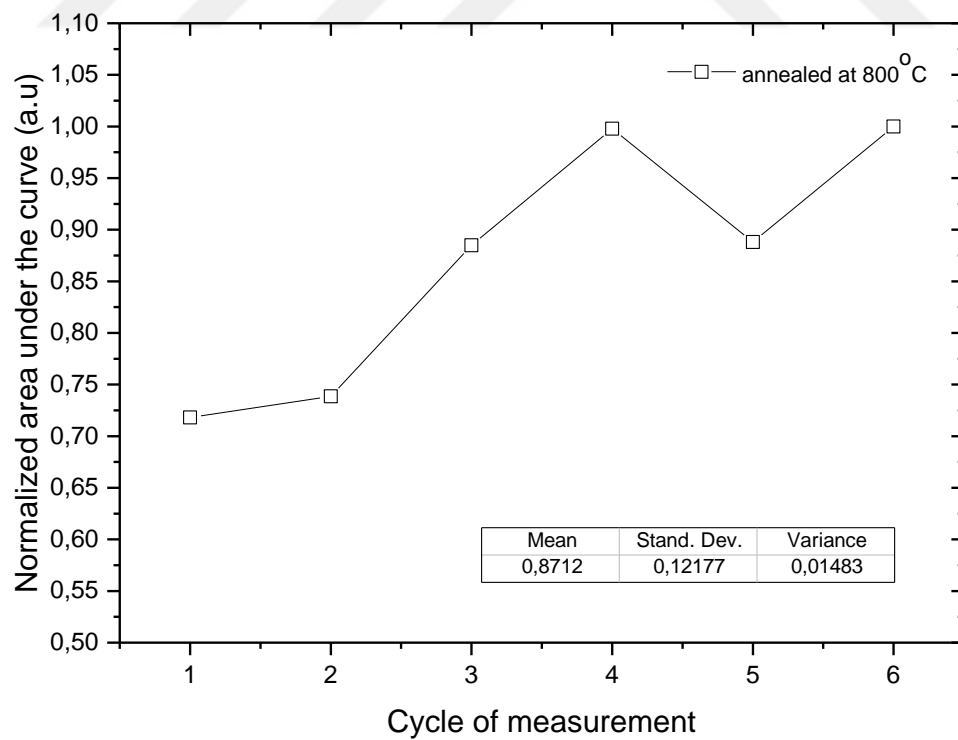


Figure 4.46 Reproducibility of the sample annealed at 800°C at fixed annealing time (30 min) and standard deviation.

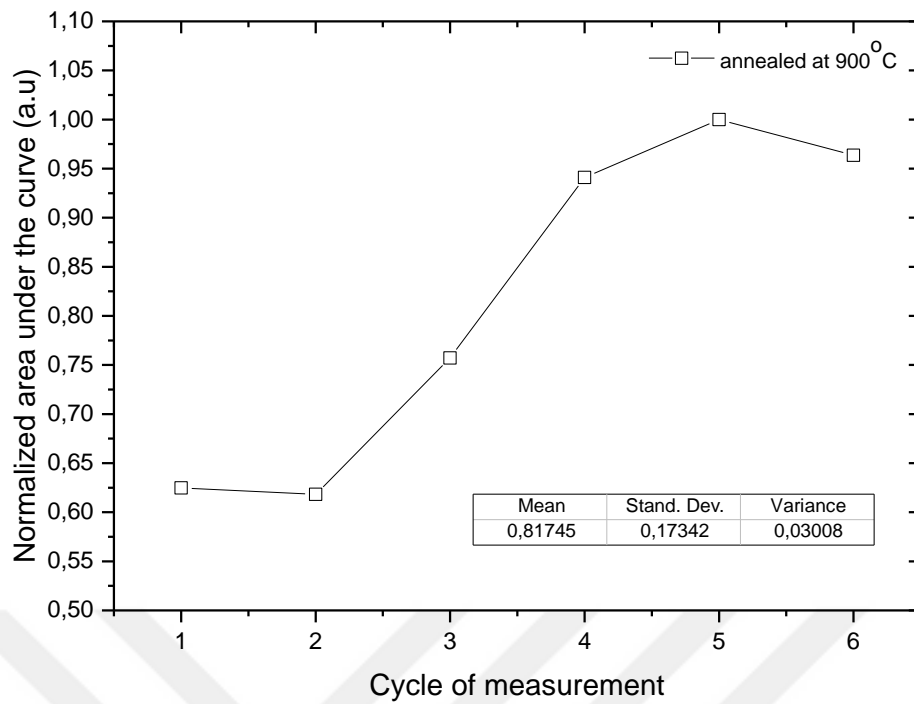


Figure 4.47 Reproducibility of the sample annealed at 900°C at fixed annealing time (30 min) and standard deviation.

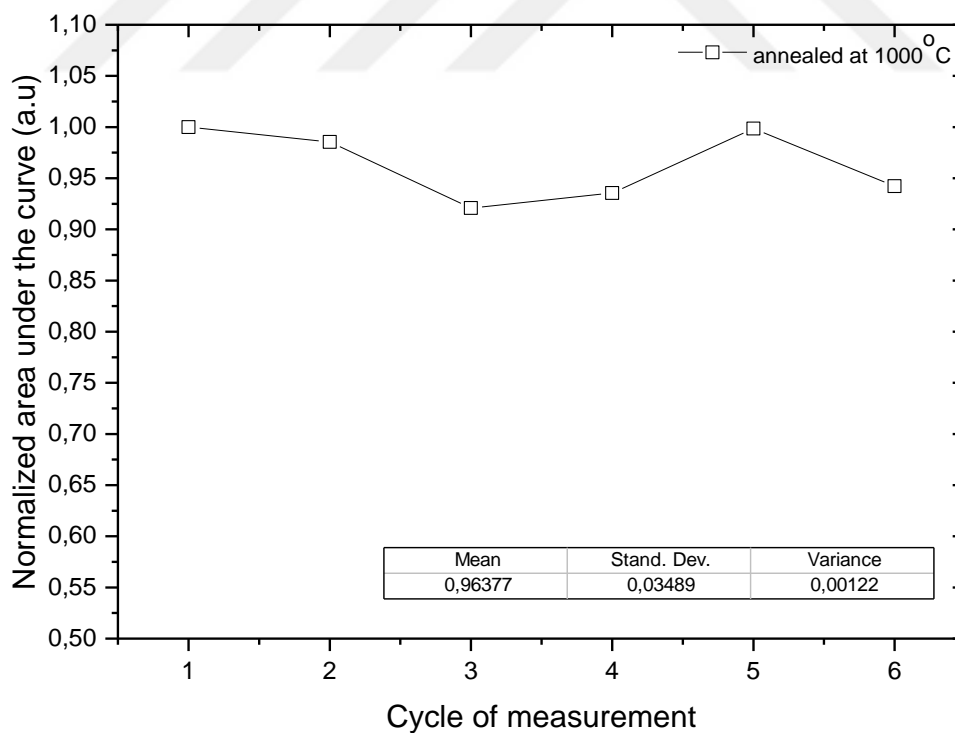


Figure 4.48 Reproducibility of the sample annealed at 1000°C at fixed annealing time (30 min) and standard deviation.

4.4.3 Biogenic Minerals Present in the Seashells

The experiments have been done to see that the effect of reproducibility of the sample on the normalized area under the glow curve at different annealing temperatures shown in Fig. 4.49 and 4.50. It is important that samples show the same sensitivity to the radiation dose for every measurement.

Firstly, the samples were annealed at fixed temperature for 30 minutes. Then they were irradiated for about 36 Gy and read out. After then they were repeated six times for each annealing time above increasing the annealing temperature of 100 °C from 500 °C till 1100 °C. Fig. 4.49 and 4.50 show the normalized area under the glow curve versus cycle of measurement for annealed samples between 500 and 700 °C, 800 and 1100 °C.

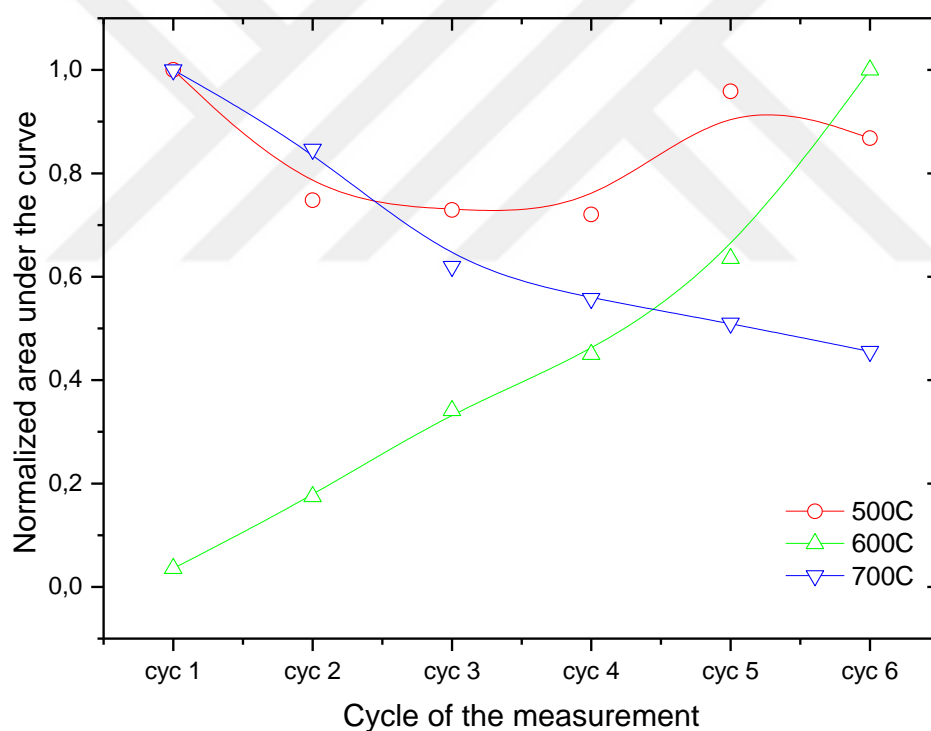


Figure 4.49 Normalized area under the glow curve versus cycle of measurement for annealed samples between 500 °C and 700 °C.

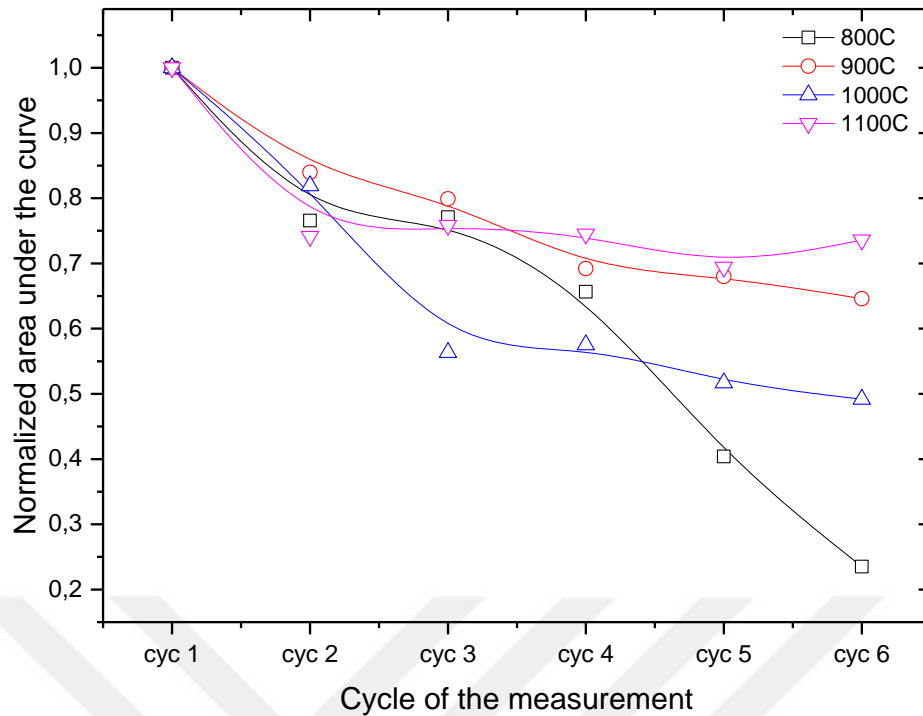


Figure 4.50 Normalized area under the glow curve versus cycle of measurement for annealed samples between 800 °C and 1100 °C.

The fluctuations in the normalized areas are seen in figure 4.49 and 4.50 and means are 0.83, 0.49, 0.67, 0.63, 0.77, 0.66 and 0.78 for annealing time of 500 °C, 600 °C, 700 °C, 800 °C, 900 °C, 1000 °C, and 1100 °C, respectively. The best reproducibility was seen at 500 °C annealing temperature.

4.4.4 Plagioclase Minerals in Basaltic Rocks

The normalized area under the glow curve versus cycle of measurement for annealed samples between 200°C-400°C, 500°C-700°C and 800°C-1100°C are shown in figure 4.51-4.53. As seen in figure 4.51-4.53 and table 4.1, the best reproducibility is seen at 500°C of annealing temperature. At this annealing temperature, mean value of normalized area under the curve and standard deviation are 0.893 and 0.0598, respectively.

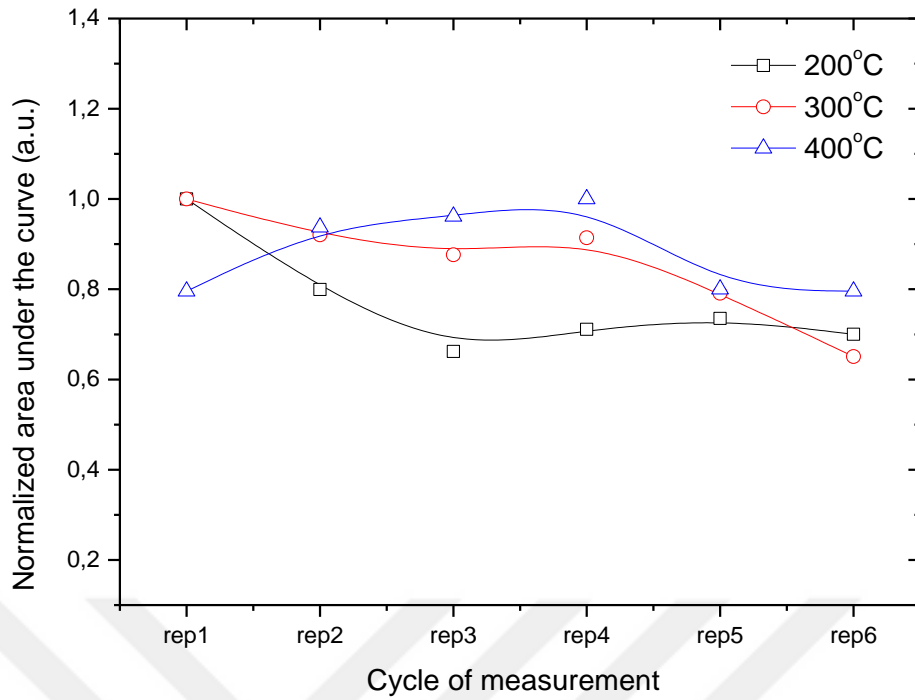


Figure 4.51 Normalized area under the glow curve versus cycle of measurement for annealed samples between 200°C-400°C.

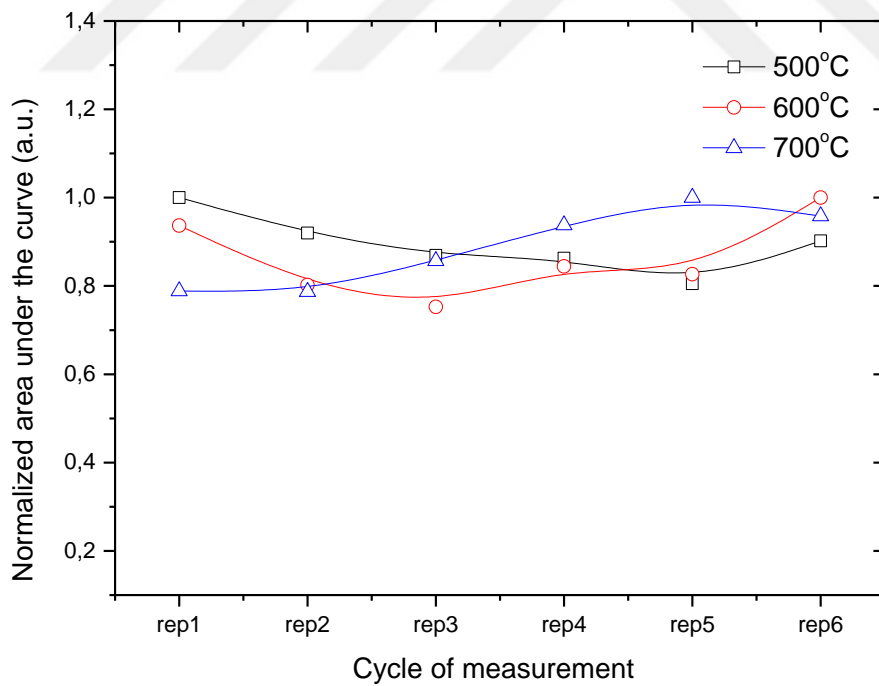


Figure 4.52 Normalized area under the glow curve versus cycle of measurement for annealed samples between 500°C-700°C.

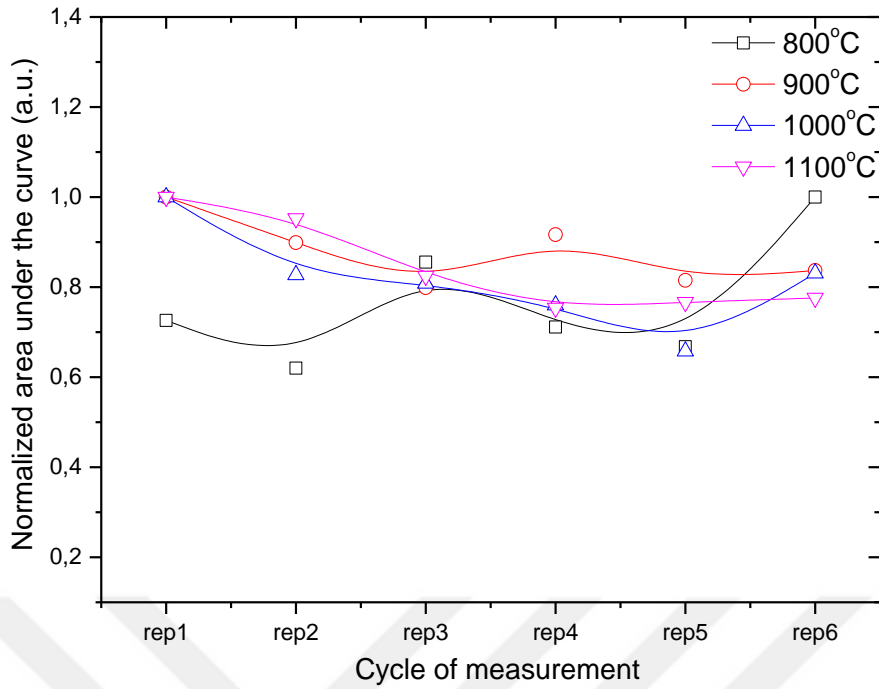


Figure 4.53 Normalized area under the glow curve versus cycle of measurement for annealed samples between 800°C-1100°C

Table 4.1 Mean and standard deviation of normalized area under the curve for different annealing temperature

Annealing Temperature	Mean of Normalized Area	Standard Deviation
200°C	0.767998	0.11177
300°C	0.858865	0.111701
400°C	0.881655	0.086625
500°C	0.893088	0.059854
600°C	0.860408	0.083396
700°C	0.888037	0.082723
800°C	0.763382	0.128009
900°C	0.877761	0.069189
1000°C	0.814043	0.101943
1100°C	0.845503	0.096027

CHAPTER 5

DISCUSSION AND CONCLUSION

Many thermoluminescence properties of dosimetric minerals may be affected by external effects and environmental condition. Annealing is one of the most known external effects and has different process. As a result of annealing process, the defect distribution of a specimen can be altered and thereby its sensitivity changes. In spite of fact that standard annealing procedures exist for the dosimetric purposes of the synthetic materials, these can be different for natural minerals. As the thermoluminescence properties of different natural minerals are unequal, different thermoluminescence properties are observed for the same natural minerals collected in the different region of the world. Therefore, annealing may alter the thermoluminescence properties of each natural minerals, differently.

This thesis reveals that how the thermoluminescence properties of different natural minerals are affected by different pre-irradiation annealing processes. The origins of natural minerals used in this thesis were different and obtained from the different regions of Turkey. The four different natural minerals which are calcite minerals in sand used in making roasted chickpea, fluorapatite minerals in tooth enamel, plagioclase minerals in basaltic rocks and biogenic minerals in seashell have been studied under different thermal treatments.

The XRD analysis of all samples were taken from Boğaziçi University Advanced Technologies R&D Center with the Rigaku D/MAX-Ultima+/PC X-ray diffraction equipment. According to the results of the XRD analysis, the main ingredient of the sand sample, tooth enamel, seashell and basaltic rocks are calcite (CaCO_3), fluorapatite ($\text{Ca}_5\text{F}(\text{PO}_4)_3$), biogenic minerals (Calcium Carbonate and Lime) and plagioclase minerals (Albite and Anorthite), respectively.

The TL glow curve obtained from the sand sample has two distinct TL peaks were observed at $\sim 110^\circ\text{C}$ and $\sim 230^\circ\text{C}$. And also, third peak is seen at $\sim 330^\circ\text{C}$ but has small intensity. This peak is due to the lattice defect not by any other impurity contents [82-

84] Marshall et al. [85] stated the low temperature peak (smaller than 200°C) is associated with migration of the CO_3^{3-} electron center and the intermediate TL peak is also associated with the destruction of the $\text{CO}_2^- \text{F}^-$ center. Macedo et al. [86] reported that the Mn^{2+} was the main luminescence center in calcite.

Fluorapatite $\text{Ca}_5\text{F}(\text{PO}_4)_3$ is a kind of important thermoluminescence dosimeter (TLD) material, because the effective atomic number of fluorapatite is close to that of human bones and teeth. Fluorapatite mineral obtained from the tooth enamel has wider TL glow curve with a peak around 230 °C.

The shellfish is one of the mollusc and its exoskeleton, called as seashell, is mainly composed of calcium carbonate minerals with very minute traces of silicate minerals. Seashell is used in lime-stone to acquire, animal feed mixtures, road construction, some chemical treatments, and the manufacture of the prosthesis and implant dentistry. Three explicit peaks are seen in the glow curves roughly at 100 °C, 180 °C, and 380°C.

Basalt is well known as an extrusive igneous rock erupts on land by volcanic eruption in a wide variety of mineral compositions and important sample for investigation of luminescence dating for formation of Martian surface [70]. It is darker, denser and finer grained compared to the familiar granite of the continents. Due to wide variety of mineral compositions, these materials display a TL glow curve with a broad peak with continuous distribution of trapping centers [73].

The plagioclase mineral group found in basaltic rocks is a kind of the two main feldspar series that have the same formula but vary in their percentage of sodium and calcium in the same crystal structure. The plagioclase feldspar subgroup consists of a continuous mineral series that is arbitrarily subdivided into six mineral categories whose composition varies from being relatively pure sodium aluminum silicate (albite) to a relatively pure calcium aluminum silicate (anorthite). Albite and anorthite are the end members of the plagioclase minerals.

Some researchers [71, 87-91] carried out the TL properties of plagioclase minerals. Huntley and Lian [71] reported fading rates for both alkali and plagioclase feldspars. They showed a correlation between fading rate and calcium content for plagioclase feldspars. Spooner [87] showed that Ca-rich plagioclase exhibits low luminescence efficiency. Huot and Lamothe [88] hypothesized that plagioclase minerals, possibility

Na-rich dominated the luminescence. Hashimoto et al. [89] mentioned that some albite (Na-feldspar) minerals displays a strong blue luminescence emission. Can et al. [90] investigated that the thermoluminescence (TL) and radioluminescence (RL) spectra in albite, which is a component of the two main feldspar series, the alkali feldspar (Na, K)AlSi₃O₈ and the plagioclases (NaAlSi₃O₈-CaAl₂Si₂O₈). In the study of Correcher et al. [91], the use of albite as a dosimeter in accident dose reconstruction was investigated. In their study, the TL emission spectra from albite (NaAlSi₃O₈) shows two characteristic bands peaked at 290 and 390 nm. At these bands, different glow curves presenting rather broad glow peaks are detected.

Plagioclase feldspars are expected to be the phosphor responsible for the main contribution of the total TL because, it is the most abundant mineral phase in these volcanic rocks, it has no iron in this lattice that can act as a TL inhibiting in the UV-blue region and the feldspar group displays the most intense glow TL signals. These naturally 'preheated' materials during recent times are homogeneous samples with a large grade of Al/Si disorder [73]. The basalt sample used in this thesis shows thermoluminescence properties with a wide peak about 200°C. Albite (NaSi₃AlO₈), anorthite-sodian (Na_{0.48}Ca_{0.52}Al_{1.52}Si_{2.48}O₈), cristobalite (high temperature polymorph of silica) and quartz (SiO₂) are the four main minerals in the basaltic rock sample.

Before starting to the annealing process, the best grain size which gives the best TL output light were obtained for these minerals. Due to lack of tooth enamel, the grain size experiment of tooth enamel wasn't carried out. The summary of grain size experiment for these three minerals are given in Table 5.1. As a result of grain size experiment, peak temperature doesn't vary for each mineral. The glow curve shapes of calcite and plagioclase minerals don't change except biogenic minerals. It means that while trap position in the forbidden band gap does not affected by the grain size, no extra peak is produced or vanished. And also, maximum area under the glow curves were seen between 100 µm and 250 µm.

The various studies [92-95] were done to observe grain size effect on TL glow curve of a dosimeter. Generally, they observed an increasing in the TL output with decreasing grain size. This increase in TL output is due to the bigger ratio of surface area per volume of grain [94]. According to their studies, carriers from surface traps cause an increase in TL output during heating process. G.D. Zanelli et al. [92]

underlined the increasing of TL output with decreasing grain size depends also on energy of the output of monochromatic x-rays.

After obtaining the best grain size, the TL properties of that minerals were investigated under the pre-irradiation thermal treatments (annealing).

The pre-irradiation thermal treatment (annealing) with three different experiments were done to see the effects of different annealing temperatures and different annealing times on TL glow curve, area under the curve, TL peak intensity and peak temperature and also reproducibility of the sample at different annealing temperatures.

Table 5.1 Summary of grain size experiment for the natural minerals used in the thesis.

	Glow Curve Shape	Peak Temperature	Maximum Area under Glow Curve
Calcite Extracted from Natural Sand Used in Making Roasted Chickpea	doesn't change	doesn't change	100 μm
Biogenic Minerals Present in the Seashells	change	doesn't change	250 μm
Plagioclase Minerals in Basaltic Rocks	doesn't change	doesn't change	100 μm

The first part of the thermal treatments (annealing) was done to see that how TL properties of the four natural minerals are effected by different annealing temperatures.

In the sand sample, it is seen that the shape of glow curve the sand sample varies at each annealing temperature shown in Fig. 4.7. Two peaks are well separated from each other at higher annealing temperatures ($>900^{\circ}\text{C}$). The area under the curve and maximum TL peak intensity increase tremendously beyond 600°C annealing

temperature shown in Fig. 4.8 and 4.9. Annealing at 900°C causes an enhancement in the area under the curve and TL peak intensity about 70 times when it is compared with no-annealed sample. This is also known as enhancement in sensitization. Sensitization is a term used to indicate an increase of sensitivity in a TL sample [24, 96, 97]. In literature, a huge increase was generally observed in TL output when the sample was annealed [98-101]. Particularly, this is observed in 110 °C TL peak of natural quartz and named as pre-dose effect [98]. The pre-dose sensitization is believed to be due to an enhanced probability of radiative recombination at the luminescence site due to transfer of holes from so-called reservoir centers to luminescence center [98]. Zimmerman proposed that competition traps where the deeper traps were partially removed during the thermal treatment. An alternate proposition to explain the mechanism of sensitization in which competing traps to the electron traps get filled by irradiation and post-irradiation thermal treatment has been suggested by Chen et al. [99] and Yang and McKeever [100]. Thermal treatment of the calcite was carried out by Engin et al. [102] Ponnusamy et al. [82], Soliman et al. [103] and Down et al. [104]. In their studies, the intensities of low and intermediate temperature peaks are increased with increase of annealing temperature up to 600 °C except high temperature peak but the intensities collapsed at 700 °C. This sensitization in TL output is due to the similar ionic motion taking place when the sample is heated at high temperatures and the atomically dispersed “Mn” ions present at high temperatures act as more efficient luminescence center than the low temperature defect complexes. Engin et al. [102] concluded that an increase in the number of luminescent ions approaching the recombination center is expected due to diffusing of impurity ions through the lattice when the crystal is heated. And also, they pointed out the increase in luminescent efficiency by heat treatment may be attributed to a reduction in the distance between recombination center and the luminescent center [105] as accomplished by diffusion of activator ions.

In the study of annealing of sand sample at different temperatures, it is also concluded that peak temperatures of TL peaks shift to higher temperature region with increasing annealing temperature shown in Fig. 4.10. Particularly, an increase is observed in peak temperatures of ~110°C peak and ~230°C peak about 30°C and 60°C, respectively, between annealing temperatures 200°C and 800°C. Annealing at 900°C about 15min gives a good glow curve shape with two distinct peaks, the biggest area under the curve

and maximum TL intensities. The increasing in annealing temperature may cause trap conversion. The shallow traps become deeper traps with increasing annealing temperature.

The pre-irradiation annealing processes at different temperatures cause to change in TL glow curve shape of fluorapatite minerals in tooth enamel seen in Fig. 4.11 and 4.12. At higher annealing temperatures, the number of distinct peak in the glow curve decreases to single peak which is located around 230°C. The possible reason may be change of position of the defects due to the annealing of sample at different pre-irradiation temperatures. This is also probably explained by thermal alkali self-diffusion through the lattice interfaces [106]. Besides, a huge increase (about 160 times) was observed in maximum TL intensities and area under the glow curve when the un-annealed sample was compared with the sample annealed at 1100°C. The annealing may cause an increase of the trap concentrations, especially at higher temperatures.

At the beginning of the studies in the powdered seashell sample, it was irradiated by a $^{90}\text{Sr}/^{90}\text{Y}$ beta source and read out without any thermal treatment. Unfortunately, no consequential TL output was observed except two peaks seen around 120°C and 230°C with incredible small peak intensities. When the sample is annealed at different annealing temperatures before irradiating and same dose was applied as unannealed case, a huge increase was observed in TL peak intensity. This increase was reported as 1500 times of unannealed case at 700 °C annealing temperature seen in figure 5.1.

As seen in fig. 5.1, the annealing affects extremely the glow curve shape and TL intensity. TL intensity increases about 1500 times when it is annealed at 700°C after irradiating 36Gy. The annealing at higher temperatures generates new traps and their capacities increase with annealing. Increasing in available trap center and recombination center increases the TL intensity.

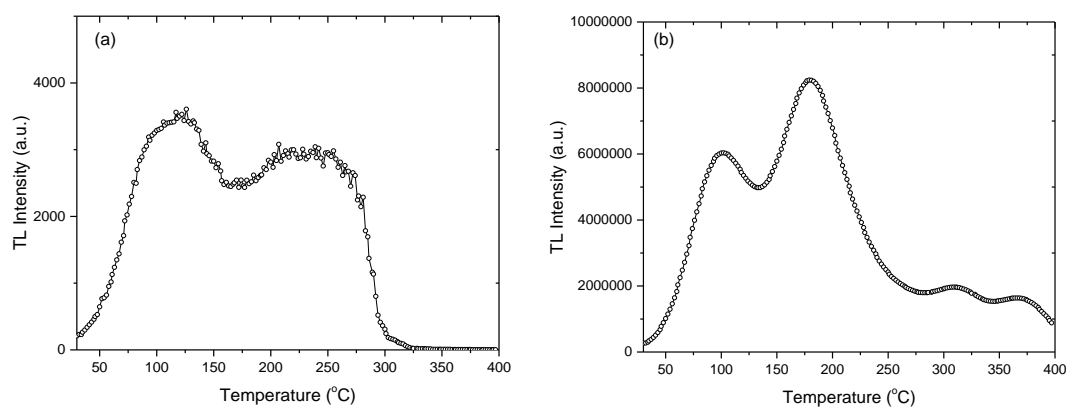


Fig.5.1 The glow curves of (a) unannealed and (b) annealed seashell samples at 700°C after irradiating 36Gy.

Another important result is that the same glow curves of annealed sample was obtained when it was reused after one day without any thermal treatments. The glow curve of the sample didn't return to its original case (unannealed). When the XRD results given in figures 3.12 and 3.13, tables 3.3 and 3.4 are examined, the aragonite and norshetite minerals are present in the unannealed seashell sample. The annealing changes its structure and calcium carbonate (CaCO_3) and calcium oxide (CaO) are found. Aragonite is a form of calcium carbonate (CaCO_3) and seen in its nature form. It has been named for its first-noted occurrence in the Aragon region, Spain and found in a wide range of geologic environments. Aragonite (density 2.95 g/cm^3) is denser than calcite (density 2.71 g/cm^3) and should thus be a higher-pressure form of CaCO_3 than calcite. Natural aragonite on heating converts to calcite, the conversion being very rapid at temperatures above 400°C [107]. In nature, calcium carbonate (CaCO_3) occurs in three structural forms: rhombohedral calcite, orthorhombic aragonite, and hexagonal vaterite. Calcite is stable at atmospheric pressure, whereas aragonite is thermodynamically stable under pressure but can be retained to ambient conditions [108]. Two phases of CaCO_3 , calcite and aragonite, are found in a wide range of geologic environments. This would indicate that calcite is a higher temperature form than aragonite, a conclusion substantiated by heat capacity measurements which show that calcite has a higher entropy than aragonite [107, 109]. MacDonald [107] concerned with the direct experimental determination of the calcite-aragonite equilibrium relations. He gave the results of subjecting calcite and aragonite to high pressures and temperatures.

Calcium oxide (CaO) is important mineral in the seashell and it is a white crystalline solid with a melting point of 2572 °C. It is manufactured by heating limestone, coral, sea shells, or chalk, which are mainly CaCO₃ to drive off carbon dioxide given eq (2.22). This reaction is reversible; calcium oxide will react with carbon dioxide to form calcium carbonate. The reaction is driven to the right by flushing carbon dioxide from the mixture.

According to the outcomes of the annealing of seashell sample at different annealing temperature, the better results in terms of TL peak intensity and area under the curve are seen annealing at 700 °C shown in Fig. 4.17. For different annealing temperatures, the shape of TL glow curve doesn't change but peak temperatures change shown in Fig 4.16.

In the basaltic rock sample, no important change is seen in the shape of TL glow curve for the different annealing temperatures shown in Fig. 4.20. However, area under the curve and TL peak intensity decrease to one-third of their initial values between 200 and 1100 °C of annealing temperatures seen in Fig. 4.21 and 4.22. This is unexpected result in this study because an increase in TL sensitivity is generally seen in the three samples mentioned above and in the literature [98-101, 110-111] when the annealing temperature increases. This extraordinary result may be due to the decreasing in number of available centers with annealing at higher temperature.

The results of the annealing of these four natural minerals at different temperatures are summarized in the Table 5.2.

As seen in Table 5.2, a change is observed in the glow curve shape of natural minerals except plagioclase minerals in basaltic rock. For all samples, peak temperature changes and the biggest area under the glow curve is observed at higher annealing temperatures except plagioclase minerals in basaltic rock.

The second thermal treatment is annealing of these four natural minerals at different annealing times. Summary of effects of annealing at different times on TL properties of the four natural minerals is given in Table 5.3.

Table 5.2 Summary of effects of annealing at different temperatures on TL properties of the four natural minerals.

	Glow Curve Shape	Peak Temperature	Maximum Area under Glow Curve
Calcite Extracted from Natural Sand Used in Making Roasted Chickpea	change	change between 200 °C and 800 °C	900 °C
Fluorapatite Mineral (Ca₅F(P04)₃) In Tooth Enamel	change	change (especially after 800 °C)	1000 °C
Biogenic Minerals Present in the Seashells	change	change between 400-700 °C (for low and intermediate temp.) change (for high temp. especially after 700 °C)	700 °C
Plagioclase Minerals in Basaltic Rocks	doesn't change	Change	200 °C

In the sand sample used in this thesis, there is no appreciable variation in glow curve shape for annealing time except 15 and 60min shown in Fig. 4.24. In addition, the peak temperatures for ~110°C peak and ~230°C peak don't vary with increasing annealing time. Annealing at 900°C about 15min gives a good glow curve shape with two distinct peaks, the biggest area under the curve and maximum TL intensities.

As a result of annealing time experiments of fluorapatite minerals in tooth enamel, variation of annealing time at fixed annealing temperature doesn't affect the shape of TL glow curve but peak temperature shifts to higher temperature region about 60°C when the sample is annealed about 120 minutes as seen in Fig. 4.28. Moreover, annealing about 120 minutes causes an enhancement (660 times) in TL peak intensity and area under the curve (carrier concentration in traps) when it is compared with un-annealed sample.

At the end of the experiments of seashell sample at different annealing times, no appreciable variation in glow curve shape for annealing time has been observed between 60 min and 360 min annealing times shown in Fig. 4.32. The largest area under the curve and TL peak intensities are seen between 150 and 180 min annealing times. Furthermore, the peak temperatures for low and intermediate peaks do not vary with increasing annealing time. But beyond 270 minutes annealing time, an increase is seen in the peak temperature of high temperature peak.

The last sample used in the experiments of the annealing at the different times is the basaltic rock. The area under the curve and TL peak intensity show different behavior at different annealing time and the best TL sensitivity is observed between 120 and 240 minutes of annealing times shown in Fig.4.36. In addition to this, the peak temperature doesn't importantly change and fluctuates between 196 and 207°C in the range of 15-360 minutes of annealing time. Martini et al. [112] demonstrated that prolonged high-temperature annealing of the samples reduces the presence of ionic charge compensators and creates luminescence traps. Generally, increasing in annealing time does not affect the glow curve shape. It means no new defect is produced and conversion of trap is not happened. But higher annealing times cause an increase in trap concentration and leads to enhancement in TL intensity.

The third thermal treatment is the cycle of measurement (reproducibility) of these four natural minerals at different annealing temperatures. Summary of effects of annealing at different temperatures on the cycle of measurement (reproducibility) of these four natural minerals is given in Table 5.4.

Table 5.3 Summary of effects of annealing at different times on TL properties of the four natural minerals.

	Glow Curve Shape	Peak Temperature	Maximum Area under Glow Curve
Calcite Extracted from Natural Sand Used in Making Roasted Chickpea	doesn't change (except 15 and 60min)	doesn't change	15 minutes
Fluorapatite Mineral (Ca₅F(P04)₃) in Tooth Enamel	doesn't change	Change (especially at 120min)	120 minutes
Biogenic Minerals Present in the Seashells	doesn't change	~100 °C and ~180 °C peaks don't change 340 °C peak changes (especially after 270 min)	150 - 180 minutes
Plagioclase Minerals in Basaltic Rocks	doesn't change	doesn't change	150 - 250 minutes

In the cycle of measurement (reproducibility) experiments at different annealing temperatures, the best reproducibilities are observed when the samples are annealed at 500°C for all natural samples except fluorapatite minerals in tooth enamel used in this thesis with good standard deviations. The stabilization of the trap is very good at this annealing temperature. That means the trap concentration does not affected by the repeat of the experiment. As it is mentioned in the theory part, annealing at low temperature may be done to stabilize traps.

Table 5.4 Summary of effects of annealing at different temperatures on the cycle of measurement (reproducibility) of the four natural minerals.

	Best Reproducibility	Mean of Normalized Area	Standard Deviation
Calcite Extracted from Natural Sand Used in Making Roasted Chickpea	at 500 °C	0.94387	0.06088
Fluorapatite Mineral (Ca₅F(P₀₄)₃) in Tooth Enamel	at 1000 °C	0.96377	0.03489
Biogenic Minerals Present in the Seashells	at 500 °C	0.837412	0.11215
Plagioclase Minerals in Basaltic Rocks	at 500 °C	0.893088	0.059854

In conclusion, the effects of pre-irradiation thermal treatments on the TL glow curves of four natural minerals whose origins are different have been done and the results obtained from all natural samples used in thesis have been compared to get common interpretations about influences of pre-irradiation thermal treatments on the TL properties of natural minerals. The outputs of the thesis have been published in the four prestigious international journals. As well as they show good TL properties, they are affected by pre-irradiation thermal treatments, efficiently. In generally, TL intensity increases enormously at higher annealing temperatures while the shape of the glow curve doesn't change with increasing the annealing temperature. Annealing of the samples at different times affects the TL peak intensities at different rates. Especially, annealing of samples about 120-180 minutes causes biggest TL intensities. And also, the annealing of the samples at 500°C gives the best reproducibility.

REFERENCES

- [1] Boss, A. J. J. (2007). Theory of thermoluminescence. *Rad. Meas.* **41**, 45-56.
- [2] Braunlich, P. (1983). *Thermally stimulated relaxation in solids*, Springer- Verlag.
- [3] HalpBran A. (1985). Evaluation of thermal activation energies from glow curves, *Phys. Rev.*, **117**, 40.
- [4] Botter-Jensen L. (1997). Luminescence technique: instrumentation and methods. *Rad. Meas.*, **17**, 749-768.
- [5] Daniels F. and Boyd C. A. (1953). Thermoluminescence as a research tool. *Science*, **117**, 343-349.
- [6] Aitken M. J., Tite M. S. and Reid J. (1964). Thermoluminescent dating of ancient ceramics, *Nature*, **202**, 1032-1033.
- [7] Aitken M. J., Zimmerman D. W. and Fleming S. J. (1964). Thermoluminescent dating of ancient pottery, *Nature*, **219**, 442-444.
- [8] Mejdahl V. (1969). Thermoluminescence dating of ancient Danish ceramics. *Archaeometry*, **11**, 99-104.
- [9] Wintle A. G. and Huntley D. J. (1980). Thermoluminescent dating of ocean sediments. *Canadian journal of earth sciences*, **17**, 348-360.
- [10] Wintle A. G. (1985). Anomalous fading of thermoluminescence in mineral samples, *Nature*, **245**, 143-144.
- [11] Wintle A. G. (1985). Thermal quenching of thermoluminescence in quartz, *Geophys. J. R. Ast. Soc.*, **41**, 107-113.
- [12] Randall J.T. and Wilkins M.H.F. (1945). Phosphorescence and Electron Traps. I. The Study of Trap Distributions. *Proc.R.Soc.London Ser. A* **184**, 366.

- [13] Chen R. and McKeever S.W.S. 1997. Theory of Thermoluminescence and Related Phenomena. Singapore: World Scientific.
- [14] Garlick G.F.J. and Gibson A.F. (1948). The Electron Trap Mechanism of Luminescence in Sulphide and Silicate Phosphors. *Proc.Phys.Soc.* **60**, 574.
- [15] May C.E. and Partridge J.A. (1964). Thermoluminescent kinetics of alpha;-irradiated alkali halides *J.Chem.Phys.* **40**, 1401.
- [16] Kitis G., Gomez-Ros J.M. and Tuyn J.W.N. (1998). Thermoluminescence glow-curve deconvolution functions for first, second and general orders of kinetics *J.Phys.D:Appl.Phys.* **31**, 2636.
- [17] Chen R. and Winer A.A. (1970). Effects of Various Heating Rates on Glow Curves. *J.Appl.Phys.* **41**, 5227.
- [18] Piters T.M. and Bos A.J.J. (1993). A model for the influence of defect interactions during heating on thermoluminescence in LiF:Mg,Ti (TLD-100) *J.Phys.D:Appl.Phys.* **26**, 2255.
- [19] Chen Reuven., McKeever S. W. S. (1997). Theory of Thermoluminescence and Related Phenomena.Singapore. *World Scientific*.
- [20] Furetta Claudio. (2008). Questions and Answers on Thermoluminescence (TL) and Optically Stimulated Luminescence (OSL).Singapore. *World Scientific*.
- [21] Driscoll C.M.H., National Radiological Protection Board, *Tech. Mem.* **5**, 82.
- [22] Busuoli G. 1981. In Applied Thermoluminescence Dosimetry. Bristol: Adam Hilger publisher
- [23] Drisoll C.M.H., Barthe J.R., Oberhofer M., Busuoli G. and Hickman C. (1986). Annealing procedures for commonly used radiothermoluminescent materials. *Rad. Prot. Dos.* **14 (1)**, 17-32.
- [24] McKeever, S. W. S. (1985). Thermoluminescence of solids. *Cambridge university Press*. Cambridge.
- [25] Daniels F. and Boyd C. A. (1953). Thermoluminescence as a research tool. *Science*, **117**, 343-349.

- [26] Teixeira M.I., Caldas L.V.E. (2002). Dosimetric properties of various colored commercial glass. *Appl. Radiat. Isot.* **57**, 407-413.
- [27] Goksu H.Y., Bailiff I.K., Mikhailik V.B. (2003) New approaches to retrospective dosimetry using cementitious building materials. *Radiat. Meas.* **37**, 323-327.
- [28] Arik R. (1992). Kubad-Abad Excavations (1980–1991). *Anatolica* **18**, 101-118.
- [29] Bernier J.L., Muhler J.G. 1970. Improving Dental Practice Through Preventive Measures. Saint Louis :The C. V. Mosby Company.
- [30] Hess J.C. 1970. Endodontie I, II. Paris: Librairie Maloine.
- [31] Sicher H., Dubrul E.L. 1970. Oral Anatomy. Saint Louis :The C.V. Mosby Company.
- [32] Fincham A.G., Moradian-Oldak J., Simmer J.P. (1999). The structural biology of the developing dental enamel matrix. *Journal of Structural Biology.* **126**, 270–299.
- [33] Macho G.A., Jiang Y., Spears I.R. (2003). Enamel microstructure – a truly three-dimensional structure. *Journal of Human Evolution.* **45**, 81–90.
- [34] Fourman P., Royer P., Lewell J.M., Morgan B.D. (1968). Calcium metabolism and the bone. *Blackwell Scientific Publication. Oxford.*
- [35] Fattibene P., Callens F. (2010). EPR dosimetry with tooth enamel: a review. *Applied Radiation and Isotopes.* **68**, 2033–2116.
- [36] Langeland K., Tagi T. (1972). Investigation on the innervation of teeth. *International Dental Journal.* **22**, 240–269.
- [37] LeGeros R.Z. (1981). Apatites in biological systems. *Progress in Crystal Growth Characterization Materials.* **4**, 1–5.
- [38] Lanjanian H., Ziaie F., Modarresi M., Nikzad M., Shahvar A., Durrani S.A. (2008). A technique to measure the absorbed dose in human tooth enamel using EPR method. *Radiation Measurement.* **43**, 648–650.
- [39] Secu C.E., Cherestes M., Secu M., Cherestes C., Paraschiva V., Barca C. (2011). Retrospective dosimetry assessment using the 380 °C thermoluminescence peak of tooth enamel. *Radiation Measurement.* **46**, 1109–1112.
- [40] Lee G.Y., Srivastava A., D'Lima D.D., Pulido P.A., Colwell C.W. (2005). Hydroxyapatite-coated femoral stem survivorship at 10 years. *Journal of Arthroplasty.* **20**, 57–62.

- [41] Matsumoto T., Okazaki M., Inoue M., Yamaguchi S., Kusunose T., Toyonaga T., Hamada Y., Takahashi J. (2004). Hydroxyapatite particles as a controlled release carrier of protein. *Biomaterials*. **25**, 3807–3812.
- [42] Ekendahl D., Judas L., Sukupova L. (2013). OSL and TL retrospective dosimetry with a fluorapatite glass–ceramic used for dental restorations. *Radiation Measurement*. **58**, 138–144.
- [43] Oliveira L.C., Rossi A.M., Baffa O. (2012). A comparative thermoluminescence and electron spin resonance study of synthetic carbonated A-type hydroxyapatite. *Applied Radiation and Isotopes*. **70**, 533–537.
- [44] Fukuda Y. (2002). Thermoluminescence in fluorapatite doped with Eu_2O_3 and PbO . *Radiation Protection Dosimetry*. **100**, 321–324.
- [45] Romanyukha A.A., Regulla D.F. (1996). Aspects of retrospective ESR dosimetry. *Applied Radiation and Isotopes*. **47**, 1293–1297.
- [46] Fukuda Y., Tanaka T. (2000). Thermally stimulated exoelectron emission and thermoluminescence in $\text{Ca}_5(\text{PO}_4)_3\text{F}:\text{Eu}$. *Proceedings of the 13th International Symposium on Exoemission and its Applications*, Jurmala, Latvia.
- [47] Furetta C. (2010). *Handbook of Thermoluminescence*, World Scientific Publishing, Singapore.
- [48] Brady J.M., Aarestad N.O., Swarts H.M. (1968). In vivo dosimetry by electron spin resonance spectroscopy. *Medical Physics*. **15**, 43–47.
- [49] Alvarez R., Rivera T., Guzman J., Piña-Barba M.C., Azorin J. (2014). Thermoluminescent characteristics of synthetic hydroxyapatite (SHAp). *Applied Radiation and Isotopes*. **83**, 192–195.
- [50] Dowling A., O’Dwyer J., and Adley C. C. (2015). Lime in the limelight. *Journal of Cleaner Production*. **92**, 13–22.
- [51] Johnson N.M. and Blanchard R. (1967). Radiation dosimetry from the natural thermoluminescence of fossil shells. *The American Mineralogist*. **52**, 1297–1310.
- [52] Köseoğlu R., Köksal F. and Çiftçi E. (2004). EPR study of radicals produced by gamma-irradiation in marine mollusc (*Venus* sp.) fossils. *Radiation Effects and Defects in Solids*. **159**, 497–502.

- [53] Aydaş C., Engin B., Kapan S., Komut T., Aydın T., Paksu U. (2015). Dose estimation, kinetics and dating of fossil marine mollusc shells from northwestern part of Turkey. *Applied Radiation and Isotopes*. **105**, 72–79.
- [54] Weightman P., Hall T.P.P. (1973). EPR studies of CaO doped with Mg. *Journal Physics C: Solid State Physics* **6**, 1292-1298.
- [55] Welch L.S. and Hughes A.E. (1980). Luminescence of the F_A center in CaO:Mg. *Journal Physics C: Solid State Physics*. **13**, 5801-5810.
- [56] Orera V.M., Sanjuán M.L. and Alonso P.J. (1986). EPR and thermoluminescence studies in RT X-irradiated CaO single crystals. *Journal Physics C: Solid State Physics*. **19**, 4763-4769.
- [57] Boas J.F. and Pilbrow J. R. (1985). Correlation of EPR and thermoluminescence in crystals of highly colored CaO:Mg: involvement of a center containing hydrogen ions. *Physical Review B*. **32**, 8258-8263.
- [58] Boas J.F. (1983). Electron spin resonance and thermoluminescence in calcium oxide crystals. *Radiation Protection Dosimetry*. **6**, 58-60.
- [59] Schmid T. and Dariz P. (2015). Shedding light onto the spectra of lime: Raman and luminescence bands of CaO, Ca(OH)₂ and CaCO₃. *Journal of Raman Spectroscopy*. **46**, 141–146.
- [60] De Freitas M. H., Blyth F.G.H. 1984. A Geology for Engineers. 6th edition. London:Elsevier.
- [61] Çanakci H., Pala M. (2007). Tensile strength of basalt from a neural network. *Engineering Geology*. **94**, 10–18.
- [62] Al-Harhi A.A., Al-Amri R.M., Shehata W.M. (1999). The porosity and engineering properties of vesicular basalt in Saudi Arabia. *Engineering Geology*. **54**, 313-320.
- [63] Gupta A.S., Seshagiri K. R., (2000). Weathering effects on the strength and deformational behaviour of crystalline rocks under uniaxial compression state. *Engineering Geology*. **56**, 257–274.
- [64] Militky J., Kovacic V., Rubnerova J., (2002). Influence of thermal treatment on tensile failure of basalt fibers. *Engineering Fracture Mechanics*. **69**, 1025 –1033.

- [65] Moore J. G., (2001). Density of basalt core from hilo drill hole. *Journal of Volcanology and Geothermal Research*. **112**, 221 – 230.
- [66] Pan Y., Christensen N. I., Batiza R., Coleman T.L. (1998). Velocities of a natural mid – ocean ridge basalt glass. *Tectonophysics*. **290**, 171 – 180.
- [67] Bell F.G., Haskins D.R. (1997). A geotechnical overview of Katse Dam and Transfer Tunnel Lesotho, with a note on basalt durability. *Engineering Geology*. **46**, 175 -198.
- [68] Morthekai P., Jain M., Murray A.S., Thomsen K.J., Botter-Jensen L., (2008). Fading characteristics of martian analogue materials and the applicability of a correction procedure. *Radiation Measurements*. **43**, 672–678.
- [69] Aparicio A. and Bustillo M. A., (2012). Cathodoluminescence Spectral Characteristics of Quartz and Feldspars in Unaltered and Hydrothermally Altered Volcanic Rocks (Almeria, Spain). *Spectroscopy Letters: An International Journal for Rapid Communication*. **45**, 104-108.
- [70] Tsukamoto S. and Duller G.A.T., (2008). Anomalous fading of various luminescence signals from terrestrial basaltic samples as Martian analogues. *Radiation Measurements*. **43**, 721–725.
- [71] Huntley D.J. and Lian O. B., (2006). Some observations on tunnelling of trapped electrons in feldspars and their implications for optical dating. *Quaternary Science Reviews*. **25**, 2503–2512.
- [72] Kayama M., Nishido H., Toyoda S., Komuro K., Finch A. A., Lee M. R., Ninagawa K., (2013). He⁺ ion implantation and electron irradiation effects on cathodoluminescence of plagioclase. *Phys Chem Minerals*. **40**, 531–545.
- [73] Correcher V., Gomez-Ros J.M., Garcia-Guinea J., Delgado A., (2004). Thermoluminescence kinetic parameters of basaltic rock samples due to continuous trap distribution. *Nuclear Instruments and Methods in Physics Research A*. **528**, 717–720.
- [74] Akber R.A. and Prescott J.R., (1985). Thermoluminescence in some feldspars: early results from studies of spectra. *Nuclear Tracks and Radiation Measurements*. **10**, 575–580.
- [75] Çanakçı H., Çabalar A.F., Kılınç E. (2002). *Geotechnical Properties of Yavuzeli Basalt Occuring in GAZİANTEP*. Harran University Faculty of Engineering, Proceedings of the Fourth GAP Engineering Congress.
- [76] Yoldemir O., (1987). Suvarlı-Haydarlı-Narlı Gaziantep arasında kalan alanın jeolojisi, yapısal durumu ve petrol olaraları: TPAO Rap. no. 2257, 60s. Ankara.

- [77] Furetta, C. and Kitis G. (2004). Review of Thermoluminescence. *Journal of Materials Science*. **39**, 2277-2294.
- [78] Garlick G.F.J. and Gibson A.F. (1948). The Electron Trap Mechanism of Luminescence in Sulphide and Silicate Phosphors. *Proc.Phys.Soc.* **60**, 574.
- [79] Vaijapurkar S.G., Raman R., Bhatnagar P.K., (1998). Sand a high gamma dose thermoluminescence dosimeter. *Radiation Measurements*. **29**, 223-226.
- [80] Teixeira M.I. and Caldas L.V.E., (2004). Sintered sand pellets for high dose dosimetry. *Nuclear Instruments and Methods in Physics Research B*. **218**, 194-197.
- [81] Fleming S.J., (1970). Thermoluminescent dating: refinement of the quartz inclusion method. *Archaeometry*. **12**, 133-143.
- [82] Ponnusamy V., Ramasamy V., Dheenathayalu M., Hemalatha J., (2004). Effect of annealing in thermostimulated luminescence (TSL) on natural blue colour calcite crystals. *Nucl.Instrum. Meth. B*. **217**, 611-620.
- [83] Lewis D.R., in: McDougall D.J. 1968. Thermoluminescence of geological material, New York :Academic Press.
- [84] Debenham N.C. (1983). Reliability of thermoluminescence dating of stalagmitic calcit., *Nature* **304**, 154-156.
- [85] Marshall S.A., McMillan J.A. (1968). Electron spin resonance absorption spectrum of Y^{3+} -stabilized CO_3^{3-} molecule-ion in single-crystal calcite. *Journal of Chemical Physics*. **48**, 5131-5137.
- [86] Macedo Z.S., Valerio M.E.G., de Lima J.F. (1999). Thermoluminescence mechanism of Mn^{2+} , Mg^{2+} and Sr^{2+} doped calcite. *Journal Physics Chemical Solids* **60**, 1973-1981.
- [87] Spooner, N.A., (1992). Optical dating: preliminary results on the anomalous fading of luminescence from feldspars. *Quaternary Science Reviews*. **11**, 139–145.
- [88] Huot S., Lamothe M., (2012). The implication of sodium-rich plagioclase minerals contaminating K-rich feldspars aliquots in luminescence dating. *Quaternary Geochronology*. **10**, 334-339.

- [89] Hashimoto, T., Yamazaki, K., Morimoto, T., Sakaue, H., (2001). Radiation-induced luminescence color images from some feldspars. *Analytical Sciences*. **17**, 825-831.
- [90] Can N., Garcia-Guinea J., Kibar R., Çetin A., Ayvacıklı M., Townsend P.D., (2011). Radioluminescence and thermoluminescence of albite at low temperature. *Radiation Measurements*. **46**, 655-663.
- [91] Correcher, V., Gomez-Ros J. M., Delgado A., (1999). The use of albite as a dosimeter in accident dose reconstruction. *Radiation Protection Dosimetry*. **84**, 547–549.
- [92] Zanelli G.D. (1968). Size on the thermoluminescence of LiF. *Physics Medical Biology*. **13**, 393-399.
- [93] Nakajima T. (1970). Effects of atmosphere and grain size on thermoluminescence sensitivity of annealed LiF crystals. *Journal. Physics. D: Application Physics*. **3**, 300-306.
- [94] Mendoza Anaya D., Angeles C., Salas P., Rodriguez R., Castano V.M., (2003) Nanoparticle-enhanced thermoluminescence in silica gels. *Nanotechnology* **14**, 19-22.
- [95] Chen, W., Wang Z., Lin Z., Lin L. (1997) Thermoluminescence of ZnS nanoparticles, *Application Physics Letter* **70**, 1465-1467.
- [96] Cameron J.R., Suntharalingam N., Kenney G.N. (1968). Thermoluminescent Dosimetry: TLD. University of Wisconsin Press, Madison.
- [97] Chen R., Kirsh Y. (1981). The Analysis of Thermally Stimulated Processes. Pergamon Press.
- [98] Zimmerman J. (1971). The radiation induced increase of the 100°C TL sensitivity of fired quartz. *Journal of Physics. C* **4**, 3265-3276.
- [99] Chen R., Yang X.H., McKeever S.W.S. (1988). Strongly supralinear dose dependence of thermoluminescence in synthetic quartz. *Journal of Physics D* **21**, 1452-1457.
- [100] Yang X.H., McKeever S.W.S. (1990). The predose effect in crystalline quartz *Journal of Physics. D* **23**, 237-244.

- [101] Lima J.F., Navarro M.S., Valerio M.E.G. (2002). Effect of thermal treatment on the TL emission of natural quartz. *Radiation Measurement* **35**, 155-159.
- [102] Engin B., Güven O., Köksal F. (1999). Thermoluminescence and Electron Spin Resonance Properties of Some Travertines from Turkey. *Application Radiation and Isotopes* **51**, 729-746.
- [103] Soliman C., Metwally M. (2006). Thermoluminescence of the green emission of calcite. *Radiation effects and defects in solids* **161**, 607-613.
- [104] Down J.S., Flower R., Strain J.A., Townsend P.D. (1985). Thermoluminescence emission spectra of calcite and Iceland Spar. *Nuclear Tracks and Radiation Measurements*. **10**, 581-589.
- [105] Medlin W.L. (1968). The nature of traps and emission centres in thermoluminescent rock materials. In *Thermoluminescence of Geological Materials* (Edited by McDougall D.J.). New York: Academic Press.
- [106] Correcher V., Garcia-Guinea J., Delgado A. (2000). Influence of preheating treatment on the luminescence properties of adularia feldspar (KAlSi₃O₈). *Radiation Measurement*. **32**, 709–715.
- [107] MacDonald G.J.F.; 1956. Experimental determination of calcite-aragonite equilibrium relations at elevated temperatures and pressure, *Am. Mineral.*; **41**, 744-756.
- [108] Suito K.; Namba J., Horikawa T., Taniguchi Y., Sakurai N., Kobayashi M., Onodera A., Shimomura O., Kikegawa T., (2001). Phase relations of CaCO₃ at high pressure and high temperature. *American Mineralogist*, **86**, 997–1002.
- [109] Anderson C. T., (1934). The heat capacities at low temperatures of alkaline earth carbonates: *J. Am. Chem. Soc.*, **56**, 340-342.
- [110] Toktamiş H., Toktamiş D., A.N. Yazici, (2014). Thermoluminescence studies of calcite extracted from natural sand used in making roasted chickpea. *J. Lumin.* **153**, 375–381.
- [111] Toktamiş H., Toktamiş D., Yılmaz S. M., Yazici A. N., Yildirim C., Özbiçki Ö., (2015). The investigation of usage of fluorapatite mineral (Ca₅F(PO₄)₃) in tooth

enamel under the different pre-irradiation thermal treatments. *Thermochimica Acta*. **600**, 102–109.

[112] Martini M., Spinolo G., Vedda A., Arena C., (1994). Phosphorescence and thermally stimulated luminescence of amorphous SiO₂. *Solid State Commun.* **91**, 751-756.



CURRICULUM VITAE

PERSONAL DATA

Full Name: Dilek TOKTAMIŞ

Maiden Surname: TUTCU

Date of Birth: 11/08/1971

Place of Birth: Gaziantep

Citizenship: T.C.

Marital Status: Married and three children

GSM: 05062424794

E-mail: dilektoktamis@hotmail.com

ACADEMIC QUALIFICATIONS

Bachelor of Science(BSc) :

University of Dicle, Faculty of Science & Art, Department of Physics

Thesis Title : *Aerodynamics and Technology Usage*

Supervisor : Assist. Prof. Dr. Kemal Akkılıç

Degree Obtained : *B.Sc.*, June 1997

Master of Science(MSc):

Graduate School of Natural and Applied Sciences, Department of Engineering Physics, Faculty of Engineering, University of Gaziantep (GAZU)

Thesis Title : *Exact Solutions of Effective Mass Schrödinger Equation*

Supervisor : Prof. Dr. Bülent GÖNÜL.

Degree Obtained : *M. Sc.* , September 2002.

WORK EXPERIENCE

1998-continue Teacher

RESEARCH SPECIALIZATION

PUBLICATIONS (SCI &SCI-EXPANDED & SSCI & Arts and Humanities)

1. Gönül B., Ozer O., Kocak M., **Tutcu D.** and Cançelik Y. (2001).
Supersymmetry and the relationship between a class of singular potentials in arbitrary dimensions. Journal of Physics A: Mathematical and General Vol34No40pp8271-8279.
2. Gönül B., Gönül B., **Tutcu D.** and Ozer O. (2002)
Supersymmetric Approach to Exactly Solvable Systems with Position Dependent Effective Masses. Modern Physics Letter A Vol17No31pp2057-2066.
3. Toktamis H. , **Toktamis D.** and Yazici A. N. (2014)
Thermoluminescence studies of calcite extracted from natural sand used in making roasted chickpea. Journal of Luminescence 153, 375--381.
4. Toktamis H. , **Toktamis D.**, Yilmaz S. M., Yazici A. N., Yildirim C. And Özbiçki Ö. (2015)
The investigation of usage of fluorapatite mineral ($\text{Ca}_5\text{F}(\text{PO}_4)_3$) in tooth enamel under the different pre-irradiation thermal treatments. Thermochemica Acta 600 (2014) 102--109.
5. **Toktamis D.**, Toktamis H. and Yazici A. N. (2016)
The effects of thermal treatments on the thermoluminescence properties of biogenic minerals present in the seashells. Radiation Effects & Defects in Solids DOI: 10.1080/10420150.2016.1259623.
6. **Toktamis D.**, Toktamis H. and Yazici A. N. (2017)
Thermoluminescence behavior of basaltic rocks collected in southeastern region of Turkey. Applied Radiation and Isotopes 121, 109--115.

CONTRIBUTION TO CONFERENCES

1. B. GONUL, B. GONUL, O. OZER ve **D. TUTCU**
Değişken Efektif Kütle İçeren Fiziksel Sistemlerin Tam Çözümleri, Türk Fizik Derneği 21. Fizik Kongresi (TFD-21), 11-14 Eylül 2002, Özetler-s.268

2. H. TOKTAMIŞ, S. ZUHUR, **D. TOKTAMIŞ**, E. BOZ, F. SAVRUN, A. TUNÇ
Gaziantep ili volkanik kayaçlardan elde edilen termoluminesans tepe şiddetlerinin
tavlama ile değişiminin incelenmesi, T.F.D 29. ULUSLARARASI FİZİK
KONGRESİ BODRUM EYLÜL 2012

3. H. TOKTAMIŞ, **D. TOKTAMIŞ** ve Ö.ÖZBİÇKİ
İnsan Diş Minesinin Farklı Tavlama Sıcaklıkları Altında Termoluminesans
Özelliklerinin Araştırılması LUMİDOZ 6, 11-13 Eylül 2012

4. **Dilek Toktamış**, A. Necmeddin Yazıcı and Hüseyin Toktamış,
Elazığ İli Leblebi Kumunun Termoluminesansışırma Tepelerine Tavlamanın Etkisi,
LUMİDOZ 6, 11-13 Eylül 2012.

5. Hüseyin Toktamış, **Dilek Toktamış**, Sinem Merve Yılmaz and A. Necmeddin
Yazıcı, Thermoluminescence Properties of Basalt Collected in Karataş Region of
Gaziantep, LUMIDOZ 8, 27-29 August 2014, Ankara, Turkey.

6. **Dilek Toktamış**, Hüseyin Toktamış and A. Necmeddin Yazıcı,
Effect of Annealing on Thermoluminescence Glow Curve of Chimera (Yanartaş)
Rock Collected Nm ear the Village of Çıralı, Antalya. LUMIDOZ 8, 27-29 August
2014, Ankara, Turkey.

7. **Dilek Toktamış**, Hüseyin Toktamış and A. Necmeddin Yazıcı,
Thermoluminescence Properties of Biogenic Minerals Present in the Seashells Under
the Different Pre-irradiation Thermal Treatments LUMIDOZ 9, 2-4 SEPTEMBER
2015, ANTALYA/TURKEY.

8. **Dilek Toktamış**, Hüseyin Toktamış and A. Necmeddin Yazıcı,
A study on Effects of Particle Size on the TL Glow Curves of Natural Minerals.
LUMIDOZ 10, 5-7 SEPTEMBER 2016, Adana/TURKEY.

9. Hüseyin Toktamış, Ömer Lütüf Unsal, **Dilek Toktamış** and A. Necmeddin Yazıcı,
Investigation of thermoluminescence properties unique Rosso Levanto marble.
TESNAT 2017, 10-12 May 2017, Adana/TURKEY

LANGUAGES

English: UDS: 62.5